28048

REFERENCE

ProQuest LLC.
789 East Eisenhower Parkway
P.O. Box 1346
Ann Arbor, MI 48106 – 1346

Detection of Protein Interactions at Cellular Membranes Using Total Internal Reflection Ellipsometry.

Rachel Ann-Selina Smith

A thesis submitted in partial fulfilment of the requirements of Sheffield Hallam University for the degree of Doctor of Philosophy.

February 2015

Declaration

I hereby declare that this thesis submitted for the degree of PhD is the result of my own research and that this thesis has not been submitted for a higher degree to any University or Institution.

Acknowledgements

I would like to thank my supervisors Dr Ben Abell and Dr David Smith for their support, patience and ideas throughout the project over the last three years. Their pep talks and encouragement have been invaluable. Also my sincere thanks to Professor Alexei Nabok for guiding me through the mysteries of the Biophysical world – I certainly mastered the art of trouble-shooting. Also to Dr Verena Kriechbaumer for all her help and guidance at the beginning of my PhD and introducing me to the realms of plant biology and TIRE!

A huge thanks to my friends in the PhD office, who listened to my rants when lab work seemed like a never-ending stretch of unanswerable questions! The endless cups of teas and cake breaks certainly kept me going. A special thanks to my lab buddy, Rebecca, I hold fond memories of sharing in-depth conversations about science, life, news...and of course gossiping and singing along with the radio – happy days!

Words cannot express enough my love and gratitude to my wonderful family and friends – old and new, your constant support and belief in me has been truly humbling, and I could not have achieved any of this without you. You were always there for me, and I hope that I have done you proud.

Abstract

The targeting and subsequent interaction of proteins with membranes and membrane bound receptors is central to numerous cellular processes. Membrane bound receptors play a vital function in cell signalling, and are thus a target for many drugs, whereas aberrant membrane interactions play a major role in human amyloid diseases such as Parkinson's disease. The analysis of these interactions in their native environments poses problems, due to the technical difficulty in depositing membranes for analysis by conventional techniques such as, surface plasmon resonance (SPR). The optical method of spectroscopic ellipsometry in its total internal reflection mode (TIRE) is a combination of spectroscopic ellipsometry (SE) and SPR. This offers sensitive detection of binding between a ligand and its receptor, and gives potential solutions to the membrane deposition issues by Langmuir-Schaefer (LS) deposition. Therefore, TIRE enables the study of natively derived membranes in addition to synthetic lipid environments.

The aim of this research was to develop the method of TIRE by focusing on the analysis of two distinct types of biological processes: model I tested protein: lipid interactions via amyloid fibrils at natively derived membrane from the neuronal cell line SH-SY5Y; and model II tested protein: protein interactions involved in the targeting and binding of molecular chaperones to cognate receptors, using natively derived chloroplast (CP) membranes. Results of Model I demonstrated how short amyloid fibrils can bring about a toxic gain of function by increased membrane disruption, and Model II showed specific chaperone binding to cognate receptors, providing evidence that there are two predominant chaperone receptors to reside at the outer CP membrane. Together the results demonstrate that TIRE can be used with natively derived membranes to obtain biologically relevant information.

The importance of studying membrane proteins is highlighted by the fact that nearly half of the top-selling drugs target membrane proteins, and organelles as potential therapeutic targets. Therefore this research will have a direct impact on the development of new therapeutics and our understanding of disease.

Contents

Abbreviations

AD	Alzheimer's Disease
AFM	Atomic force microscopy
AMP	Antimicrobial peptide
APP	Amyloid precursor protein
At	*Arabidopsis Thaliana*
Aβ	Amyloid-β peptide
CP	Chloroplast
Cys-HCl	Cysteamine-Hydrochloride
d	Thickness
DDM	Dodecyl β-D-Maltopyranoside
DEPC- water	Diethylpyrocarbonate- water
DMEM	Dulbecco's Modified Eagle's Medium
DPI	Dual-polarization interferometry
DTT	Dithiothreitol
EDTA	Ethylenediaminetetraacetic acid
EIS	Electrical impedance spectroscopy
EPP	Ethanol and 1,2-epoxypropane
ER	Endoplasmic Reticulum
F	Force
FRET	Fluorescence resonance energy transfer
gDNA	Genomic DNA
Get	Guided entry for tail anchored proteins
GK	Gabi-Kat
GPCRs	G-protein-couple receptors

HEPES	4-(2-hydroxyethyl)-1-piperazineethanesulfonic acid
HFIP	Hexafluorisopropanol
HOP	Hsp70/90 organising protein
Hsc	Heat shock constitutively expressed
Hsp	Heat shock proteins
ImageJ	Image processing and analysis in Java
k	Co-efficient
KOAc	Potassium acetate
KOH	Potassium Hydroxide
LB	Langmuir Blodgett
LB	Lewy bodies
LB	Langmuir-Blodgett
LS	Langmuir-Schaefer
LUV	Large unilamellar vesicles
MS agar	Murashige Skoog agar
NAC	Non-amyloid-β component
NP	Nanoparticles
OEP61	Outer envelope protein 61kDa
PAH	Polyallylamine hydrochloride
PI	Propidium iodide
PMSF	Phenylmethylsulphonyl flouride
PrP	Prion protein
PTD	Protein transduction domains
QCM	Quartz crystal microbalance
QCM-D	QCM with dissipation
RFU	Relative fluorescence units
RI	Refractive index

RNC	Ribonascent Chain
SE	Spectroscopic Ellipsometry
SGTA	Small glutathione-rich tetratricopeptide repeat-containing protein alpha
SLB	Supported lipid bilayers
SNARE	Soluble *N*-ethylmaleimide-sensitive factor attachment protein receptors
SPR	Surface Plasmon Resonance
SPRM	SPR with microscopy
SRP	Signal recognition particle
SUBA database	SUB-cellular location database for Arabidopsis proteins
SUV	Small unilamellar vesicles
TA	Tail anchored
TA protein	Tail-anchored membrane protein
TAIR	The Arabidopsis Information Resource
TBS-T	Tris-Buffered Saline and Tween 20
TE	Transverse electric
ThT	Thioflavin-T
TIC	Translocon at the inner envelope membrane of the chloroplast
TIRE	Total Internal Reflection Ellipsometry
TM	Transverse magnetic
TMD	Transmembrane domain
TOC	Translocon at the outer envelope membrane of the chloroplast
TPR	Tetratricopeptide repeat
TRC	Transmembrane recognition-complex
Vipp	Vesicle-inducing protein in plastids

1.1. The biological importance of protein interactions.

Proteins play a central role in biological function, and it is these protein-protein interactions that mediate metabolic and signalling pathways, cellular processes and organismal systems. Protein structures and subsequent interactions are predominantly governed by non-covalent bonding: hydrophobic and Van der Waals forces, and electrostatic interactions. Whilst hydrophobicity is the major driving force in protein folding, electrostatic interactions also play a critical role in protein folding, specificity of protein binding, flexibility, stability and function (Kumar *et al.,* 2002). The careful management of protein synthesis and folding is vital for healthy conditions, with errors leading to a diseased state in organisms. Diseases are often caused by mutations affecting the binding interface or leading to biochemically dysfunctional allosteric changes in proteins. For example, a point mutation causes the replacement of a single nucleotide base and can result in encoding for an entirely different amino acid. It was shown that a point mutation in the endoplasmic reticulum (ER) SEC61 gene was found to cause diabetes in mice via β-cell apoptosis, due to a loss of function downstream causing ER stress (Lloyd *et al.,* 2010). Furthermore, protein misfolding and their undesired interactions can alter homeostasis causing the loss of vital cellular functions resulting in cytotoxicity. A group of protein folding diseases known as amyloidosis arise as a result of specific proteins misfolding and their abnormal accumulation in deposits, for example Lewy bodies (Parkinson's disease) and plaques (Alzheimer's disease) associated with the impairment of cellular function and neurodegeneration (Stefani *et al.,*

2003). Therefore, the study of protein interactions can help to elucidate the molecular basis of disease and an understanding of cellular control, which in turn can inform methods for prevention, diagnosis, and treatment (Gonzalez *et al.,* 2012).

1.2. Classic *in vitro* analysis of protein interactions using biochemical methods

It is estimated that over 80 % of proteins do not operate alone but in complexes (Berggard *et al.,* 2007), whereby protein: protein interactions can include: altering the kinetic properties of enzymes, acting as a common mechanism for substrate channelling, constructing new binding sites for small effector molecules, inactivating or suppression of protein activity and finally can alter the specificity of a protein for its substrate via its interaction with alternative binding partners (Phizicky *et al.,* 1995). As a result their study requires a range of biochemical techniques to identify and analyse their interactions and subsequent roles within cellular processes, of which discoveries of such interactions can lead to the identification of possible drug targets (Pedamallu *et al.,* 2010). Classic *in vitro* techniques for the study of protein interactions include affinity chromatography, used to analyse interactions including; enzyme-enzyme, subunit-oligomer, protein-antibody and protein-chaperone (Muronetz *et al.,* 2001). It is a highly sensitive technique and can detect interactions with a binding constant as weak as 10^{-5} M if high enough concentrations of protein are immobilised on the

column (Phizicky *et al.,* 1995). However, a potential problem of its sensitivity is that it is also prone to false-positive results due to the broad specificity of binding amongst proteins (Rao *et al.,* 2014). Furthermore, the forces involved in protein: protein interactions as well as the forces stabilising the three-dimensional structures of proteins are often complex, thus the immobilisation and elution of such proteins and/or complexes whilst maintaining their native form and biological activity pose significant problems. Stringent elution conditions such as change of pH or denaturing conditions can overcome such difficulties, but can abolish biological function as a result of protein unfolding (Muronetz *et al.,* 2001). Another technique is co-immunoprecipitation, where the protein of interest is isolated with a specific antibody and can be identified via electrophoretic analysis. It is considered the gold standard for the analysis of protein: protein interactions in the context of a living cell or organism (Van der Geer 2014). The utilisation of eukaryotic cells therefore allows for the study of proteins in their native state, enabling posttranslational modification that may be essential for protein function and for subsequent interactions such as phosphorylation, of which could not have occurred in a prokaryotic expression system (Rao *et al,.* 2014). Nevertheless, issues with transient interactions which may go undetected (Van der Geer 2014) and the requirement of highly specific antibodies to avoid false positive results and decrease background noise are a few of the limitations faced using this method (Berggard *et al.,* 2007). Protein microarrays are also another powerful tool for detecting protein interactions, this method can perform a large volume of tests in parallel, thereby functioning as a high-throughput technique (Rao *et al.*, 2014).

However, the use of microarrays as routine diagnostics face some operational challenges, including probe specificity, cross-reactivity between antibodies in complex mixtures leading to background noise and false positive results, and finally, the production of monoclonal antibodies as capture agents is expensive and a labour-intensive process (Cretich *et al.,* 2014). Alternatively the direct labelling of proteins such as fluorescence-based technologies can enable spatial and temporal changes in protein complexes to be measured. For example, fluorescence resonance energy transfer (FRET) detects the proximity of fluorescently labelled molecules over distances < 100 Å, and has been used to map *in vivo* protein: protein interactions (Kenworthy 2001). However, like other label-based techniques it is mainly an end point assay measuring changes in fluorescence signals before and after binding, which is not directly suitable when determining binding kinetics (Wang *et al.*, 2012). Furthermore, the addition of a synthetic label to proteins may affect protein conformation and subsequent biological activity by interfering with native-folding and thus its function (Arnau *et al.,* 2006).

With the human genome consisting of 20, 000 – 30, 000 genes coding for over 500 000 different proteins (Berggard *et al.,* 2007), membrane proteins are estimated to be encoded by over 30 % of the genome (Arslan *et al.*, 2013), and their significance is highlighted by the fact that they are targets for almost half of the top selling drugs in the current market (Gonzalez-Maeso 2010). The technique blue native polyacrylamide gel electrophoresis (BN-PAGE) has been used to separate native membrane complexes, involving the careful solubilisation of protein complexes with non-denaturing

detergents, followed by their separation using electrophoresis. Protein separation is based on binding of Coomassie blue G which provides negative charges to the surface of the proteins, during which protein complexes separate according to molecular mass and/or size. The detergent enables the extraction of membrane proteins whilst maintaining their intactness by disrupting membrane lipid bilayers and lipid-protein assemblies. Detergents are classified into three groups: anionic, non-ionic and zwitterionic with non-ionic detergents being used primarily for the isolation of native membrane protein complexes due to preferentially disrupting lipid-lipid and protein-lipid interactions, for example Triton X-100 and DDM. Once optimal solubilisation protocols have been established according to the nature of the protein and the detergent type and concentration (between 0.5 - 2 % w/v final concentration), there are many different methods available for further analysis of separated protein complexes, including immuno-detection using pecific antibodies (Reisinger *et al.,* 2008). Difficulties posing BN-PAGE and membrane protein analysis entails the screening and identification of a detergent compatible with the target protein. The detergent micelles which form a soluble protein-detergent complex are often unsatisfactory substitutes for native lamellar membranes (Long *et al.,* 2013). Furthermore, the use of detergents can decrease protein stability, interfere with assays and cause the partitioning of substrates and products into the excess detergent micelle (Kriechbaumer *et al.,* 2012 (C)).

The study of membrane-associated events is technically challenging when monitoring in lipid environments, and therefore there is a lack of experimental systems which can mimic native environments and quantify subsequent

protein-protein and protein-membrane interactions. This is mainly due to the difficulties in replicating the intrinsic complexity of the cell membrane with its varied components of lipids, sterols, proteins, *etc.*, and also by the purification and correct folding of the recombinant proteins of interest (McGillivray *et al.,* 2007).

1.3. Biosensing techniques and the study of bimolecular interactions

The labelling of proteins, for example the addition of an affinity tag, has been employed to improve protein yield, folding and purification, however as previously noted, it can also exert negative effects resulting in a change in target protein conformation, inhibition of enzyme activity, altered biological functions and toxicity (Arnau *et al.,* 2006). Thus the development of label-free methods for the analysis of molecular interactions has been established whilst aiming for increased sensitivity in a native-like environment. This has been primarily through the coupling of a molecular recognition element such as an antibody or target receptor, to a transducer that acts to convert a chemical or biological interaction into an electrical signal, termed a biosensor (Cooper *et al.,* 2007). A type of biosensor includes optical, which provides powerful detection and analysis with numerous applications in biomedical research, healthcare and pharmaceuticals. By employing label-free optical detection it is relatively cheap to perform and allows for quantitative and kinetic measurements of molecular interactions (Fan *et al.,* 2008).

1.3.1. Surface Plasmon Resonance

A well-established analytical method of surface plasmon resonance (SPR) was pioneered by Ingemar Lundström and his team at Linköping University in collaboration with the BIAcore™ Company, whose SPR machine monitors biological binding interactions in real-time (Turner 2013). This optical method measures changes in refractive index (RI) of a medium in close vicinity to a metal surface (typically gold), thus enabling monitoring of binding of analyte molecules to immobilised receptors at the sensors surface. SPR exploits the phenomenon of surface plasmon resonance between plasmon oscillations in thin metal films. The incident light from a laser source is coupled through a prism at total internal reflection conditions at a surface-solution interface, generating an evanescent wave which penetrates the thin metal layer propagating along the metal/prism interface, extending into the solution (~300 nm) (Fig. 1.1). The changes in the surface plasmon resonance caused by binding of biomolecules alter the RI which is measured to derive binding kinetics (Patching 2014).

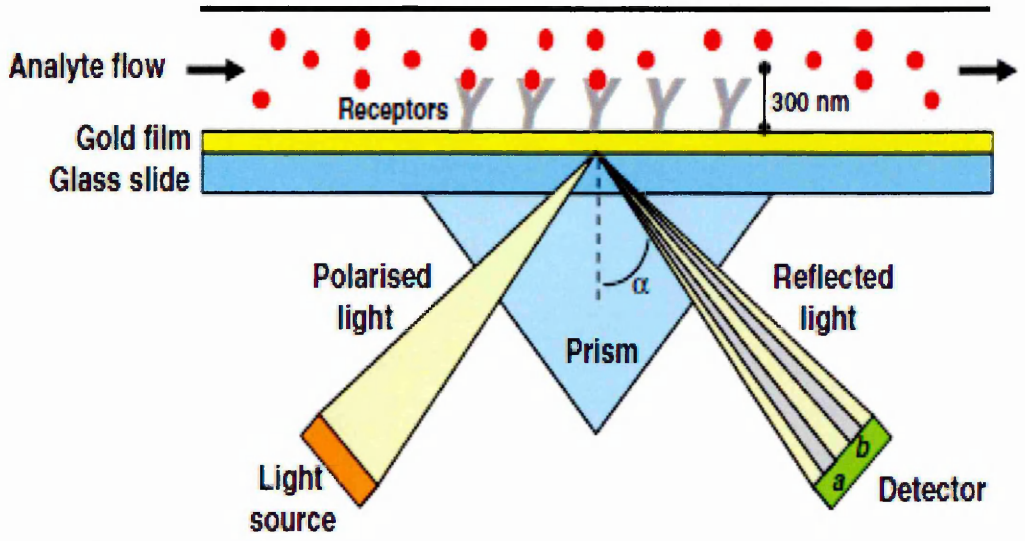

Figure 1.1. Schematic illustration of the basic SPR experimental set-up. (Patching 2014).

SPR requires several steps to achieve immobilization of proteins onto SPR chips including extraction, purification and selective chemistry for attachment, which is not only time-consuming but also changes the native environment of the proteins (Wang *et al.*, 2012). The deposition of membranes is technically challenging, limiting the sensitivity of SPR particularly when studying ligands in native membranes of low abundance. Developments over the years include utilising solid supports for the stabilisation of biomimetic and tethered bilayer membranes, maintaining the fluidity of proteins within the bilayer to study protein-ligand interactions. However, the additional cushions added to help lift the bilayer away from the sensor chip surface, can result in the decrease in sensitivity of SPR (Maynard *et al.*, 2009). Although the use of an artificial membrane mimic

provides a robust experimental platform for many surface-base-characterisation techniques (Yildiz *et al.,* 2012), the capability to directly study binding kinetics of proteins within their native environment is highly desired, not only to validate *ex situ* methods but also in revealing novel features (Wang *et al.,* 2012). An extensive review of SPR and its applications by Patching (2014) highlights the developments of next-generation SPR instruments in screening small molecule compounds for drug discovery. Next generation SPR instruments use a sensor based on nano-structured materials, using extraordinary optical transmission as opposed to a prism in BIAcore to focus the light, where specific wavelengths are transmitted through nanopores in thin metal films. The sensing capability due to the large number of nanopores is much greater than can be achieved by a conventional SPR instrument, overcoming sensitivity issues caused by the cushioning of the lipid bilayer for substrate accessibility to both sides.

One particular method combines SPR with microscopy (SPRM) allowing simultaneous optical and fluorescence imaging in single living cells without extracting the proteins from the cell membranes (Fig 1.2). Wang *et al.,* (2012) studied the specific interactions between glycoproteins (membrane protein) and lectin (ligand) by culturing human epithelial cells (SH-EP1) on a gold film modified with poly-L-lysine solution, and visualised using an inverted microscope.

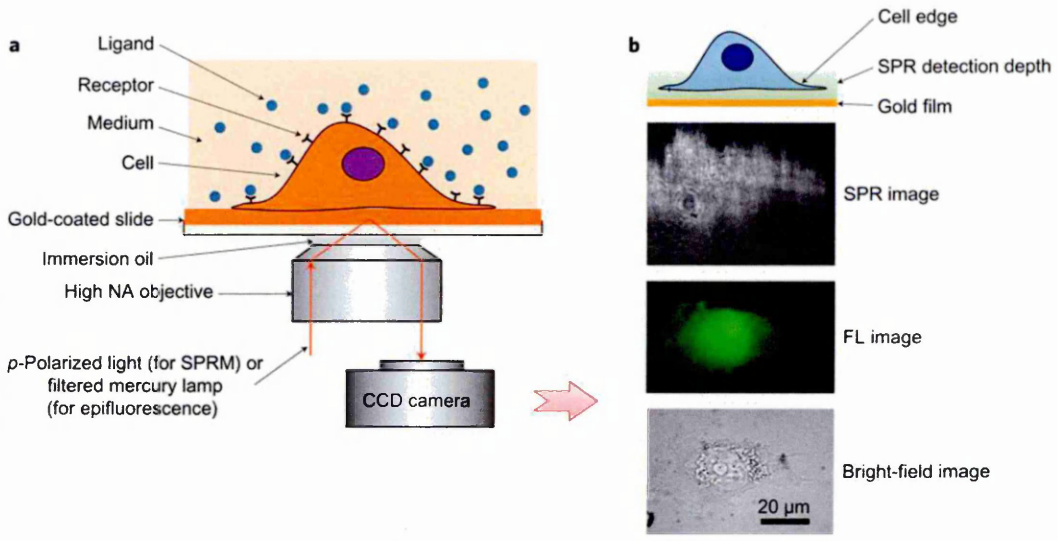

Figure 1.2. Next-generation SPR instrumentation for measuring membrane protein- ligand binding. (a) Surface plasmon resonance microscopy schematic experimental set-up; (b) demonstrating contact depth of the entire cell edge regions are located within the typical detection depth of the SPRM, in order below: examples of SPR image, fluorescence (FL) and bright-field images of living cell (Wang *et al.*, 2012).

Using SPRM Wang *et al.,* (2012) determined kinetic constants of membrane proteins in single live cells and subsequent binding of ligands. This novel combination of SPR and microscopy enabled the label free detection of protein interactions within a native membrane environment. This was achieved by gold film modification with a solution of positively charged poly-L-lysine to promote the subsequent adhesion of cultured cells, similar to that performed by Kriechbaumer *et al.,* (2011) for the deposition of proteins on gold slides using polyallylamine hydrochloride (PAH). Wang *et al.,* (2012) compared the binding of live and fixed cells which had been subjected to fixation prior to measurements with 4 % paraformaldehyde solution. The

fixation of cells can cause membrane disruption and artificial protein import and redistribution as seen by Lundberg *et al.,* (2003) who studied the mechanism of translocation of protein transduction domains (PTD) involved in protein delivery across the membrane. When comparing results of protein import in fixed (methanol fixation) and unfixed cells, they found that proteins in fixed cells were able to adhere to intracellular structures resulting in the redistribution of proteins and causing apparent but not true protein translocation. Similarly, Richard *et al.,* (2003) also found that PTD derived peptides in cells after fixation by paraformaldehyde caused membrane barrier dysfunction, allowing peptide relocation and resulting in artefactual redistribution and subsequent binding of intracellular structures. Wang *et al.*, (2012) further demonstrate a difference in binding capabilities and dissociation rates between live and fixed cells; attributing damage during cell fixation resulting in reduced ligand binding and membrane-associated events such as receptor mediated endocytosis. These studies highlight the difficulty of monitoring protein interactions *in situ* and the need for alternative cell deposition methods that avoid the use of chemical fixatives like paraformaldehyde and methanol, to maintain native cell activity.

1.3.2. Quartz crystal microbalance

Other techniques used for measuring thin films include quartz crystal microbalance (QCM) a piezoelectric method based on oscillations of a quartz crystal when an alternating voltage is applied. QCM relates a frequency

change (Δf) from the oscillating crystal to the mass adsorbed (Δm) on the surface in gas-phase measurements, as demonstrated by Sauerbrey in 1959: (Equation 1.1. C = sensitivity factor of crystal, and n = harmonic number)

$$\Delta m = \frac{C}{n} \Delta f$$

Equation 1.1

Any changes to the crystals surface is reflected by changes in the resonant frequencies and depict surface-bound mass, thus immobilization of substrates and subsequent binding of ligands can be tested. QCM measurements are frequently used to follow a range of biomolecular processes, such as; protein-protein interactions: antigen-antibody binding or ligand-receptor interactions (Wegener *et al.,* 2001) and newer applications involving complex biochemical and biomimetic systems in drug discovery and biosensors.

Figure 1.3 was taken from the survey of the Quartz crystal microbalance review by Speight *et al.,* (2012) depicting the applications of QCM, highlighting the focus of a vast majority of papers on small molecules and the adsorption of proteins. To name but a few, QCM has been used for detection of bacteria, eukaryotic cell interactions, protein adsorption and binding and biochemical assays.

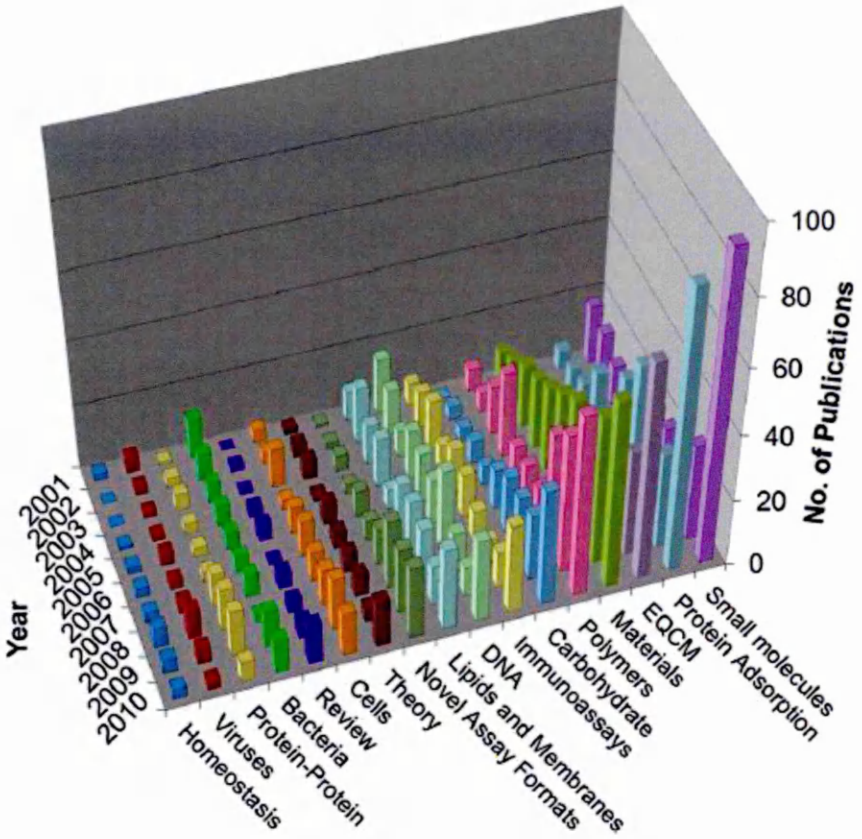

Figure 1.3. Number of publications per annum using a QCM sensor. Defined by the field of application from 2001 to 2010 (Speight *et al.*, 2012).

A study by Shammas *et al.,* (2011), utilised QCM to measure the rate of amyloid fibril elongation via its covalent attachment to the sensors surface in the presence of the small heat shock protein αB-crystallin. It was concluded that fibril elongation was inhibited in the presence of αB-crystallin, which may act to prevent the development of disease based on protein mis-folding and aggregation. Biochemical binding assays at lipid membranes using artificial systems have also been tested using tethered liposomes. The impact of the membrane binding antimicrobial peptide melittin was studied, with the interaction shown to cause liposome rupture (Briand *et al.,* 2010). QCM has also been used as an alternative to the traditional enzyme-linked

immunosorbent assay (ELISA) as an immunosensor, offering a fully automated and label free method with a rapid response time and requirement for only a single analyte-specific antibody (Cooper *et al.,* 2007). Mass sensitivity has been shown to increase with increasing resonant frequency; therefore a higher resonance frequency requires even thinner crystals making them fragile and expensive to produce (Marx *et al.,* 2003).

An important consideration for biosensing applications is that the deposited material does not act as a thin rigid layer during QCM measurements, and therefore can poise complications. This is a result of non-rigid molecules attached to the surface causing the frequency-mass relationship to deviate from the Sauerbrey equation, therefore leading to an overestimation of the mass accumulation. Thus the development of QCM with dissipation monitoring (QCM-D) coupled the measuring of changes in resonant frequency with a simultaneous parameter related to the energy loss or dissipation caused by surface inhomogeneity (viscoelasticity). This allows for two independent properties to be measured; mass changes at the sensor surface and viscoelastic properties - particularly important in biomolecular applications, for example, cell adsorption and structural changes (Dixon 2008).

QCM-D was combined with data from electrical impedance spectroscopy (EIS), a method that characterises cellular changes quantitatively as a function of an applied electrical current, and together the methods investigated the structure-function relationships of proteins and peptides interacting with lipid membranes. In particular, recording membrane disruption caused by a snake venom toxin and a pore-forming peptide

respectively, by simultaneously measuring membrane resistivity and viscoelastic properties of the lipid membrane (Briand *et al.,* 2010).

1.3.3. Dual-polarization interferometry

Dual-polarization interferometry (DPI) is another optical method that uses the evanescent field of laser light as a sensing element. DPI utilises a waveguide structure consisting of a stack of vertical dielectric layers, the top (sensing) waveguide surface is exposed for protein adhesion and the lower waveguide experiences no changes, providing an optical reference (Swann *et al.,* 2004). Light from a laser passes through the sandwiched waveguide structure and the output light combines with each other to produce a series of light and dark bands known as interference 'fringes' (Fig 1.4). Any changes to the refractive index of the sensing layer alter the optical path length of the top waveguide and cause a shift of the interference fringes (Mashagi *et* al., 2008). Unlike SPR which measures only a single polarized light mode (transverse magnetic, TM), DPI measures two independent measurements with two different polarizations (TM and transverse electric, TE), providing quantitative determination of both refractive index and the thickness of the adsorbed layer (Mashagi *et al.,* 2008) to subatomic resolutions; 0.01 nm (Swann *et al.,* 2004). DPI applications have proven to be useful in monitoring biomolecular structural changes for various interactions including; protein: protein (Biehle *et al.,* 2004), protein: small molecule (Swann *et al.,*

2004 and Ozalp *et al.,* 2012) and artificial lipid bilayer membranes (Mashagi *et al.,* 2008).

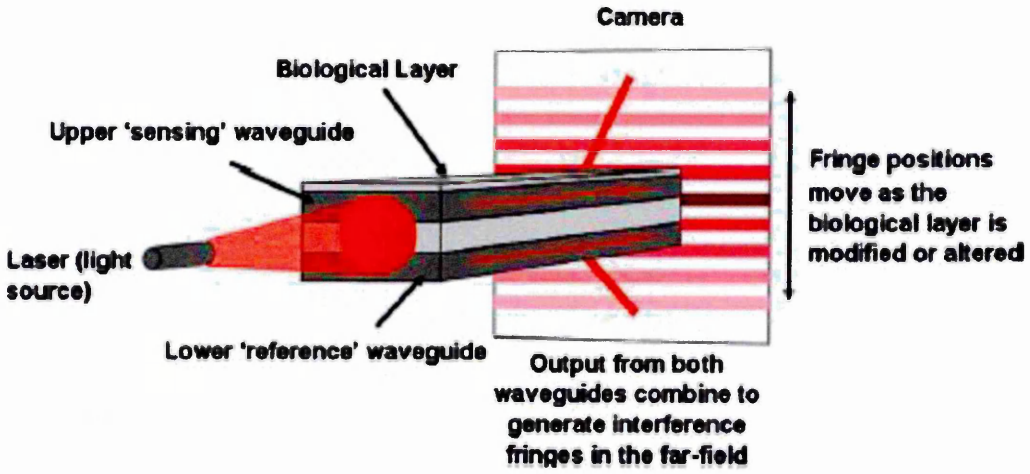

Figure 1.4. Schematics of a dual polarization interferometry sensor. Determination of thickness and RI is derived from using information from both the absolute and relative changes in optical path length for propagation of two waveguide modes (Swann *et al.,* 2004).

Supported lipid bilayers (SLB) are an important model system used in optical biosensors which mimic cell membranes for subsequent measurements of bimolecular interactions. However, there is a lack of understanding of the driving forces responsible for SLB formation from liposomes, beyond the qualitative effects of electrostatic attraction and repulsion, with common optical techniques like SPR incorrectly determining film thickness and estimated mass etc., due to the assumption of an isotropic SLB RI (Mashaghi *et al.,* 2008). A molecule that is optically anisotropic has a *n* that depends on the polarization and propagation direction of light (birefringent) causing each molecule to respond differently depending on their alignment

(Edvardsson *et al.,* 2009). Mashaghi *et al.,* (2008) showed that DPI could sensitively detect the different stages of SLB formation initiating from liposomes, by measuring the birefringence of the bilayer and using anisotropy to calculate the isotropically averaged RI for each time point, therefore removing the differences in mass load and providing accurate and sensitive measurements of vesicle and SLB coverage during the course of formation. As a result, Mashaghi *et al.,* (2008) proposed that DPI has the potential to study transitions in SLB membranes, for example caused by membrane-interacting peptides or membrane active drugs.

DPI has been coupled with methods such as QCM-D and atomic force microscopy (AFM) to study protein adsorption mechanisms and direct membrane interactions respectively (Xu *et al.,* 2013 and Ouberai *et al.,* 2013). Xu *et al.,* (2013) elucidated the mechanism of lysozyme adsorption, identifying different orientations of adsorbed layers dependent on protein concentration by combining the two techniques DPI and QCM-D, extracting values of adsorbed mass with layer thickness and density. Ouberai *et al.,* (2013) investigated the mode of interaction of α-syn with physiological lipid membranes employing DPI with *in situ* AFM. Results revealed an enhancement of α-syn binding attributed to electrostatic interaction with acidic lipid bilayers, and that lipid packing defects of the SLB modulated α-syn binding as well. This effect was found to be similar to that of the antimicrobial peptide (AMP); melittin, which contain amphipathic lipid-packing sensor motifs that sense membrane curvature. DPI and AFM results correlated α-syn binding interactions with that of melittin; causing lipid

membrane thinning and lateral expansion of lipid head-groups linked to membrane remodelling effects.

Specific emphasis has been given to the description and application of classic *in vitro* biochemical methods, and the development of biophysical methods in the characterisation and identification of protein: protein interactions and subsequent binding in lipid model membranes. Difficulties that have been documented include: attaining the required concentration and purity of protein preparations (membrane proteins), sensitivity and specificity of methods to derive accurate data avoiding false-positive results, establishing immobilisation protocols which retain ligand activity whilst using membrane mimetics to replicate a native-like environment, and deriving binding kinetics. These methods have provided an invaluable insight into the binding dynamics of proteins and modes of interactions in relation to their roles within the pathogenesis of disease, proving to be incredibly powerful when two complementary techniques have been combined. Thus highlighting the importance of these studies, but nevertheless recognising the need for the development of novel biophysical techniques that can characterise protein: protein and protein: lipid interactions within a native *in vivo* environment.

1.4. Optical method of Ellipsometry and Total Internal Reflection Ellipsometry (TIRE)

1.4.1 Spectroscopic Ellipsometry (SE)

Spectroscopic ellipsometry is a well-established reflection based technique recognised for its optical properties measurements with regards to studying organic materials, such as polymer thin films (Mutschler *et al.,* 2002), self-assembled layers (Zhou *et al.,* 2011) and Langmuir Blodgett (LB) films (Zeng *et al.,* 2008). It is a non-destructive optical method, measuring the changes in the polarisation of light upon its reflection from a sample. The method of SE does not measure directly the optical parameters of the material but the ellipsometric angles Psi (Ψ) and delta (Δ), making it extremely sensitive to changes in optical parameters of the reflecting substrate and the mass of adsorbed material. The state of polarisation described by two ellipsometric angles; Ψ and Δ, represent the ratio of Fresnel reflection amplitudes and phase shift between *p*- and *s*- components of polarised light respectively, defining the shape and position of the ellipse of polarisation in *p*- and *s*- co-ordinates; 'p' in the plane of incidence and 's' in the plane of the substrate (Equation 1.2, J.A. Woollam 2002):

$$tn\Psi = \frac{R_p}{R_s}, \qquad \Delta = \delta_p - \delta_s$$

Equation 1.2

The values of thickness, refractive indices and extinction coefficients can be obtained for the substrate and coating layers by fitting the experimental spectra to a particular model, such as Fresnel equations – which describes the behaviour of light when moving between media of varying refractive indices. The applications of ellipsometry can be seen as to focus mainly on surface characterisation, but in the last decade ellipsometry has been utilized as a biosensor (Nabok *et al,.* 2005 and 2008) due to its high sensitivity to thickness increment at surface layers; ~ 0.01 nm (Arwin 2000).

The main scheme for the J.A. Woollam M2000 spectroscopic ellipsometric instrument exploits the principle of a rotating compensator, consisting of a light source in the spectral range of 370 – 1000 nm, two polarising elements (polarizer and analyser) and a photodetector (Fig. 1.5). The use of the rotating compensator enables the registration of two minima of light intensities passing through the polarisation elements allowing for the direct evaluation of both ellipsometric parameters; Ψ and Δ, making ellipsometry equally as sensitive to SPR but with the advantage of measurements of both the amplitude (Ψ) and phase (Δ) related parameters (Nabok *et al.,* 2008).

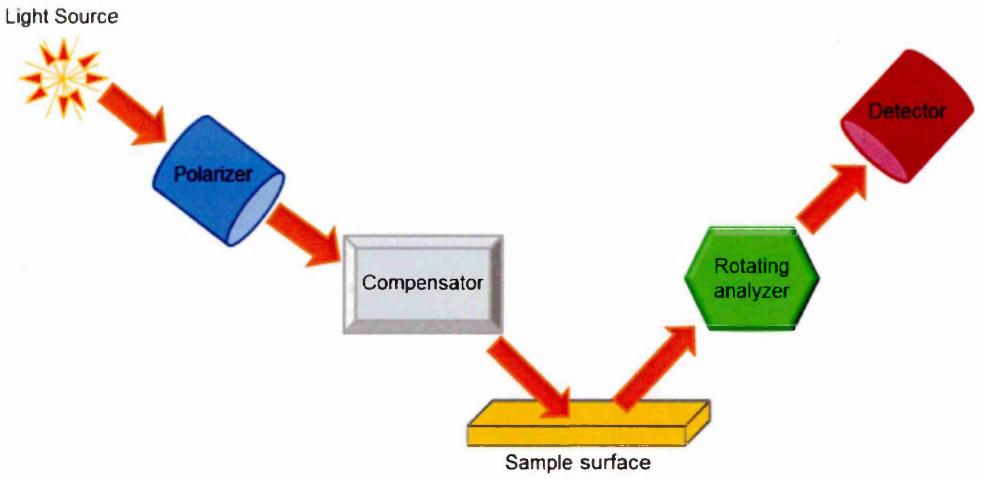

Figure 1.5. A schematic diagram of the ellipsometry set-up. Comprised of a light source, two polarising elements: the polariser and rotating analyser respectively and a photodetector.

Some of the advantages of spectroscopic ellipsometry as a biosensor are summarised in Table 1.1 (adapted from Arwin 2001).

	Features of ellipsometry	Comments
Advantages	Measurements based on reflection of polarized light.	Requires no reference beam and label-free.
	Thin molecular layers can be measured (~ 0.01 nm).	Fast response of sensor.
	In situ dynamic monitoring of both parameters Ψ and Δ during bio-reaction.	Enables the study of binding and kinetics such as affinity reactions in real-time.
	Monitoring the optical parameter Δ (phase shift between p- and s- components of polarized light).	Increased sensitivity to thickness increments.
	Used in any transparent ambient.	Measurements in liquid are possible.

Table 1.1. Summarising the advantages of the method of ellipsometry (Arwin 2001).

However, the experimental application of conventional ellipsometry within biosensing is limited due to experimental difficulties of the light beam passing directly through the investigated medium, and the variations of the medium RI can affect subsequent measurements, particularly if *in-situ* (Nabok *et al.,* 2008).

1.4.2. Total Internal Reflection Ellipsometry (TIRE)

The experimental set-up of TIRE is also based on the commercial M2000 J. A. Woollam spectroscopic ellipsometer (Fig. 1.6 A) and enables the separation of the light beam passing through the investigated medium via the addition of a prism and fluid cell (Fig. 1.6 B). The choice of a 68° prism is dictated by the conditions of total internal reflection on glass-water interface. The TIRE fluid cell was specifically designed to cater for small-volumes (~200 μL), substantially decreasing analyte consumption of which may be expensive or difficult to produce in large quantities. To avoid an air gap between the prism and gold coated glass slide, index matching fluid is used for optical contact. The O-ring (Fig. 1.6 C) seals the gold slide to the cell, pairing the two surfaces together and providing a contained area to perform binding experiments.

(A)

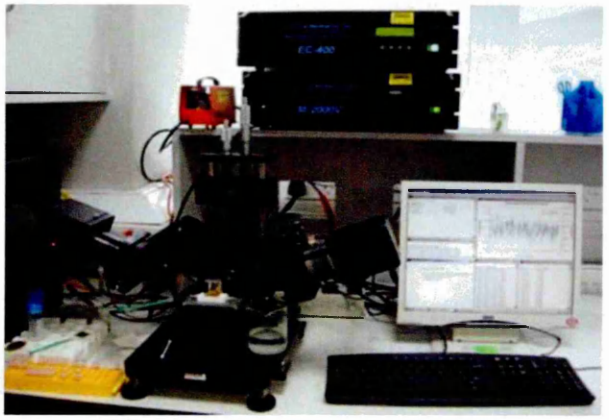

(B)

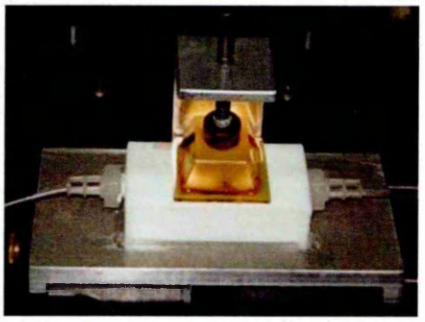

(C)

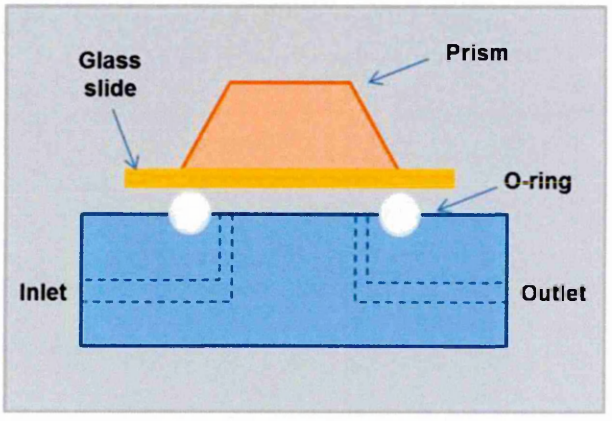

Figure 1.6. The instrumental set up of TIRE. (A) J.A. Woollam M2000 Ellipsometer (B) TIRE cell including 68° prism placed on top of a 2 x 2 cm gold slide sitting on the ellipsometer sample stage and (C) Schematic of TIRE cell operating in liquid.

Unlike TIRE, SPR uses only *p*-polarised light which corresponds to the reflection amplitude only; this is similar to the parameter Ψ used in TIRE. Therefore, in contrast to the conventional bio-sensing tool of SPR monitoring the intensity of reflected *p*-polarised light only, the TIRE method can detect both parameters Ψ and Δ of polarised light. Nabok *et al.,* (2008) demonstrated that Ψ(λ) spectra are equivalent to SPR curves and the additional Δ(λ) spectra provided new information on the phase shift of polarised light which is ~10 times more sensitive than Ψ to changes in both refractive index of thin films and thickness, concluding that TIRE is 10 times more sensitive than conventional SPR.

However, a limitation of SPR, ellipsometry and TIRE is that the simultaneous evaluation of *d* (thickness) and *n* (RI) of thin dielectric films (< 10 nm) is theoretically not possible, and either one of the parameters must be fixed during data fitting; hence the current method of data analysis is not strictly true by fixing *n,* but is necessary. The RI (*n*) for the deposited organic layers using TIRE was previously described (Nabok *et al.,* 2008, Mustafa *et al.,* 2010 and Kriechbaumer *et al.,* 2011 and 2012 (A)) and used the Cauchy dispersion model (Equation 1.3) for all adsorbed layers, yielding a value of RI $n = 1.42$ (at 633 nm), representative of the 'real' situation since all molecular layers, such as polymers and proteins have similar or close RI to 1.42. Comparable results for the RI utilised within this research have also been reported for organic substances between 1.44 -1.49 (Striebel *et al.,* 1994 and Finot *et al.,* 2013). A zero value for the coefficient ($k= 0$) was used as the adsorbed molecular layers are considered to be optically transparent within the 370-1000 nm spectral range.

$$n = A + \frac{B}{\lambda^2} + \frac{C}{\lambda^4} + \cdots, k = 0$$

Equation 1.3

TIRE data processing involves the building of an optical model accounting for each of the samples specifications. The model consists of the BK7 glass as the ambient (3), whereby the light passes through the prism attached to the glass slide with the evaporated Cr-Au film (2) - upon which has the adsorbed molecular layer - Cauchy (1), and finally reaches the aqueous buffer solution within the cell which acts as the substrate (0) (Fig.1.7).

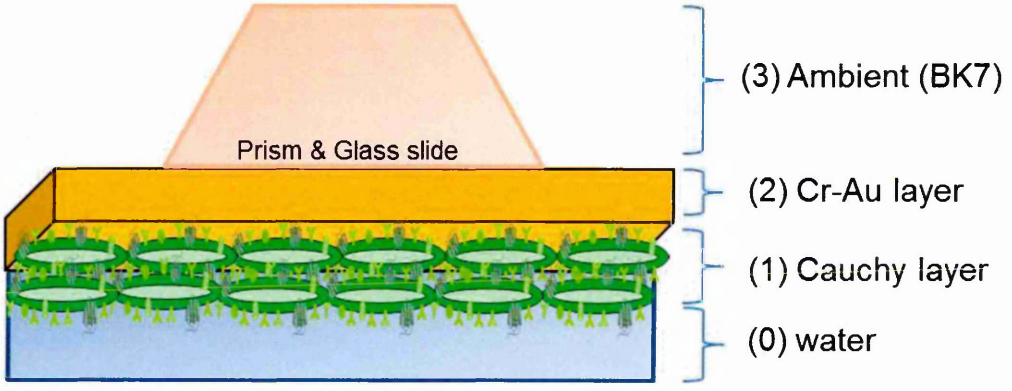

Figure 1.7. Illustration of the four-layer model used in data-fitting for adsorbed molecular layer. The model consists of the BK7 glass as the ambient (3), whereby the light passes through the prism, the difference between total internal reflection ellipsometry and conventional ellipsometry is the addition of the glass prism, which depending on the ambient; air/water or aqueous solutions, are 45° or 68° respectively. The prism is attached to the glass slide with the evaporated Cr-Au film (2) - upon which has the adsorbed Cauchy layer (biological sample) (1), and finally reaches the aqueous buffer solution within the cell which acts as the substrate (0).

Dielectric functions of particular layers including BK7 glass, gold and water are known parameters and can be found in the WVASE software library (J.A. Woollam 2002). The characteristic values of *n* and *k* for glass and water are given at 633 nm, which is the wavelength of the helium-neon (HeNe) laser widely used in ellipsometric instruments. Parameters of unknown layers can be found by fitting the experimental data to the model layer which has been selected from the WVASE library, with the most common model for adsorbed molecular layers is Cauchy. TIRE measurements consist of two types of scans: (i) dynamic spectral measurements which are performed during the course of sample adsorption, recording multiple spectra's over a set period of time; (ii) single spectroscopic scan which are performed in steady state conditions after completion of each adsorption step.

TIRE data modelling typically starts with a single spectroscopic scan of the bare gold film in a selected buffer, to obtain the thickness (*d*) and dispersion curves for optical parameters $n(\lambda)$ and $k(\lambda)$ of the Chromium-Gold (Cr-Au) layer. An inital three layer model was used, made up of: an ambient (BK7 glass), Cr-Au (regarded as Au) and substrate (water). The parameters are fixed for glass and water however, the thickness and optical constants of the metal layer are varied due to metal evaporation differences, typical thickness of gold layer is 25 – 27 nm, which is monitored by a quartz crystal microbalance sensor and thickness derived by TIRE measurements (Fig. 1.8). The selected parameters for the Cr-Au layer obtained by fitting for that particular sample are then fixed and used for further fitting upon addition of a new layer (*i.e.* molecular layer). Therefore, the only variable parameter is

thickness (d), and any changes at the adsorbed layer are associated with changes in film thickness.

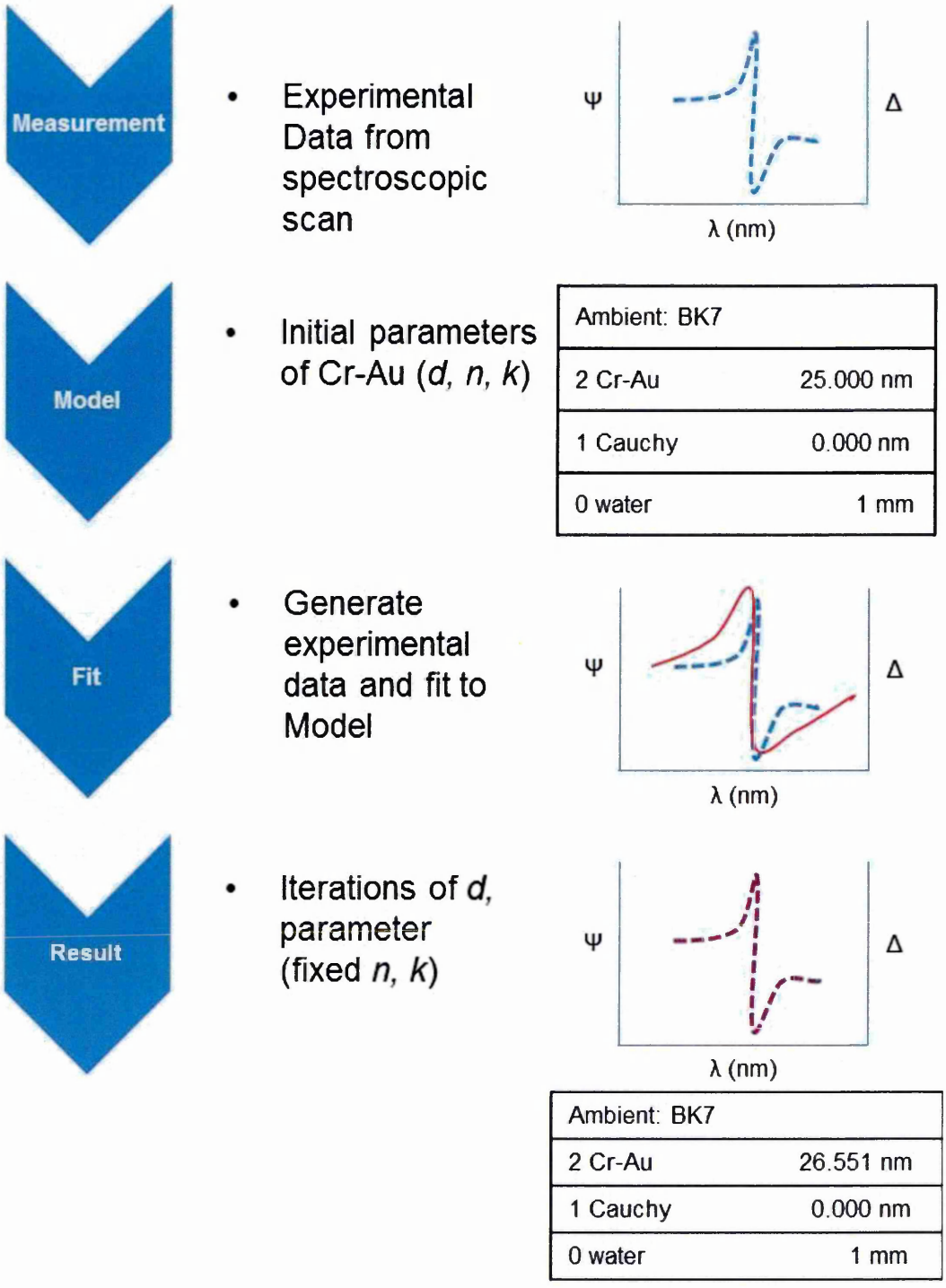

Figure 1.8. A flowchart of data analysis and fitting in TIRE. An initial spectroscopic scan of sample (e.g. Cr-Au) provides experimental data, following the construction of the optical model from WVASE library to account for sample specifications, experimental data is fitted to model parameters. (Adapted from J.A. Woollam Manual 2002).

Table 1.2 provides a detailed description of the four-layer model utilising the J.A. Woollam (2002) material library for the fixed optical dispersion characteristics with regards to BK7 glass (3) and water (0). The initial building of the four-layer model starts with the effective values for thickness and refractive index dispersion for Cr-Au by fitting TIRE data for a bare gold slide. The thickness *(d)* and dispersion functions for *n* and *k* of the Cr-Au layer (2) were then kept fixed in subsequent TIRE fittings on the sample after deposition of Cauchy (molecular) layers (1).

N°.	Layer	Thickness (*d*) refractive index (*n*)	Comments
3	BK7 glass (ambient)	*n, k* dispersions from WVASE32 library *n* = 1.515, *k* = 0 at 633 nm	Parameters are fixed.
2	Cr/Au	*n* = 0.359 ±0.078; *k* = 2.857 ± 0.114 at 633nm *d* is varied in the range of ~25-30 nm	The values of *d*, and dispersions for *n* and *k* were obtained by fitting TIRE data for every new sample, then kept fixed in further fittings.
1	Cauchy layer	Cauchy model: A= 1.396 B= 0.01 C= 0 *n* = 1.42, *k*= 0 at 633 nm	*n* is a fixed parameter, *d* is varied.
0	Water	n, k dispersions from WVASE32 library *n* = 1.33, *k* = 0 at 633 nm	Parameters are fixed.

Table 1.2. The four-layer model for TIRE experimental data fitting.

1.5. Biosensing applications and TIRE.

The combination of the SPR effect with ellipsometry in total internal reflection mode provides a technique with very high sensitivity in comparison to traditional ellipsometry and SPR, enabling quantitative measurements in opaque solutions and of biomolecules (Arwin 2000 and Poksinski *et al.,* 2004). Poksinski *et al.*, (2007) employed TIRE for ultrahigh sensitivity for protein adsorption on metal surfaces studying monolayer adsorption. Using the ellipsometric parameter Δ, they demonstrated that TIRE provided the quantification of protein adsorption according to surface-mass concentration, proposing its potential for the study of protein layer microstructure. Further applications include the analysis of interactions between ligands and antibodies (Nabok *et al.,* 2008), and the analysis of low molecular weight analytes such as pesticides and mycotoxins, with detection levels reaching as low as 0.1 ng/ml (Nabok *et al.*, 2011). Kriechbaumer *et al.,* (2011) utilised TIRE to determine the binding affinity of the molecular chaperone Hsp70 for a soluble form of a chloroplast (CP) chaperone receptor; outer envelope protein 61 kDa (OEP61), bound to a gold surface by electrostatic immobilisation. TIRE was sensitive enough to distinguish between the binding affinities of closely-related isoforms of the chaperone Hsp70. This highlighted the discriminatory powers of TIRE and the ability to attain quantitative data on specific protein-protein interactions.

Protein adsorption studies have been carried out over the years using biosensing applications that utilise the evanescent field of laser light as a

sensing element. Well-established techniques include SPR, with developments of alternative label-free optical techniques such as DPI (Daghestani *et al.,* 2010). Unlike SPR which measures only a single polarized light mode (TM), DPI measures two independent measurements with two different polarizations (TM and TE). Sonesson *et al.*, (2007) showed that DPI and SPR data can be directly related to each other, which is important since protein adsorption studies are usually coupled with additional techniques. However, whilst the strengths of each method differ: DPI provides information about the thickness and RI of the adsorbed protein layer, and SPR is more accurate for studying initial quantitative kinetics of adsorption to surfaces, they both lack the ability to study such interactions in an *in vivo* –like environment. Therefore, TIRE with its enhanced biosensing capability, utilising a fluid-cell and the ability to analyse protein interactions at natively derived membranes offers quantitative studies *in situ.*

1.5.1. Langmuir-Schaefer (LS) method and cell deposition for TIRE analysis

The study of molecular interactions within their native environment has been limited by the lack of experimental systems which can mimic their natural setting without the need to over express proteins in non-native cell lines, or synthetically producing lipid model membranes, such as; liposomes, to study protein-membrane interactions (Kriechbaumer *et al.,* 2012 (C)). For example, the study of membrane proteins is hindered by difficulties in their expression

and purification in large quantities, due to the instability of hydrophobic membrane regions within aqueous buffers. This can result in the formation of insoluble aggregates; inclusion bodies, which subsequently abolishes functional activity and become toxic in high concentrations. In addition the use of detergents to extract and solubilise membrane proteins requires a screening procedure to liberate proteins in a functional state (Eriksson *et al.,* 2009). Therefore a novel technique has been developed using LS deposition, resulting in natively derived lipid membranes being deposited as a thin film where subsequent protein interactions can then be monitored by changes in layer thickness using TIRE.

1.6. An introduction to Langmuir-Schaefer method

The formation and deposition of a monolayer thick film formed at an air-water interface, was founded as early as the 12th century. Examples include the use of colour dyes mixed with proteins to create patterns which were transferred onto paper by lowering it onto the air-water interface; horizontal dipping. Langmuir was awarded the Nobel Prize in 1932 for his study of the formation and stability of monolayer films, who reported that the film formed at the air-water interface, could be transferred to a substrate. Initially the study of sequential and controlled transfer by vertical dipping was developed by Katharine Blodgett, and together the Langmuir Blodgett (LB) method was defined (Blodgett 1934 and 1935). Later the collaboration between Langmuir and Schaefer focussed on protein deposition, and in 1938 reported a new

approach to protein deposition; where the sample plate was lowered onto the air-water interface in an almost horizontal position, giving rise to the LS deposition (Langmuir and Schaefer 1938).

A key element in monolayer formation is the molecular amphiphiles, molecules consisting of hydrophobic and hydrophilic parts responsible for their water solubility capabilities. A classic sub-phase at which the monolayer forms requires demineralised deionised water (~18.5 MΩ) where the low ion content ensures that the polar head of the molecule will not interact with minerals in natural water, protecting the monolayer properties from disruption. The Langmuir trough holds the bulk water, upon which the amphiphiles are distributed at the surface. Surface tension (Υ) is vital in enabling monolayer formation, the interaction of water molecules in the liquid state are held by electrostatic forces and its net attraction controls its viscosity. The intermolecular forces at the surface are measured in N/m units and are indicative of any contamination at the water's surface, such as a molecular film. The total surface pressure (Π) can be defined as the difference between the initial sub-phase surface tension (Υ_0) (e.g. water) and the sub-phase after the film deposition (Υ) (Equation 1.4).

$$\Pi = \Upsilon_0 - \Upsilon$$

Equation 1.4

Surface pressure is measured using the Wilhelmy plate (Fig. 1.9) which is directly coupled to a sensitive electro-balance. It is usually made from paper

and is partially submerged into the trough water, during its immersion the force acting on the plate is the sum of three forces; gravity and surface tension acting downwards and the buoyancy of the plate acting upwards. Therefore surface pressure is deduced by a change in force (F), thus any change in mass at the water's surface is subsequently detected.

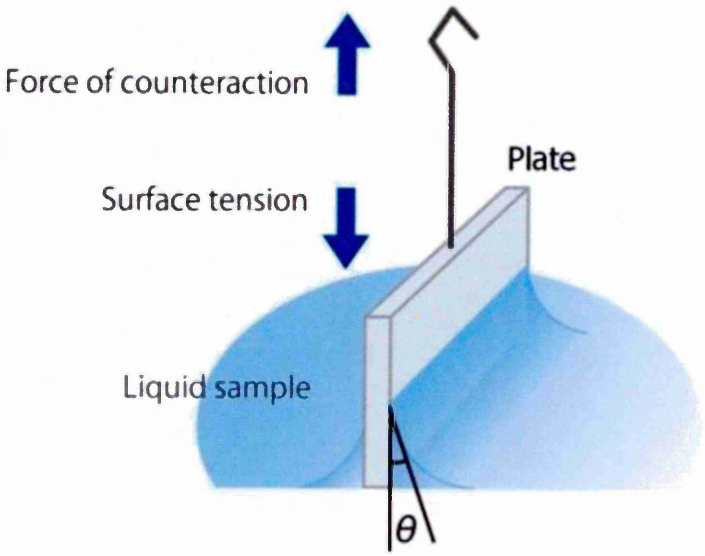

Figure 1.9. Illustration of the Wilhelmy plate method. The Wilhelmy plate detects the pulling force at the water's surface and determines the surface tension whilst attached to an electro-balance (Kyowa Interface Science Co 2014).

A typical experiment utilises a water-filled Langmuir-trough with a barrier(s) which are controlled remotely and can be moved to compress molecules at the air-water interface to a desired target surface pressure. This is translated into a pressure isotherm by the Wilhelmy plate recording surface pressure (Π) as a function of area (cm^2), and upon removal of cells from the water

surface the barriers compress the water again to reach the target Π (Gengler 2010).

Kriechbaumer *et al.,* (2012 (B)) analysed protein interactions at natively derived outer envelope chloroplast (CP) membranes, using TIRE and LS film deposition to successfully deposit natively derived CP membranes onto metal (Au) coated slides, which retained fully-functional receptors capable of binding chaperones with high affinity and specificity. Binding and affinity constants were quantified using TIRE to detect specific interactions between low-abundance chaperone receptors within natively derived CP membranes, and their soluble chaperone partners. Further work by Kriechbaumer *et al.,* (2012 (C)) performed LS deposition using human derived Ishikawa cells, and quantified the ligand binding of CXCL12α to the G-protein-coupled receptor (GPCR) CXCR4. Using light microscopy the viable integrity of deposited membranes was confirmed, presenting receptor proteins in their native membrane environment and enabling subsequent ligand binding to be quantified. Using TIRE with LS deposition, interactions in a native lipid environment were performed without the need for recombinant expression of membrane proteins, showing potential applications in investigating functions of cell membrane receptors, and the identification of their binding partners which could be useful in screening for new pharmaceuticals.

The novel combination of TIRE and LS methods has shown that the bio-sensing capability of TIRE has been enhanced, enabling the deposition of natively derived cells for the quantification of protein-protein interactions. Together they could be developed to be made applicable to a wide variety of membranes and membrane protein receptors - allowing for quantification of

protein interactions involved in fundamental cellular processes and human diseases enabling the rapid screening of drugs that target membrane proteins.

1.7. Aims and objectives

The main aim of this research was to develop and highlight the versatility of the optical biosensor TIRE method via two working models: (I) the toxic effects of amyloid proteins at natively derived lipid membranes (protein: lipid interactions) and (II) regarding the targeting and binding of molecular chaperone protein to cognate receptors at natively derived CP membranes (protein: protein interactions).

To achieve this aim, the following objectives were identified:

Model I:

I. To employ the TIRE method for the detection of fibril interaction derived from amyloid proteins at the neuronal cell line membrane; SH-SY5Y.

II. To identify and differentiate the effects of membrane binding capabilities of fibrils of reduced sizes; comparing full length and fragmented fibrils.

III. To perform *in vitro* assays to support biophysical data from TIRE using dye release assays with synthetic liposome membranes to assess amyloid fibril binding *in vitro.*

IV. To measure cellular integrity of cultured human neuronal cells; SH-SY5Y, after incubation of full length and fragmented fibrils using an *in vitro* cell viability assay.

Model II:

I. To employ the TIRE method for the detection of binding of molecular chaperones to outer envelope CP membranes lacking specific chaperone receptors, focusing on the role of the chaperone receptor OEP61.

II. To assess and identify the binding of molecular chaperones with CP membranes in their complexes with pre-proteins (tail-anchored membrane proteins).

III. The genetic phenotypic analysis of receptor deficient CP membranes of *Arabidopsis thaliana* plants by RNA tissue extraction and electron microscopy.

2.1. Molecular Biology techniques

The following Molecular techniques were performed in order to express, purify and/or analyse prepared samples such as DNA, RNA and plasmids.

2.1.1. Plasmid-mini-prep

Plasmid mini-prep kit materials:

- cell lysis buffer (containing sodium-dodecyl-sulfate (5-10 % v/v) and sodium hydroxide (< 2.5 % v/v))
- neutralization solution (guanidinium chloride and unspecified acetate)
- endotoxin removal wash (guanidinium chloride and propan-2-ol)
- column wash (95 % v/v ethanol (EtOH))
- elution buffer (10 mM Tris-Hydrochloride (pH 8.5) 0.1 mM EDTA)

Plasmid isolation and purification was performed using a PureYield plasmid mini-prep system kit (Promega, A1222), following manufacturers guidelines. Briefly the sample was subjected to cell lysis and neutralisation for column binding of deoxyribonucleic acid (DNA), with purification by centrifugation removing protein, ribonucleic acid (RNA) and endotoxin contaminants from the plasmid DNA. The eluted plasmid DNA (< 15 μg) was stored at -20 °C.

2.1.2. DNA isolation and purification

Wizard gel/PCR clean up system kit materials:

- membrane binding solution (4.5 M guanidine isothiocyanate, 0.5 M potassium acetate (KOAc)
- membrane wash solution (10 mM KOAc (pH 5.0)
- 80 % v/v EtOH, 16.7 µM EDTA (pH 8.0))
- nuclease free water

The extraction and purification of DNA fragments was performed using a gel/PCR clean up system kit (Promega, A9281), following manufacturers guidelines. Briefly membrane binding solution was added to the DNA sample, if excised from a gel band it was incubated at 50 - 65 °C for 10 min. DNA binding to the silica membrane within the column occurs in the presence of chaotropic salts whilst subjected to washes and elution by centrifugation. Eluted DNA was stored at -20 °C.

2.1.3. Polymerase Chain Reaction (PCR)

Standard PCR was performed using Q5 polymerase as recommended by manufacturer (NEB) using a thermocycler (Techne thermocycler TC-3000).

Name	Primer	Sequence 5' to 3'	Size of expected PCR product (bp)
At1g17780.1	Forward	TAA TAC GAC TCA CTA TAG GG ATG GAG GGG GAT GGT TTT	570
At1g17780.1	Reverse (– STOP codon)	TTT TTC TCT GAT GAT TAT GAT AAA G	570
At3g63160.1	Forward	TAA TAC GAC TCA CTA TAG GG ATG GTG GAG AAG TCA GGA	210
At3g63160.1	Reverse (– STOP codon)	GGC GCC CGA CGG	210

Table 2.1. Tail-anchored protein primers for gene sequence amplification.

Step	Temperature	Time
Initial Denaturation	95°C	30 seconds
35 Cycles	98°C	10 seconds
	60°C	30 seconds
	72°C	1min30 seconds
Final Extension	72°C	5 minutes
Hold	4°C	Continuous

Table 2.2. At3g63160.1 thermocycling conditions for PCR.

Step	Temperature	Time
Initial Denaturation	95°C	30 seconds
35 Cycles	98°C	10 seconds
	63°C	30 seconds
	72°C	1min30 seconds
Final Extension	72°C	5 minutes
Hold	4°C	Continuous

Table 2.3. At1g17780.1 thermocycling conditions for PCR.

2.1.4. RNA Transcription

Components were mixed on ice and added in the following order and were incubated at 37 °C for 90 minutes and analysed on a 1 % w/v agarose gel.

Component	Volume (µL)
DEPC-treated H_2O	57
10x RNA polymerase buffer (NEB)	10
rNTPs (10 mM)	5
7mGG Cap analogue (10 mM)	10
RNasin Plus (40 U/µL)	1
Template DNA	15
T7 RNA polymerase (50 U/µL)	2
TOTAL	100

Table 2.4. RNA Transcription.

2.1.5 RNA purification - Phenol: Chloroform: Isoamyl Alcohol (IAA) extraction and ethanol precipitation

100 µL phenol: chloroform: isoamyl alcohol (IAA) (25:24:1) was added to total RNA sample and subjected to vortexing and centrifugation for 1 min at maximum speed (14,800 rpm benchtop centrifuge). The lower phase (phenol) was removed and discarded. The previous step was repeated using chloroform only. Ten microliters of NaOAc (3 M, pH 4.5) and 250 µL of 95 % (v/v) ethanol were added and mixed thoroughly, and stored at -20 °C for 60 minutes to precipitate the RNA. The sample was centrifuged (14,800 rpm, 20 minutes) followed by the removal of liquid without disturbing the RNA pellet. The RNA pellet was washed with 95% (v/v) ethanol (180 µL) at room temperature, and the liquid was removed immediately, taking care not to dislodge the pellet. The RNA pellet was air-dried for 5 min at room temperature. The pellet was resuspended in a 10 % (v/v) elution buffer (10 mM Tris-HCl, 0.1 mM EDTA) (50 µL). RNA analysis was performed using a 1% (w/v) agarose gel with 2 µL 6x loading buffer and 5 µL DEPC-water to 5 µL RNA.

2.1.6. Ribonascent Chain (RNC) Translation with ^{35}S labelling

Components were thawed on ice including TA RNA transcripts lacking the stop codon. Components were added and incubated at 30 °C for 7 min. Initial

analysis of labelled RNC products was performed by SDS-PAGE (16 % w/v); 2 µL RNC added to 18 µL SDS loading buffer and 10 µL loaded onto the gel.

Component	Volume / µL
Wheatgerm	50
DEPC-H_2O	26.5
Amino-acid (met)	8
RNasin Plus	0.5
^{35}S-met	5 (0.135 µCi)
RNA (0.1 µg/µL)	10
TOTAL	100

Table 2.5. RNC translation.

2.1.7. Ribonascent chain (RNC) purification

After translation the reaction was kept on ice and supplemented with cycloheximide (2.5 mM) and KOAc (500 mM). The ^{35}S-RNC sample was layered over 400 µL ice cold HSCC buffer (500 mM sucrose, 500 mM KOAc, 5 mM magnesium acetate, 50 mM Hepes- potassium hydroxide (KOH) pH 7.9 with 2.5 mM cycloheximide and 1 mM Dithiothreitol (DTT)) and subjected to centrifugation at 213,000 x g for 20 minutes. The RNC pellet was then resuspended in 50 µL HSCC with reduced sucrose (100 mM) and layered onto 150 µL HSCC, followed by centrifugation at 213,000 x g for 20 minutes. The ^{35}S-pellet was finally resuspended in 40 µL LSC buffer (100 mM sucrose, 100 mM KOAc, 5 mM $Mg(OAc)_2$, 50 mM Hepes-KOH pH 7.9, 1 mM

DTT), resulting in a translation reaction 5 x more concentrated than the initial translation. Samples were stored at -80 °C.

2.1.8 ^{35}S-Tail Anchored (TA) protein Binding Assay

4µL of RNC was made up to 10 µL in LSC buffer, with 10 µL chloroplast suspension and puromycin (1mM) which was added last for the release of the RNC from its incomplete translation by ribosome organelles. This was considered to be a control reaction with no additional components. Various binding reactions were then performed with CP membranes and TA-proteins, including the addition of molecular chaperones (Hsp70/Hsp90 purchased from Boston Biochem) or binding proteins SGTA (2 µM) (provided by S.High Group, Manchester University) in the presence of ATP (1 mM). Components were incubated for 30 mins at 30 °C, followed by the addition of apyrase (0.1 U/ µL) for 5 min on ice for the stabilisation of interactions. Chloroplast membranes were washed and purified by centrifugation (3000 x g for 5 min) with 50 mM HEPES (pH 8.0). Protease treatment used thermolysin (40 U/mL) (Sigma) for 5 min at 30 °C, followed by the addition of EDTA (10 mM) to stop reaction.

2.1.10. ^{35}S-TA Protein binding analysis

Samples were loaded onto a 16 % (w/v) SDS-PAGE gel and run at 150 V for 1 hour 10 min. Gels were fixed by two 5 min washes in de-staining buffer (10 % v/v acetic acid, 40% v/v methanol) with agitation, transferred to Whatman paper (3M) and placed on a vacuum dryer (Welch Rietschle Thomas Gel Master Model 1426, Biorad gel dryer vacuum system, Model 583) for 3 hours at 60 °C. Dehydrated gels were then exposed on phosphor plates for 24-72 hours and scanned on the Cyclon phosphorimager (Cyclone storage phosphor screen, Packard) using Optiquant software (150 dpi medium plates). Protein bands of interest were corrected against background, and run alongside a molecular weight marker (GE Healthcare, CFA626).

2.1.11. cDNA Synthesis and RT-PCR

Complementary DNA (cDNA) synthesis was performed using the Protoscript First stand synthesis NEB kit (E6560). Firstly, 1 µg of RNA was subjected to genomic DNA removal using gDNA wipeout buffer (Qiagen 205310) and enzyme inactivation at 80 °C for 5 min. Followed by initial denaturation in the presence of a gene specific primer at 70°C for 5 min before addition of enzymes and polymerase. This was finally followed by incubation at 42 °C for one hour with the addition of and enzyme inactivation at 80 °C for 5 min. cDNA was analysed on a 1 % (w/v) agarose gel with comparable RNA sample. The cDNA was subsequently used for gene specific reverse

transcription- PCR (RT-PCR) reactions using primers (Table 2.6) for cDNA RT-PCR amplification (Table 2.7). The thermocycling conditions were adapted for optimum annealing temperatures with regards to specific genotype primers. (TAIR Accession numbers: OEP61 At5g21990 and Actin At2g37620).

Name	Primer	Sequence 5' to 3'	Size of expected product (bp)
OEP61 (1)	Forward	CATCAAGAGGTGTGGTGATTG	828
OEP61 (1)	Reverse	CTCTCAGAGATAATCCA	
OEP61 (2)	Forward	AAGCAATCAG AACTTTCCAG	813
OEP61 (2)	Reverse	CTCGGCTATATTGGAAACT	
OEP61 intron	Forward	CATCAAGAGGTGTGGTGATTG	166
OEP61 intron	Reverse	CTGGAAAGTTCTGATTGCTTC	
Actin	Forward	TGGAACTGGAATGGTTAAGGCTGG	435
Actin	Reverse	TCTCCAGAGTCGAGCACAATACCG	

Table 2.6. Gene specific primers for cDNA synthesis.

The RT-PCR primer annealing temperatures for OEP61 (1) and (2) was set to 55.3 °C, actin and OEP61 intron primers was set to 62 °C.

Step	Temperature	Time
Initial Denaturation	95°C	30 seconds
30 Cycles	98°C	10 seconds
	? °C	30 seconds
	72°C	30 seconds
Final Extension	72°C	5 minutes
Hold	4°C	Continuous

Table 2.7 Thermocycling conditions for RT-PCR. Annealing temperature (symbolized as '?') varied for different primers.

2.2. Plant preparations

2.2.1. Chloroplast isolation from pea leaves

Pea plants were grown for 10-14 days in 50:50 soil-vermiculite and extracted using a chloroplast isolation kit (Sigma-Aldrich, CO-ISO). 30 g of pea leaves were harvested and subsequently purified following Sigma-Aldrich manufacturer protocol. Briefly, leaves were cut into 1 cm pieces and homogenised in 1 x chloroplast isolation buffer (CIB) by three 30 sec bursts with a polytron homogenizer (IKA T 18 basic ULTRA-TURAXX, intensity level 2). The macerate was passed through a filter mesh into 50 mL tubes and centrifuged for 3 min at 200 x g to remove whole cell debris. The supernatant

containing broken and intact chloroplasts was purified using a 40/80 % (v/v) Percoll gradient by centrifugation; intact chloroplasts were collected from the interface band between the two Percoll layers. Excess Percoll was removed by additional centrifugation (15 min at 3200 x g and 1 min at 1700 x g respectively). Isolated chloroplast pellet was re-suspended, with membrane intactness visualised by phase microscope and stored at -80 °C.

2.2.2. Gene expression of mutant seedlings

Qiagen RNeasy plant kit materials (74903):

- RNeasy Mini Spin Columns (pink)
- QIAshredder Spin Columns (lilac)
- Buffer RLT (lysis buffer)
- Buffer RW1 (wash buffer)
- Buffer RPE (concentrate) (wash buffer)
- RNase-Free Water

Arabidopsis thaliana seeds collected from mature mutant plants were washed in 50 % (v/v) bleach with 0.05 % (w/v) tween-20 for 20 mins with agitation, after which seeds were subjected to 5 washes in sterile water (1 mL) with vortexing to remove any remaining bleach and detergent. Seeds were re-suspended in ~500 µL sterile water and dispensed evenly across autoclaved MS (Murashige Skoog medium, Sigma-Aldrich) agar plates. The plates were placed in the dark for 3 days at 4 °C to break dormancy. Plates

were then transferred to a growth chamber (21 °C, 55 % humidity). After 10 days the leaves were harvested using an RNeasy plant mini kit for RNA extraction (Qiagen), following manufacturer guidelines. Briefly, *Arabidopisis thaliana* leaves were removed from individual plants and moved to -80 °C overnight. Frozen leaves were crushed using a plastic pestle (~100 mg tissue), and lysed using RLT buffer with 2 mM DTT. The homogenate was passed through a QIAshredder column to remove insoluble material and reduce the viscosity of the sample. Ethanol was included to promote RNA binding to RNeasy columns during the wash step, and RNA was eluted in RNase free water. RNA concentrations were determined using a Nanodrop (ND-1000 Spectrophotometer) and stored at -20 °C. RNA was confirmed by electrophoresis of 1 µg of RNA on a 1 % (w/v) agarose gel.

2.2.3. Electron Microscopy (EM) and mutant CP analysis

8 day old *Arabidopsis thaliana* plants consisting of the genotypes: Wild type CP, GabiKat (transposon insertion mutant) and Toc64 were harvested (by V.Kriechbaumer, Abell Group, SHU) and sent for EM analysis at the Biomedical Science Electronic Microscopy Unit at Sheffield University. The leaves were subjected to 1 week primary tissue fixation, 1% Osmium tetroxide (OsO_4) for 1 hour followed by tissue dehydration and embedding; in ethanol and 1, 2-epoxypropane (EPP) respectively, with sample remounting and staining using Araldite resin.

2.2.4. Mutant chloroplast morphological analysis

The ImageJ analysis tool (Image processing and analysis in Java) was obtained from the National institutes of Health online. The drawing tools were used to scale the length, width and outline of all chloroplasts attained from EM analysis.

Total surface area calculation for EM CP analysis:

1. The area of the CP was extracted from ImageJ (AU)
2. The scale bar's length was measured (AU)
3. Pixels/μm was calculated for the scale bars length by dividing its length by the stated EM scale measurement (e.g. 0.5/2 μm)
4. The value for pixels/ μm was then multiplied to the power of 2 to reach μm^2
5. Finally the original area measured for the CP in question was divided by the scale bar in μm^2 to attain its total surface area in μm^2.

E.g. Area of CP: 150000

Length of scale in units (240) / said μm (2) = pixels/ μm = 120

$1\ \mu m^2 = 120^2 = 144000$ pixels

Area of CP/ 144000 $\approx \mu m^2$ total surface area = 150000/144000 = 1.041 μm^2

Length and width for CP measurements:

1. Length/width of CP recorded using ImageJ
2. Length of scale bar was measured and recorded
3. The length/width was then divided by the length of the scale bar and multiplied by the said μm scale (0.5/2 μM).

2.3. Protein Expression

2.3.1. Expression and purification of recombinant wild type α-synuclein

The vector pET 23 b+ containing the human wild-type (WT) α-synuclein (α-syn) sequence was used to transform *Escherichia coli* (*E. coli*) BL21 (DE3) competent cells (Agilent Technologies).

BL21(DE3) cells transformed with pET 23 b+ encoding the human wild-type (WT) α-syn were freshly grown on ampicillin agar plates, where a single colony was transferred to 100 ml of LB medium with 100 μg/ml ampicillin and incubated overnight at 37 °C with shaking (pre-culture). The preculture was used to inoculate 1 L of LB/Ampicillin medium. Expression was induced when the OD_{600} of the cultures reached 0.5 with 1M isopropyl-β-D-1-thiogalactopyranoside (IPTG) for 3 h at 37 °C. Cells were harvested by centrifugation at 20 °C, 10 000 rpm and the pellet was resuspended in lysis buffer (10 mM Tris-HCl (pH 8.0), 100 μg/ml lysozyme, 100 mM

phenylmethylsulphonyl fluoride (PMSF), 20 µg/ml DNase, 20 µg/ml Rnase) and incubated for 30 min before the addition of 1 mM EDTA. Cells were further lysed by sonication (Branson 1210 sonicator). The lysate was centrifuged at 10 000 rpm (using Sorvall F10s-6x500Y rotor) for 40 min for the removal of debris, the remaining supernatant was acidified to pH 4.5 and centrifugation was repeated at 10 000 rpm (using Sorvall F10s-6x500Y rotor) for 30 min allowing the removal of any aggregated protein. This was followed by a final neutralisation step of the supernatant to a pH of 8.0. The crude lysate was subsequently injected onto a 50 ml Q-Sepharose column (GE Healthcare) for anion exchange at 4 °C. Equilibration of the column required 2 column volumes of buffer A - 25 mM Tris-HCl (pH 8.0), α-syn was eluted with a linear gradient of buffer B - 25 mM Tris-HCl (pH 8.0) at ~ 300 mM sodium chloride (NaCl). Enriched α-syn fractions (6 ml) were identified by a distinctive broad UV peak, which were collected and subjected to SDS-PAGE analysis; selected fractions were then pooled and dialysed extensively in MilliQ water at 4 °C, followed by lyophilisation. The lyophilised protein was re-dissolved and loaded onto a High-load 26/90 SuperdexTM 75 prep grade size exclusion column (Amersham Biosciences) with 20 mM Tris and 25 mM NaCl (pH 8.0) as the running buffer. The process was repeated with the pooling and purifying of fractions, followed by dialysis using snakeskin 10K MWCO dialysis tubing (Thermoscientific 88243) and re-lyophilisation. Purified α-syn was stored at -20 °C. Protein concentration was measured using a UV/Vis spectrophotometer (Jenway 6715) at absorbance 280 nm with an extinction coefficient of 5960 $M^{-1}cm^{-1}$.

2.3.2. Preparation of amyloid fibrils

α-syn fibrils were prepared by dissolving lyophilised α-syn protein to a final concentration of 70 μM in 25 mM sodium phosphate buffer (pH 7.4), and incubating on an orbital shaker at 37 °C, 300 rpm for 7 days. Quiescent Aß40 fibrils were prepared by dissolving 1 mg of lyophilised Aß40 (purchased from Bachem Bubendorf, Switzerland), without further purification in 200 μL hexafluorisopropanol (HFIP) and vacuum dried for 24 hours for HFIP removal. The peptide film was re-suspended in 20 mM NaOH, MilliQ water, 10 x PBS in a 2:7:1 ratio and incubated at 37 °C for 7 days. Lysozyme (Sigma Aldrich) fibrils were prepared by dissolving 1 mg of lyophilised protein in 1 mL 0.1 M HCl diluent (pH 1.6) and incubated overnight at 65 °C with agitation, 550 rpm. Fragmented fibrils were formed by freeze-thawing (-20 °C) each sample followed by 30 min sonication (Branson 1210 sonicator).

2.4. *In vitro* assays

2.4.1. ThT Assay

A discontinuous growth assay was used to measure fibril assembly using the benzothiazole dye; thioflavin-T (ThT). The dye when bound to β-sheet rich structures, displays enhanced fluorescence and a characteristic red shift of its emission spectrum. Samples (10 μl) were removed from each sample and

added to 90 µl of a 20 µM ThT solution at pH 7.4 in 20 mM Tris (pH 7.4). The ThT fluorescence was quantified on a Tecan Infinite plate reader at 20 °C by exciting at 480 nm and scanning the emission wavelengths in the range of 470 - 600 nm with slit widths set at 2 nm.

2.4.2. Dot Blotting

Nitrocellulose membranes (0.45 µM, GE Healthcare, Sweden) were spotted with 1 µl of monomeric or fibrillar species alongside bovine serum albumin (BSA) as a negative control. The membrane was blocked with 5% (w/v) milk in 1 x Tris-Buffered Saline and Tween 20 (pH 7.4) containing 0.1% Tween 20 (TBS-T). Primary antibody; anti-amyloid fibril LOC (Millipore, UK) (fibril specific antibody), was diluted in TBS-T (2 % milk w/v) at 1:1000 and incubated with membrane for 1 hour. Three wash steps were performed for 10 min with TBS-T. Secondary antibody CW conjugated polyclonal anti-rabbit IgG (H+L) (Li-Cor) was applied at 1:20000 dilution, incubated at RT for 1 hr. Visualisation was performed using the Li-Cor Odyssey and Odyssey Infrared Imaging software at wavelength 800 nm.

2.4.3. Liposome Dye Release Assay

Large unilamellar vesicles (LUV) were prepared as previously described by Xue *et al.*, (2009). Briefly LUVs were made using a lipid mixture of 1.6

mg/mL phosphatidylcholine (PC) and 0.4 mg/mL phosphatidylserine (PS) purified from chicken egg (Avanti lipids) to give 20 % negatively charged head groups. The lipids were dissolved in 1 ml 1 M chloroform and evaporated under a stream of nitrogen leaving a lipid film. The lipid film was resuspended in 50 mM carboxyfluorescein in 50 mM sodium phosphate, 10 mM sodium chloride and 1 mM EDTA (pH7.4) (Sigma) and subjected to extrusion through a polycarbonate filter with 0.1 µm pore size. The carboxyfluorescein encapsulated LUVs were washed by ultracentrifugation (Beckman Optima TLX) at 100,000 x g for twenty minutes (x3) and resuspended in liposome buffer: 50 mM sodium phosphate, 107 mM sodium chloride and 1 mM EDTA (pH7.4) and used within 48 hours. Dye release assay reactions consisted of 2 µl of LUV stock solution diluted with 188 µl liposome buffer, fibril sample (10 µl) was added to the solution giving a final volume of 200 µl. Fluorescence emission of carboxyfluorescein was quantified at 520 nm using an excitation wavelength of 480 nm using a Tecan Infinite plate reader. Positive controls performed using LUV with liposome buffer only and/or addition of 20 % (v/v) triton X-100 were also included for every reaction.

2.4.4. CellTox Green Membrane integrity Assay

The cyanine dye preferentially stains the DNA from dead cells, excluding viable cells. When the dye binds DNA released from cells, its fluorescence

properties are enhanced. Thus the fluorescence signal produced by the binding of dead cell DNA is proportional to cytotoxicity.

Following manufacturer guidelines the Express, No-Step Addition at Seeding method (5C) was performed using the human neuronal cell line; SH-SY5Y. Briefly the fluorescent dye was added to the desired density of cells ($2x10^4$ cells/well) in phenol free media with 10 % (v/v) FCS using sterile black 96 wellplates (50 µl), and allowed to adhere overnight at 37 °C, 5 % CO_2. The test compound was added at the required concentration with a volume-matched negative control (CDMEM) and a positive control for primary necrosis using the kits lysis solution at 1:25. Fluorescence was measured using a Tecan Infinite plate reader; excitation 485 nm and emission 520 nm. The experiment was performed over a 72 hour period, with readings every 24 h.

2.5. TIRE: cell deposition and spectroscopic analysis

2.5.1. SH-SY5Y Cell Line Culture

All cell culture methods were carried out under sterile conditions in a class II laminar flow cabinet. The neuronal cells SH-SY5Y was obtained from the European Collection of Cell Cultures. Thawed stocks of adherent cells were routinely grown and passaged in a cell culture incubator at 37 °C and 5 % CO_2 in 75 cm^2 cell culture flasks with 20 mL of DMEM (Dulbecco's Modified

Eagle's Medium supplemented with 2 % (v/v) L-alanyl-L-glutamine (GIBCO GlutaMAXTM) and 2 % penicillin-streptomycin (Invitrogen). Cell monolayers were determined to be near-confluent at approximately 80 %. The cells were detached from the flask by incubating in 3 ml of trypsin/EDTA solution (containing 0.25 % trypsin and 0.02 % EDTA) at 37 °C for 5 min. Trypsin digestion was stopped by addition of 7 mL of supplemented DMEM. The resulting cell solution was placed into 50 ml Falcon tubes and centrifuged for 5 min at 300 x g and the supernatant discarded. Cell pellets were washed three times by re-suspension and centrifugation in 10 ml of 1 x phosphate buffered saline (PBS). The pellet was re-suspended, aliquotted and snap-frozen in liquid nitrogen and stored at -80 °C.

2.5.2. Langmuir-Schaefer deposition

Cell deposition and TIRE analysis were performed as previously described by Kriechbaumer *et al.*, 2011 and 2012).

Standard microscopic glass sides (1" x 1") were coated with chromium (Cr 3 nm thick) and gold (Au 25 nm thick) via thermal evaporation without breaking vacuum of 10^{-6} Tor (Edwards Lifesciences A360 metallizing unit, Irvine, CA). The metal coated slides were incubated overnight at 4 °C in a 0.1 M cysteamine-hydrochloride (Cys-HCl) solution to achieve positively charged slides. A Langmuir-trough (Nima PS4) was used for the deposition of chloroplast or SH-SY5Y cells onto gold coated glass slides. Membrane layers were subsequently assembled on the surface of deionised water (~18.5 MΩ) of the cleaned trough (using 100 % (v/v) chloroform and

isopropanol respectively). A strip of filter paper was slightly submerged in the water which was connected to the surface pressure sensor; allowing surface contamination to be monitored using the 'isotherm' graph and therefore any particles were removed by suction. After thorough cleaning, 300-500 µL of cell solution in PBS (1 x) was dotted onto the water surface using a Hamilton syringe; the droplets were gently brought into contact with the water's surface of Langmuir trough and were distributed evenly across the trough's surface area. Upon compression of the water's surface, a linear rise in surface pressure reflects the formation of a two-dimensional solid phase of cells. A pressure of 20 mN/m was chosen for deposition. The LS method of horizontal lifting (Petty 1996) was utilized for transferring membranes onto the glass slides. The slide was fixed horizontally but with a slight angled tilt to enhance deposition, onto the sample holder and was lowered down slowly (10 mm/min) until touching the water surface allowing for full coverage with membrane of interest. The slide was not allowed to be fully submerged, and was lifted up again resulting in a negatively charged layer of cell membranes electrostatically attached to the positively charged surface of gold. Deposition was monitored by the recording of surface pressure (Π) and thin film slides were kept hydrated in 1 x PBS and used within 48 hours, stored at 4 °C.

2.5.3. TIRE measurements and data fitting

TIRE measurements were performed using the J.A Woollam spectroscopic ellipsometer M2000 with a rotating compensator, operating in the spectral

range 370 - 1000 nm. Optical contact between the 68° trapezoidal glass-prism to the glass slide (opposing side of deposited material) is achieved via index matching fluid (ethyl-salicylate). The thin metal (Au) film slide faces down onto a rubber O-ring which seals the slide forming the TIRE cell. The cell has a 0.2 mL volume with inlet and outlet tubes enabling the washing (3 x cell volume) and sample incubation with subsequent analysis of adsorption at the films surface.

Software provided by J.A Woollam Ltd (Woollam 2002) enabled the modelling of the reflection system and its subsequent evaluation of the *d* and *n* of adsorbed molecular layers, comparing experimental and theoretical values of Ψ and Δ (Chapter 1 Table 1.2 for full details on TIRE four-layer model utilised in TIRE set-up). Briefly, the construction of the optical model used dielectric functions of particular layers including BK7 glass; gold and water which were all known parameters and found in the WVASE software library (J.A. Woollam 2001). Parameters of unknown layers were found by fitting the experimental data to the model layer using the Cauchy model for adsorbed molecular layers. TIRE data modelling started with a single spectroscopic scan of the bare gold film in 1 x PBS buffer, to obtain the thickness (*d*) and dispersion curves for optical parameters $n(\lambda)$ and $k(\lambda)$ of the Cr-Au layer. All parameters were fixed apart from *d*, thus any subsequent changes were associated with changes in film thickness. Therefore, a second spectroscopic scan of the next layer: the adsorbed Cauchy layer was fitted to the optical model of the Cr-Au layer, providing the new thickness.

This was repeated for subsequent protein adsorption steps during each experiment. During sample incubation (30 min), two types of ellipsometric measurements were performed: (1) dynamic TIRE spectral measurements where multiple TIRE spectra's were recorded during protein adsorption and (2) TIRE single spectroscopic scan recording after completion of every adsorption step using standard buffer solution (1 x PBS, pH 8.0). The spectroscopic scan performed after adsorption provided the change in thickness (Δd (nm)) which is recorded and interpreted into graphical representation using excel.

3.1. Introduction

3.1.1. Protein - lipid interactions brought about by protein misfolding.

Proteins are the major components of the living cell and a play a crucial role in the maintenance of life, acting as building blocks of all organisms (Uversky 2008). They are composed of amino acids which are connected by peptide bonds, and whose sequence forms its primary structure. Folding of this chain forms the secondary structure, consisting of α-helices, β-sheets and random coils. The interactions between these elements create the tertiary structure and subsequent functionality. The final native conformation fold is stabilized by a range of interactions, including hydrophobic and Van der Waals forces, and electrostatic interactions. Protein misfolding is a major cause of a broad range of human diseases which arise from the failure of a specific protein to adopt its native functional conformation. Misfolding is influenced by various internal or external factors including; amino acid sequence and mutations, or environmental changes in temperature and pH respectively. The aberrant folding and loss of structural integrity can lead to protein aggregation and the appearance of various intermediate structures; amorphous aggregates, known as oligomers as well as highly ordered fibrils known as amyloid (Fig. 3.1) (Herczenik *et al.*, 2008).

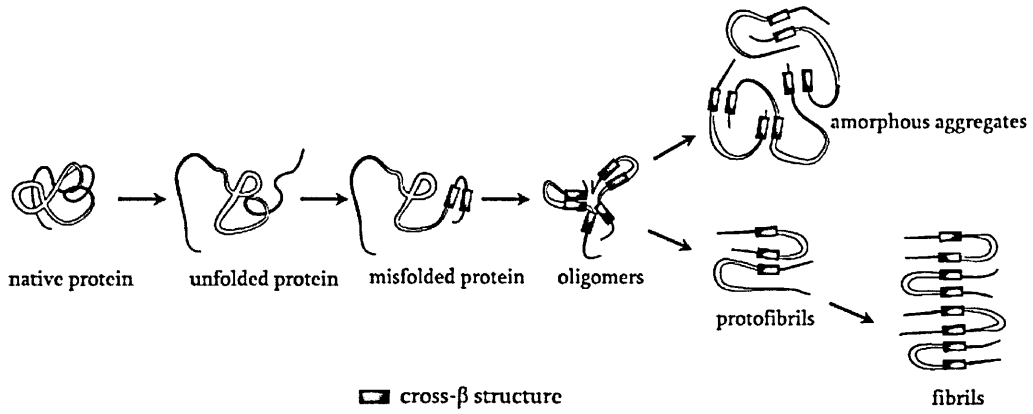

Figure 3.1 Protein misfolding and aggregation. Under various environmental conditions it can result in proteins undergoing conformational changes that result in its unfolding and partial misfolding which is associated with protein aggregation causing different structural appearances (cross-β structure) including unordered aggregates to ordered fibrils called amyloid (Herczenik *et al.,* 2008).

Oligomeric species have been shown to induce seeding of the amyloid protein; α-synuclein (α-syn) causing its aggregation, directly relating their roles as cytotoxic species in the spread of α-syn pathology (Danzer *et al.,* 2007 and 2009), furthermore amyloid fragmented fibrils have also been identified to induce seeding (Xue *et al.,* 2009) correlating their cytotoxic capabilities to that of oligomers. To date, >25 amyloid forming proteins have been identified in disease-associated amyloid deposits, including α-syn in Parkinson's Disease (PD), amyloid-β peptide (Aβ) in Alzheimer's disease (AD), and prion protein (PrP) in transmissible spongiform encephalopathy's (Eisenburg *et al.*, 2012).

3.1.2. Amyloid Protein

In 1854 the term 'amyloid' (amylo (starch) & oid (like)) was first coined by Rudolph Virchow due to its reaction with iodine, assuming that amyloid deposits were derived solely from carbohydrates and lipids, until 1859, when Friedreich and Kekule demonstrated both the presence of protein in 'mass' deposits and the absence of carbohydrates (Sipe *et al.,* 2000). Over the years aniline dyes such as methyl violet and congo red were used to stain amyloid protein, and in 1959, Vassar and Culling used Thioflavin T (ThT) as a diagnostic tool to detect amyloid deposits. To date, a combination of atomic structural studies and conformational antibodies show a typical cross-β X-ray diffraction pattern (Eanes *et al.*, 1968 and Makin *et al.,* 2005) along with a common generic epitope shared amongst disease-related amyloid fibrils that can be recognised by specific antibodies (O'Nuallain *et al.,* 2002, Yoshiike *et al.,* 2008 and Kayed *et al.,* 2007) (Fig. 3.2).

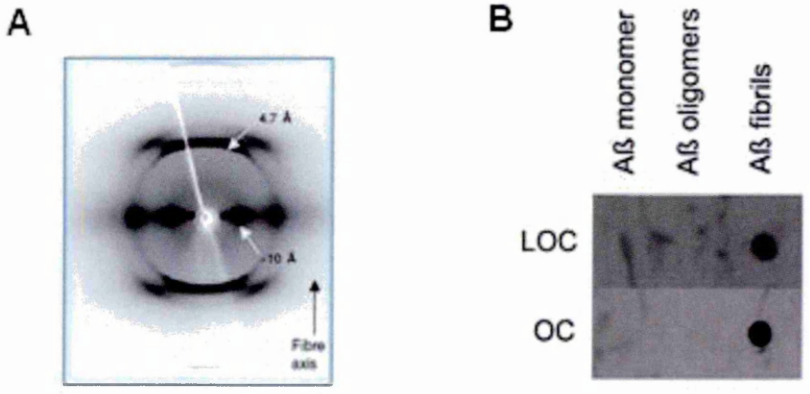

Figure 3.2. (A) X-ray fibre diffraction pattern from amyloid fibrils, showing the positions of the 4.7 Å meridional and 10 Å equatorial reflections in a cross-β pattern (Makin *et al.,* 2005). (B) Common epitope to amyloid fibrils detected by anti-amyloid fibril (OC) and LOC (Like-OC) antibodies (Kayed *et al.,* 2007).

As shown in Fig. 3.2 (B), the conserved structural similarity of fibrillar species has enabled the development of conformation specific antibodies via the identification of generic epitopes, resulting in their immunological characterisation (O'Nuallain *et al.,* 2002). Therefore, it is possible to distinguish between different amyloid structures - independent of the peptide sequence. Fig. 3.3 demonstrates the pathways of monomer misfolding resulting in different conformational species that can be identified using conformation-specific antibodies. Prefibrillar oligomers are recognised by the A11 antibody and these species are transient intermediates that ultimately become fibrils via protofibril formation. Alternatively the amyloidogenic monomer can aggregate to adopt a fibrillar conformation recognised by the OC antibody, and is prone to elongation by recruiting additional monomers resulting in direct fibril growth (Kayed *et al.,* 2007). These have been extensively used in studies as described in further detail later (section 3.1.3).

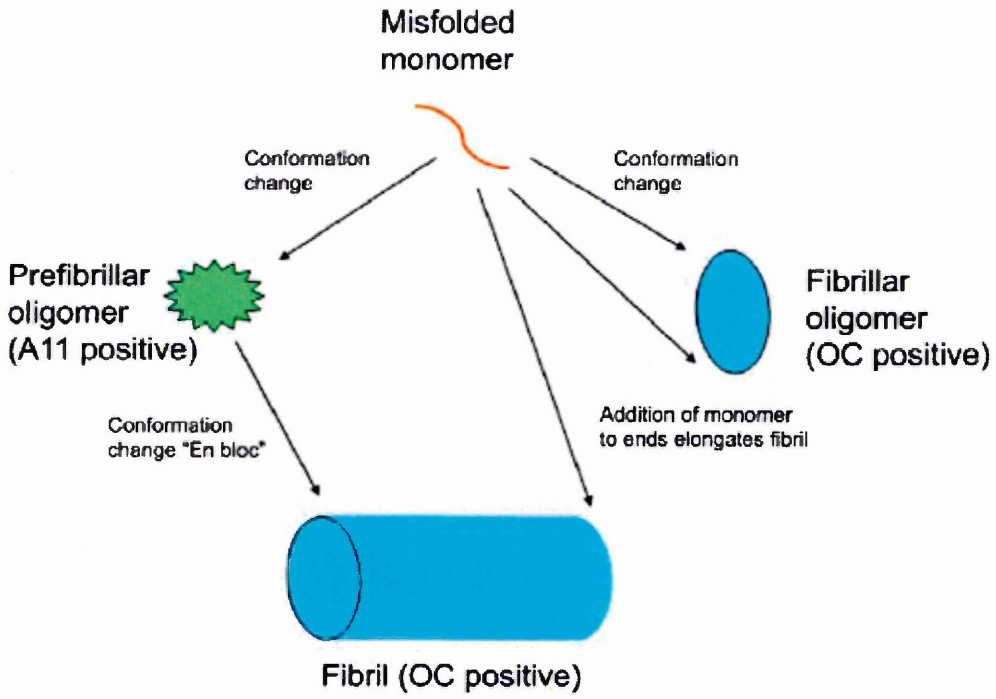

Figure 3.3. Schematic representation of the distinct types of amyloid oligomers and their relationships to amyloid fibrils (Kayed *et al.,* 2007).

The definition of amyloid has evolved in parallel with our understanding of its molecular structure, "an unbranched protein fibre whose repeating substructure consists of β-strands that run perpendicular to the fibre axis, forming a cross-β sheet" (Greenwald *et al.*, 2010). It is thought that virtually any protein can be induced into forming amyloid structures, and the ability to form amyloid fibrils is a generic property of peptides and proteins. This is a result of the inherent physicochemical properties of the polypeptide main-chain which is a structural feature common to all sequences, rather than interactions of specific side-chains. Thus the composition and sequence of a

peptide or protein can affect its propensity to form amyloid structures. However, the properties of side-chains should not be overlooked as they can influence the details of amyloid structures giving rise to variations in fibrillar assembly (Stefani *et al.,* 2003).

3.1.3. Structural traits of amyloid fibrils

The process of formation for oligomeric and fibrillar species remains equivocal as to whether amyloid oligomers are an obligate intermediate, described as either 'on-pathway' for which all protein molecules must pass through during fibril formation, or represent an alternate 'off-pathway' that may or may not result in fibril formation (Necula *et al.*, 2007). The various intermediate structures are maintained by intermolecular interactions between side chains, and it has been suggested that the balance between the hydrophobic and electrostatic interactions, could be the underlying cause for which different pathways for oligomeric and subsequent fibrillar species are formed from. In lysozyme, a well-known amyloidogenic protein, the extent of charge repulsion has been shown to determine the assembly pathway and morphology of fibrillar aggregates (Hill *et al.*, 2011). Furthermore, solution conditions and peptide sequence mutations have also been found to modulate the nature of oligomers switching between on- and off-pathways, supporting the argument that the structural features of the oligomers determine which pathway is followed (Bemporad *et al.*, 2012). A result of genetic mutations associated with familial forms of diseases, such

as the point mutations A53T, A30P and E46K in early onset Parkinson's disease (Fredenburg *et al.*, (2007), Conway *et al.,* (1998), Li *et al.*, (2001), Kang *et al.*, (2011)) have shown aggregation rates to be increased, with the extent of protein aggregation giving rise to fibrils with varying degrees of cytotoxicity according to the cross-β-core size (Mossuto *et al.*, 2010).

The characteristic feature of fibrils is the cross-β sheet entailing protein backbones aligned perpendicularly to the main fibril axis, and linked to one another via two distinct sets of hydrogen bonds (Breydo *et al.,* 2012). Electron and atomic force microscopy have provided insights into the macromolecular structure of amyloid fibrils, showing them as long, straight and unbranched (Fig. 3.4). Fibrils are comprised of individual subunits named 'protofilaments', of which fibrils usually consist of between two to six, and these are observed to twist around one another to form the mature fibril. Amyloid proteins including lysozyme, Aβ and α-syn fibrils are composed of several protofilaments wound around one another (Rambaran *et al.,* 2008 and Breydo *et al.,* 2012). Currently the mechanisms for fibril formation is an active area in research, with evidence that fibril ends are responsible for extension and fibril breakage affecting the kinetics of fibrillar growth (Tanaka *et al.*, 2006) whilst also modulating their cytotoxic potential (Xue *et al.,* 2009).

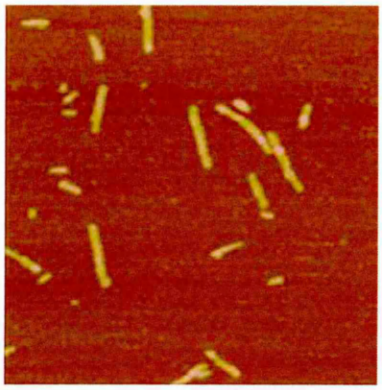

Figure 3.4. Fibril characterisation by atomic force microscopy (AFM) image. 2x2 μM image of β-2-micrglobulin fibrils on a mica surface, accentuating typical un-branch like structural features of fibrils (Xue *et al.,* 2009).

There is ongoing controversy with regards to the primary culprits of cytotoxicity associated with amyloid disorders, due to the complex heterogeneity between different species identified during amyloid formation and their subsequent interactions (Stefani 2012). During fibril formation oligomeric species accumulate and can contribute to the nucleation dependent polymerisation of fibrillar aggregates, therefore making it difficult to identify a sole culprit of cytotoxicity. A plethora of studies have focused on the soluble prefibrillar oligomers as active toxic agents (Bucciantini *et al.,* (2002). Kayed *et al.,* (2003) and Glabe (2006)). However, there are increasing examples of fibrils associated with toxic effects. Studies by Jakhira *et al.,* (2014) and Xue *et al.,* (2009) relate the physical dimensions of fibrils to their biological properties and cytotoxic potential respectively, Martins *et al.,* (2008) showed Aβ fibrils releasing cytotoxic species and finally

Engel *et al.*, (2008) demonstrated membrane disruption of liposome vesicles using human islet amyloid fibrils.

3.1.4. α-Synuclein (α-syn)

α-syn is a 14 kDa soluble neuronal protein which is typically natively unfolded, found abundantly at presynaptic termini of neurons within close association to synaptic vesicles. Several physiological functions of α-syn have been suggested, including synaptic vesicle release and trafficking, fatty acid binding and physiological regulation of certain enzymes, transporters, and neurotransmitter vesicles, as well as roles in neuronal survival (Dev *et al.,* 2003). α-syn is implicated in various neurodegenerative diseases including Parkinson's Disease (PD), with characteristic hallmarks presenting deposition of Lewy bodies (LBs) in the substantia nigra pars compacta and selective loss of dopaminergic neurons (Jellinger 2011). LBs are spherical inclusions bodies containing predominantly fibrillar α-syn protein, and are found in the cytoplasm of surviving *substantia nigra* neurons. These fibrils are structurally similar to those seen in other amyloid diseases, appearing as linear rods of 5-10 nm diameters (Pirc *et al.,* 2011). PD affects more than 2 % of the population over the age of 65 years (Gallea *et al.,* 2014) and the cause of PD remains unknown, but substantial evidence indicates that fibril formation is a critical step in the aetiology of PD (Pirc *et al.*, 2011).

The amino acid sequence of α-syn is composed of three domains: residues 1-60 contain four 11-amino acid imperfect repeats with a conserved

KTKEGV motif; residues 61-95 is the central region known as the non-amyloid-β component (NAC) which is highly hydrophobic and propagates protein aggregation and generation of β-sheets - a prominent feature in fibrils, and finally residues 96-140 are enriched in acidic residues and prolines at the C-terminal region (Fig. 3.5). The first two domains entail a membrane-binding domain, and the C-terminal tail contains sites for protein-protein and protein-small molecule interactions (Breydo *et al.*, 2012).

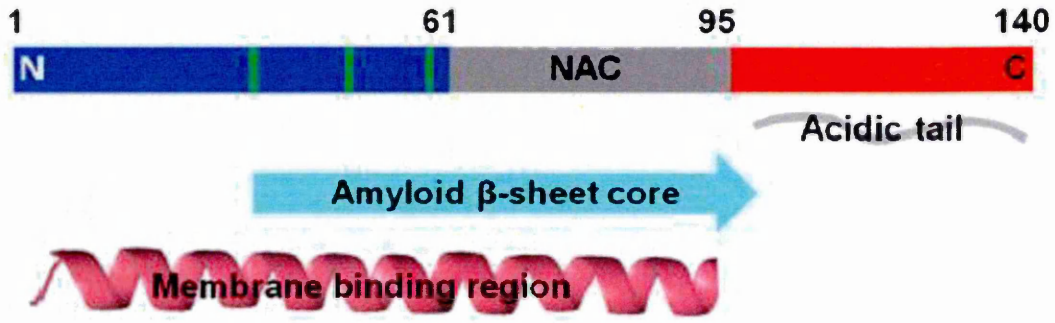

Figure 3.5 Schematic representation of the primary amino acid sequence of α-syn. Upon amyloid formation the fibril core region is composed of residue 30-100, while the N- and C- terminal regions are disordered. In the presence of model membranes such as acidic micelles and phospholipid vesicles, residues 1-95 bind; adopting a α-helical structure (McGlinchey *et al.,* 2011).

The set of seven 11-residue repeating motifs featured in the α-syn amino acid sequence are reminiscent of the amphipathic α-helical domains of apolipoproteins, which are involved in mediating lipid and protein binding (Davidson *et al.,* 1998). Thus these structural features enable α-syn to bind to synthetic vesicles and cellular membranes, resulting in a variety of helical

structures upon membrane binding (Breydo *et al.,* 2012). Zhu *et al.,* (2003) demonstrated that membrane binding of α-syn affected both protein and membrane properties, with electrostatic and hydrophobic interactions governing protein-bilayer associations, with large fibrillar structures causing greater disruption of the membrane than its monomeric form. Furthermore, α-syn binding has been found to cause membrane remodelling via membrane thinning (Ouberai *et al.,* 2013) and the permeabilisation of model membranes via the formation of pore-like channels (Fig. 3.6) (Giehm *et al.,* 2011 and Quist *et al.,* 2005). The mechanical disruption of lipid membranes therefore, could be considered as an alternative cell death mechanism to the traditional notion of cell death directed by chemical effects of biomolecules (Lee *et al.,* 2012).

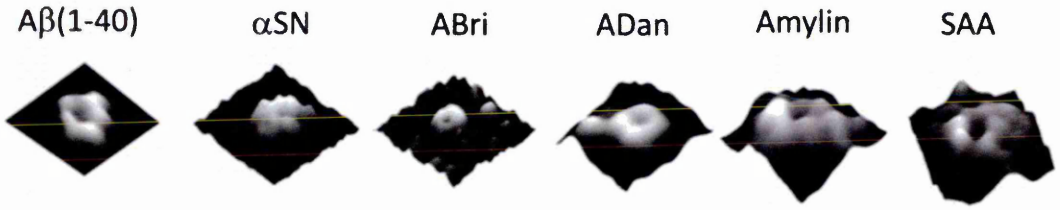

Figure 3.6. AFM images of annular, pore-like structures for oligomeric species of a range of amyloid-forming proteins. An example for each molecule is shown, in which a central pore can be observed (Quist *et al.,* 2005).

In vitro studies of α-syn binding to lipid membranes have utilised artificial membranes of various sizes (small unilamellar vesicles (SUV) and large unilamellar vesicles (LUV)) composed of different combinations of phospholipids head groups: negatively charged phosphatidylglycerol (PG),

phosphatidic acid (PA), phosphatidylserine (PS) and phosphatidylinositol (PI), while the uncharged, neutral lipids commonly used include phosphatidylcholine (PC) and phosphatidylethanolamine (PE) (Pirc *et al.,* 2011). The array of *in vitro* literature on α-syn and membrane interactions is vast, with contrasting reports stating α-syn binds preferentially to SUVs containing acidic phospholipids, but not to vesicles with a net neutral charge (Davidson *et al.,* 1998), on the other hand, Narayanan *et al.,* (2001) states that α-syn binds strongly to LUVs composed of either anionic or zwitterionic (neutral) head groups. This highlights the lack of data on native membranes and their importance in consequently identifying target organelles. *In vivo* studies have identified the correlation between mitochondrial dysfunction and PD, which has prompted significant interest in α-syn mitochondrial membrane interactions. Nakamura *et al.,* (2008) using FRET-based reporters confirmed that the conformation of α-syn is altered in the presence of natively derived mitochondrial membranes, indicating a direct link between α-syn and an organelle which is strongly implicated in the pathogenesis of PD. The importance of understanding the dynamic and heterogeneous nature of α-syn when bound to native membranes and its amyloid form, underscores the significance of biophysical techniques that can provide an insight into their properties and their involvement in the pathogenesis of PD, particularly in natively derived conditions.

3.1.5. Amyloid β (Aβ)

Aβ is a small proteolytic product (~4 kDa) derived from the human amyloid precursor protein (APP) gene. The accumulation of abnormally folded Aβ proteins and tau form the basis of senile plaques and neurofibrillary tangles (NFTs) respectively, and are the hallmarks for the neurodegenerative disease; Alzheimer's Disease (AD). AD has been identified as a protein misfolding disease, and is the most common form of dementia. Neuropathological examination of the AD brain reveals the loss of neurons and synapses causing cognitive impairment (Fodero-Tavoletti *et al.,* 2011). The main constituent of senile plaques is Aβ fibrils, and their formation via intermediate aggregates and subsequent neurotoxic properties are of great research interest to identify therapeutic and/or diagnostic biomarkers in this currently incurable disease.

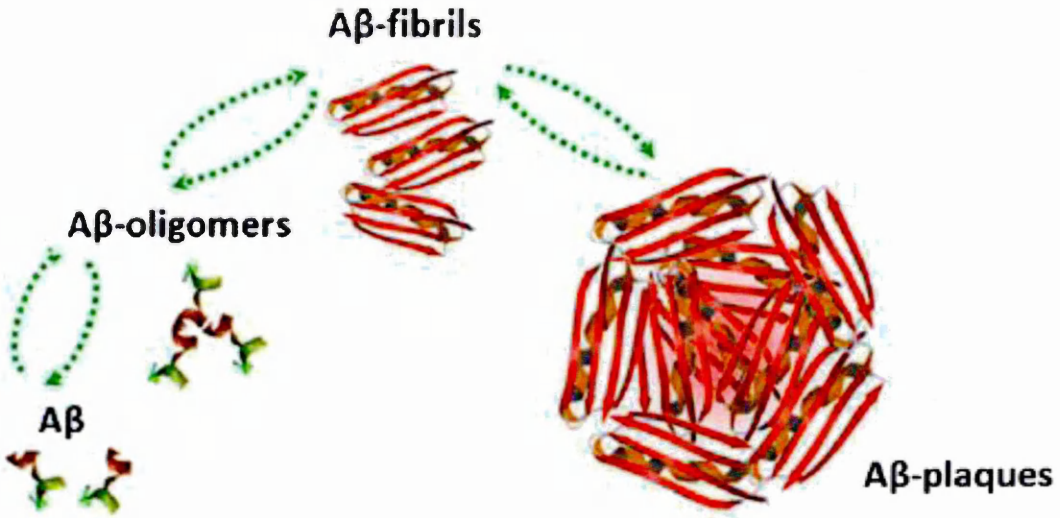

Figure 3.7. Mechanistic pathways of fibril formation/amyloidogenesis. Ribbon schematics showing the Aβ peptide self-aggregating, forming oligomers prior to the formation of fibrils that comprise the main constituents of the characteristic extracellular AD plaques (Fodero-Tavoletti *et al.,* 2011).

The interactions between Aβ peptides and cellular membranes have been shown to lead to the disruption of membranes and cause subsequent cytotoxicity. Lashuel *et al.*, (2002) demonstrated enhanced neurotoxic properties upon accumulation of protofibrillar intermediates, causing pore formation and subsequent membrane disruption. The interactions between Aβ and membranes have been found to be regulated by not only the peptides structural conformation (e.g. soluble monomer) but also the lipid composition and charge at target membranes. Tofoleanu *et al.,* (2012) utilised model bilayers and identified electrostatic interactions between charged peptide residues of Aβ fibrils and lipid head groups as the major driving force for membrane binding. Results showed membrane perturbations and thinning effects upon binding, suggesting a direct

interaction between fibrils and lipid bilayers and a similarity to the formation of amyloid channel-like structures. The observation that membrane composition affects peptide binding was also observed by Wong *et al.,* (2009) who determined that charge is important in the initial membrane binding; however, permeabilisation depended on membrane fluidity. Wong *et al.,* (2009) proposed an insight into how Aβ becomes cytotoxic *in vivo*, that increased charge density on the outer leaflet due to damage during aging or due to disease, and differences in cholesterol content altering membrane fluidity, can alter membrane composition, resulting in enhanced Aβ membrane interactions and subsequent permeabilisation.

3.1.7. Lysozyme

The human protein lysozyme is an enzyme for which gene mutated variants underlie non-neuropathic amyloidosis. The disease-related lysozyme mutants are structurally identical to their native counterpart, whilst their thermal stability is reduced resulting in a decrease in the stability of the native state and an increased propensity to form amyloid fibrils (Booth *et al.,* 1997). The formation of amyloid fibrils *in vivo* can result in large quantities, often kilograms, of aggregated protein to accumulate in organs such as the liver, kidney and spleen (Chamberlain *et al.*, 2000). The amyloid fibrils formed by disease mutants are morphologically indistinguishable from those formed by native lysozyme, and thus results obtained with native lysozyme can be directly applicable to their disease-related mutants (Hill *et al.,* 2011).

Using hen egg-white lysozyme amyloid, Gharibyan *et al.,* (2007) demonstrated using a range of toxicity assays that both lysozyme oligomers and fibrils exerted toxicity on SH-SY5Y neuroblastoma cells, but within different time-scales and via different mechanisms. Oligomers were found to induce apoptosis-like cell death via caspase activation after 24h but no changes in morphology or staining by the DNA fluorescent dye; propidium iodide (PI) were observed. However, within 6h fibrils caused an increased permeability of cell membranes leading to the rapid release of lactate dehydrogenase (LDH) and of the intake of PI. Furthermore, it was noted that all amyloid samples observed a concentration-dependent cellular effect such as the release of LDH. In contrast to the fibrils however, even the lowest concentration of oligomeric sample affected cell viability, indicating that the oligomers must act via specific mechanisms as opposed to a generic direct membrane disruption by fibrils. The direct membrane disruption by fibril binding was also observed by Xue *et al.,* (2009) who showed that lysozyme fibrils along with β_2-microglobulin (β_2m) and α-syn caused damage to liposome membranes and disruption to cellular function, and as previously mentioned Xue *et al.,* demonstrated that fibril length contributes to cytotoxicity effects, with short fibrils resulting in enhanced cytotoxicity. A strong correlation amongst structural, conformational and stability features of amyloid assemblies and their ability to permeabilise membranes has been reported (Kastorna *et al.,* 2012). Specifically, Mossuto *et al.,* (2010) reported that intrinsic differences in physicochemical properties of lysozyme fibrils gave rise to different degrees of cytotoxicity. Results showed that lysozyme fibrils formed at a physiological pH were found to be less ordered in the

cross-β structure, resulting in a substantial increase in cytotoxic effect when compared to fibrils prepared at an acidic pH. Furthermore, the high ordering of mature lysozyme fibrils with increased structural stability and reduced exposed hydrophobic patches led to bilayer dehydration, and/or increase in lipid packing density reducing membrane permeabilisation effects (Kastorna *et al.,* 2012).

The outline of three amyloid proteins (α-syn, Aβ and lysozyme) have identified several different factors affecting fibril binding and cytotoxic-related effects, including changes in intermolecular forces (Hill *et al.,* 2011), lipid to protein ratio's (Shvadchak *et al.,* 2011) and physical dimensions of amyloid material (Xue *et al.,* 2009 and Jakhira *et al.,* 2014). These studies suggest that fibrils contribute to membrane disruption via direct interactions, which could contribute to cellular dysfunction associated with amyloid diseases. However, these biophysical investigations have mainly used *in vitro* techniques such as; LUVs as a lipid model system for binding interactions, emphasising a lack of studies at native cellular membranes. The aim of this research is to utilise the human neuroblastoma cell line; SH-SY5Y to determine cellular effects in an *in vivo* model of amyloid fibril binding.

3.2. Aims of Model I – protein: lipid interactions

In order to explore the hypothesis that fragmented amyloid fibrils exert enhanced cytotoxic effects (Fig 3.8) the binding of three amyloid proteins (α-syn, Lysozyme and Aβ40) using full length and fragmented fibrils was established and were incubated with the natively derived neuroblastoma cell line; SH-SY5Y. The protein: lipid interactions were quantified using the novel biophysical technique; TIRE.

To demonstrate amyloid fibril interaction *in vitro* with artificial membranes using dye encapsulated liposome vesicles, and cellular viability assay to determine cytotoxic effects of amyloid fibrils with the neuronal cell line; SH-SY5Y.

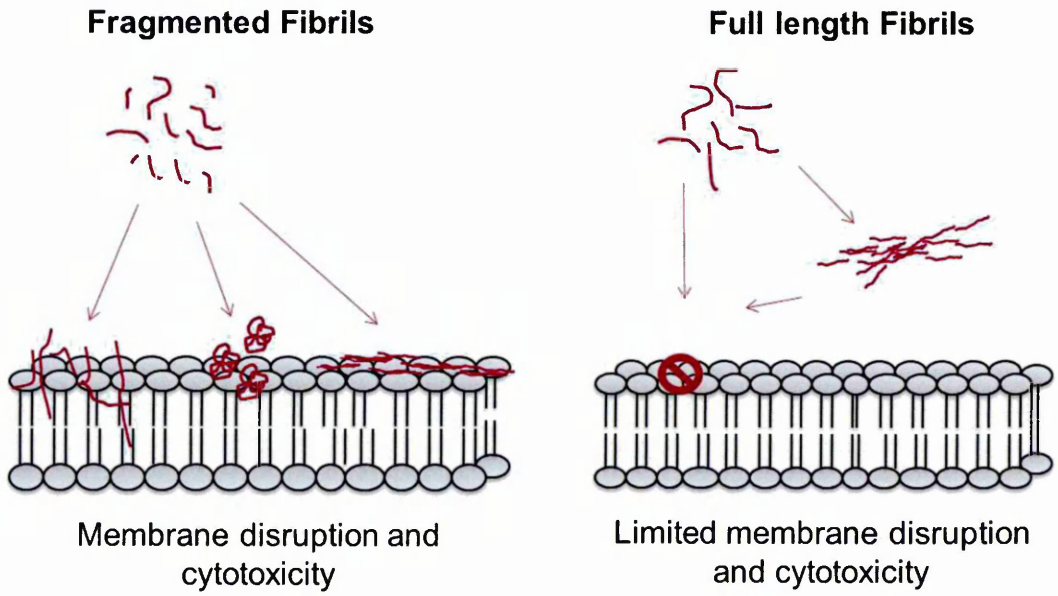

Figure 3.8. Schematic illustrations of amyloid fibril and cellular membrane interaction. Fragmented fibrils are postulated to elicit increased membrane disruption and cytotoxic effects compared to their full length counterparts.

3.3. Results

3.3.1. Amyloid Fibril characterisation

To investigate the effects of fibril-membrane interactions, amyloid fibrils were produced following previously described methods for α-syn (Xue *et al.*, 2009), Aβ40 (Ciccotosto *et al.,* 2004) and lysozyme (Ow *et al.,* 2013). AFM imaging (Fig. 3.9 A, B and C) was performed on full length and fragmented fibrils for each protein, along with excitation/emission scan utilising thioflavin-T (ThT), to confirm the presence of β-pleated sheet structures – a predominant feature of amyloid fibrils. The full length fibrils observed here present a network of linear unbranched structures (Fig. 3.9); the AFM images for fragmented fibrils demonstrate a notable change in their macromolecular structure, showing a loss of entwining networks of the linear un-branched structures as seen by their full length counterparts. As such, the physical characteristics of fragmented fibrils have been altered, for example; α-syn full length fibrils display a network of aggregated and overlapping fibrils noting their height reaching 10 nm, compared to the dispersed fragmented fibrils at 4 nm. (Fig 3.9 A). Size and morphological features are typical of full-length and fragmented amyloid fibrils and corresponded to the linear unbranched structures documented previously by Xue *et al.,* (2009). Fibril incubation with ThT - widely used as an amyloid dye (Biancalana *et al.,* 2010) presented a characteristic peak of increased fluorescence intensity at 480 nm, indicative of the presence of fibrils. Immunological characterisation was also

demonstrated using a conformational specific primary antibody, anti-amyloid fibril LOC (Millipore UK). This particular antibody recognises generic epitopes specifically common to amyloid fibrils; excitation at 800 nm with infra-red secondary antibody binding which confirmed the presence of amyloid fibril material in all three proteins (Fig. 3.9 D). A negative control using BSA showed no immunoreactivity confirming the antibody specificity for fibrils. Similar antibody binding intensities for full and fragmented counterparts were observed, demonstrating that fragmentation had not resulted in a loss of the generic epitope. AFM, ThT and dot-blotting have confirmed generic amyloid presence of fibrils. However, differences in protein load have shown differences in fibril morphology, the extent of epitope binding and ThT intensities. For example, AFM imaging of α-syn and lysozyme full length fibrils with regards to the length of fibrils seen in Fig. 3.9 A and B. This shows that the degree of fibril formation is protein specific, with no one amyloid protein being the same, intrinsic factors such as peptide sequence and subsequent peptide-backbone interactions could all contribute to the extent of protein load and aggregation (Breydo *et al.,* 2012). However, it is clear in all cases that amyloid material is present, but with differences in total load and absolute morphology.

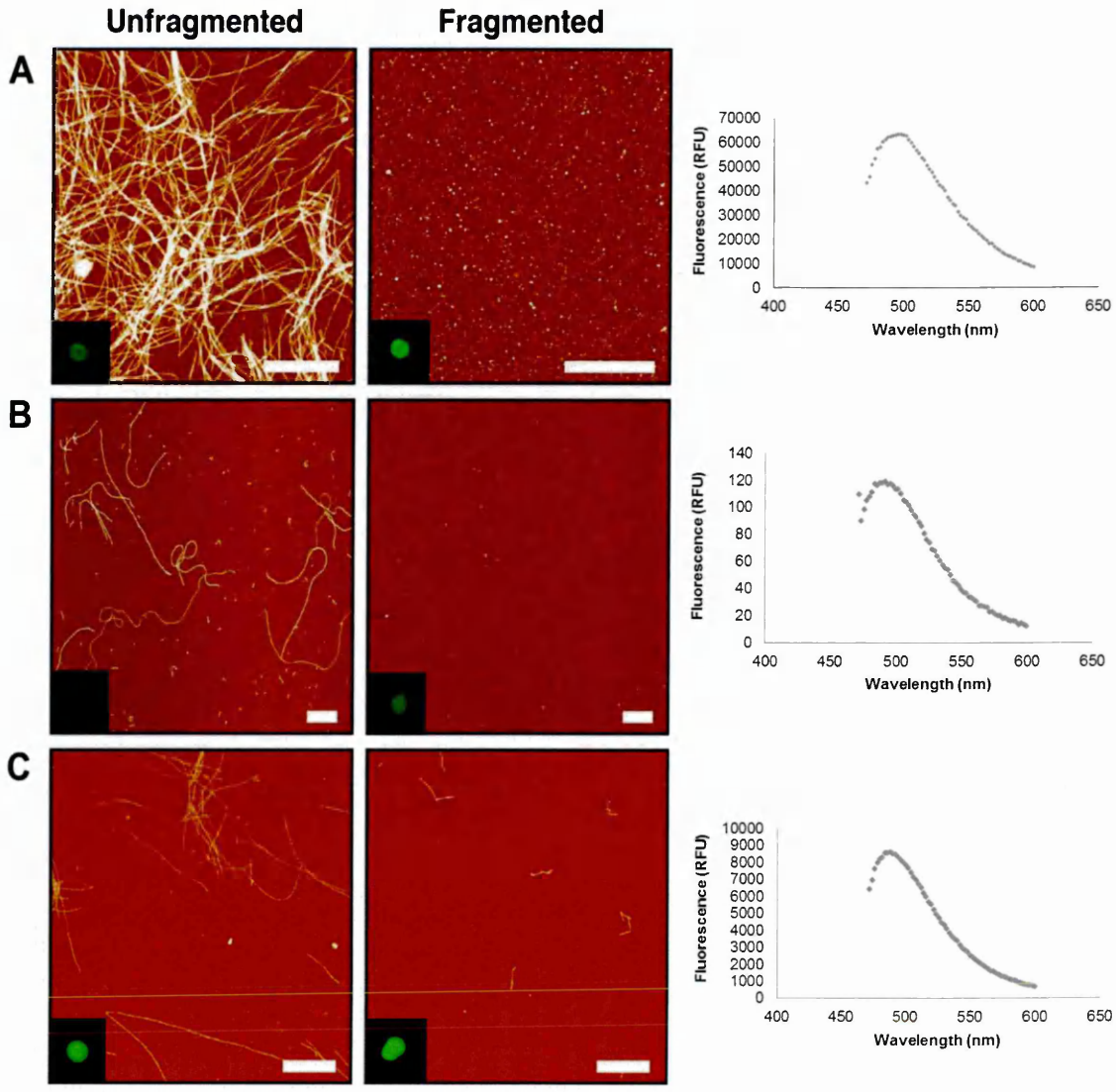

Figure 3.9. Amyloid fibril characterisation. TM-AFM images of fibril samples adhered to mica surface (1 μM); with dot blot analysis of fibrillar samples inset, using anti-fibril LOC antibody specific to generic epitopes common in amyloid fibrils. Using thioflavin-T (ThT) a discontinuous growth assay was performed, showing an emission scan (470-600 nm) and relative fluorescence units (RFU). (A) α-syn, (B) Lysozyme and (C) Aβ40.

3.3.2. Liposome dye release assay

It has been shown that fibril-membrane interactions cause membrane disruption (Martins *et al.*, 2008 and Milanesi *et al.,* 2012) and in particular that fragmented fibrils have an enhanced membrane disruption than their longer counterparts (Xue *et al.*, 2009). In order to confirm the fibrils produced acted in the same manner as those published previously we monitored the ability of both fibril samples to disrupt synthetic membranes. Dye-release assays were performed using LUVs formed from 80 % PC and 20 % PS - a physiological composition and charge of the plasma membrane (Knight *et al.*, 2004), within which the self-quenching fluorescent dye carboxyfluorescein was encapsulated at pH 7.4. The release of the encapsulated dye to the bulk solvent decreases the self-quenching of fluorescence of the dye within liposomes, thus an increase in fluorescence reflects membrane disruption.

Positive controlled membrane disruption was demonstrated by the addition of Triton X-100 (20 % v/v), and a negative control of LUVs in buffer only (Fig 3.10). Successful dye encapsulation in LUVs was demonstrated by the ability to trigger dye release with the addition of Triton X-100 (20 % v/v) which is known to dissolve membranes.

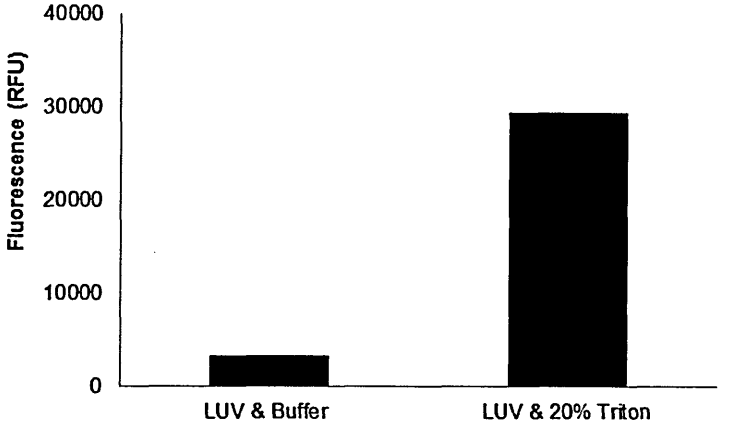

Figure 3.10. Controlled dye release. Dye release (RFU) of LUVs after 30 min in buffer only (negative control) and Triton X-100 (20% v/v) (positive control).

Upon the addition of fibrils to the dye encapsulated LUVs, the fluorescence intensity was seen to increase by all three amyloid proteins studied, indicating liposome disruption was due to the presence of fibrils. Initial time dependent dye-release assays were performed over a 60 minute period (Fig. 3.11); the findings demonstrate that full length fibrils achieve lower levels of dye release than fragmented fibrils. The overall difference in dye release (fluorescence) from start to end caused by fragmented fibrils, is between 1000 - 4000 RFU higher than the full length fibrils (Fig. 3.11 A, B and C). After 30 minutes a plateau in the fluorescence can be seen, particularly in Fig. 3.10 B and C. Therefore, a direct comparison of the differences between fluorescence intensities at 30 minutes was selected to compare the extent of membrane disruption caused by full length and fragmented fibrils.

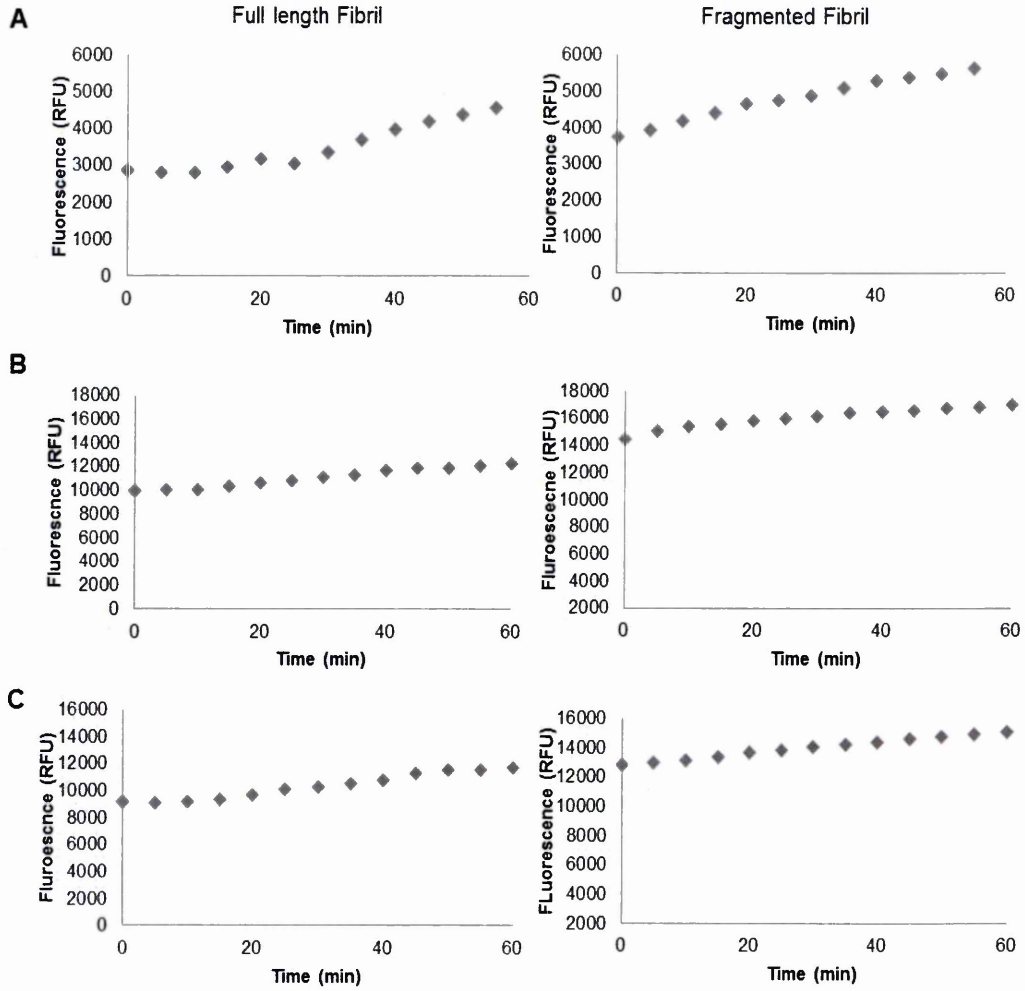

Figure 3.11. Dye release assay with amyloid fibril incubation. Dye-encapsulated vesicles were incubated with amyloid fibrils: (A) α-Syn (100 μg/mL), (B) Lysozyme (20 μg/mL) and (C) Aβ40 (20 μg/mL) and time-dependent fluorescence (RFU) was recorded (520_{Em}/ 480_{Ex}) over a 60 minute period.

To compare the extent of membrane disruption caused by full length and fragmented fibrils, fluorescence was recorded at 30 minutes and normalised against full length fibrils (derived from Fig. 3.11 data). Fig. 3.12 shows a ≥ 0.5 fold increase in dye release for all three fragmented amyloid proteins compared to their full length counterparts. This reflects an enhanced ability of fragmented fibrils to disrupt dye-encapsulated liposomes.

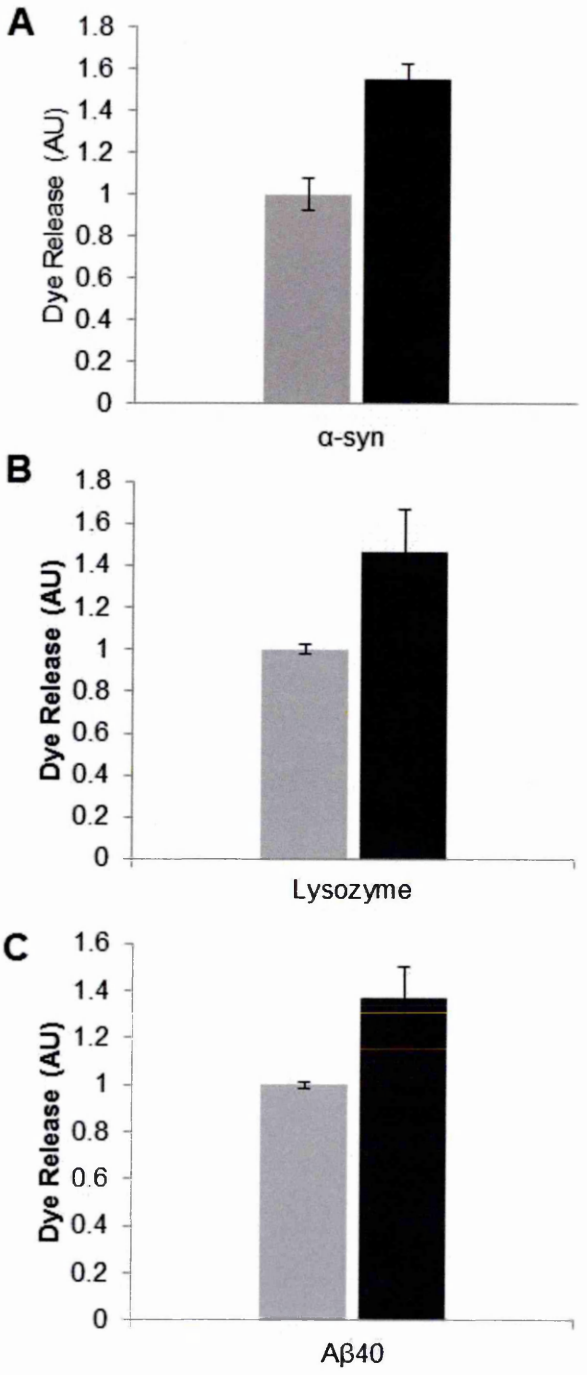

Figure 3.12. The effect of fibril fragmentation on length and its capacity to cause membrane disruption. Dye-encapsulated vesicles were incubated with amyloid fibrils for 30 mins, and fluorescence was recorded (520_{Em}/ 480_{Ex}). The fold increase of dye release was normalised against full length fibril fluorescence (AU). (A) α-Syn 100 μg/mL (B) Lysozyme 20 μg/mL and (C) Aβ40 20 μg/mL. Light grey (full length fibril) and dark grey (fragmented fibril) (n=3, SE).

3.3.3. Cell (SH-SY5Y) viability assay treatment using CellTox green assay.

Cells were seeded and left for 24 hours to adhere in which the celltox probe was incorporated within the media/cells immediately. Fibrils were added and left for three days in total, with readings every 24 hours. The CellTox green assay (Promega) is designed to measure changes in membrane integrity that occurs as a result of cell death; the dye preferentially binds to dead cell's DNA and thus excludes viable cells. Upon binding of cell DNA the fluorescence properties of the dye is greatly enhanced and thus fluorescence signal is proportional to cytotoxicity. Fig. 3.13 presents primary necrosis as a positive control using reagent supplied by manufacturer (Promega).

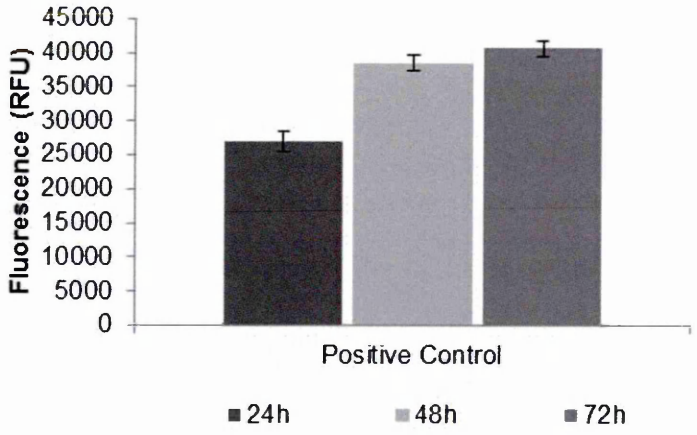

Figure 3.13. Primary cell necrosis. Lysis Solution was added to replicate wells at a ratio of 1:25 (4 µl per 100 µl of cells) for toxicity control, showing the minimum positive control signal obtainable from proliferating cells at the end of the exposure period (72 h) (n=6 SE).

To determine if the enhanced liposome membrane disruption by fragmented fibrils is replicated within live cells, the human neuroblastoma cell line; SH-SY5Y was selected. Full length and fragmented fibrils from each protein were incubated with seeded cells and cell membrane integrity was measured over 72 hours to assess cell viability and subsequent cytotoxic effects.

The resulting data (Fig. 3.14) revealed that treatment with fragmented fibrils from α-syn and Aβ40 caused higher fluorescence intensity, reflecting loss of membrane integrity and increased cytotoxicity. The fragmented fibrils from α-syn and Aβ40 both exhibit cytotoxic effects within 24 hours, with fluorescence intensity nearly three times higher than incubation with full length fibrils. Lysosomal fibrils were prepared in pH 1.0 buffer and in this case the solvent control proved toxic to the cells, with equivalent fluorescence after 24 h as the positive control (Fig. 3.13). The membrane integrity based assay therefore supports the increased fibril-membrane interaction by fragmented fibrils which result in greater membrane disruption. A generic mode of action is being observed with regards to the amyloid fibrils studied, in that they are able to disrupt both synthetic vesicles (Fig. 3.12) and bring about cytotoxicity in human cells, as measured by assays for membrane integrity (Fig. 3.14).

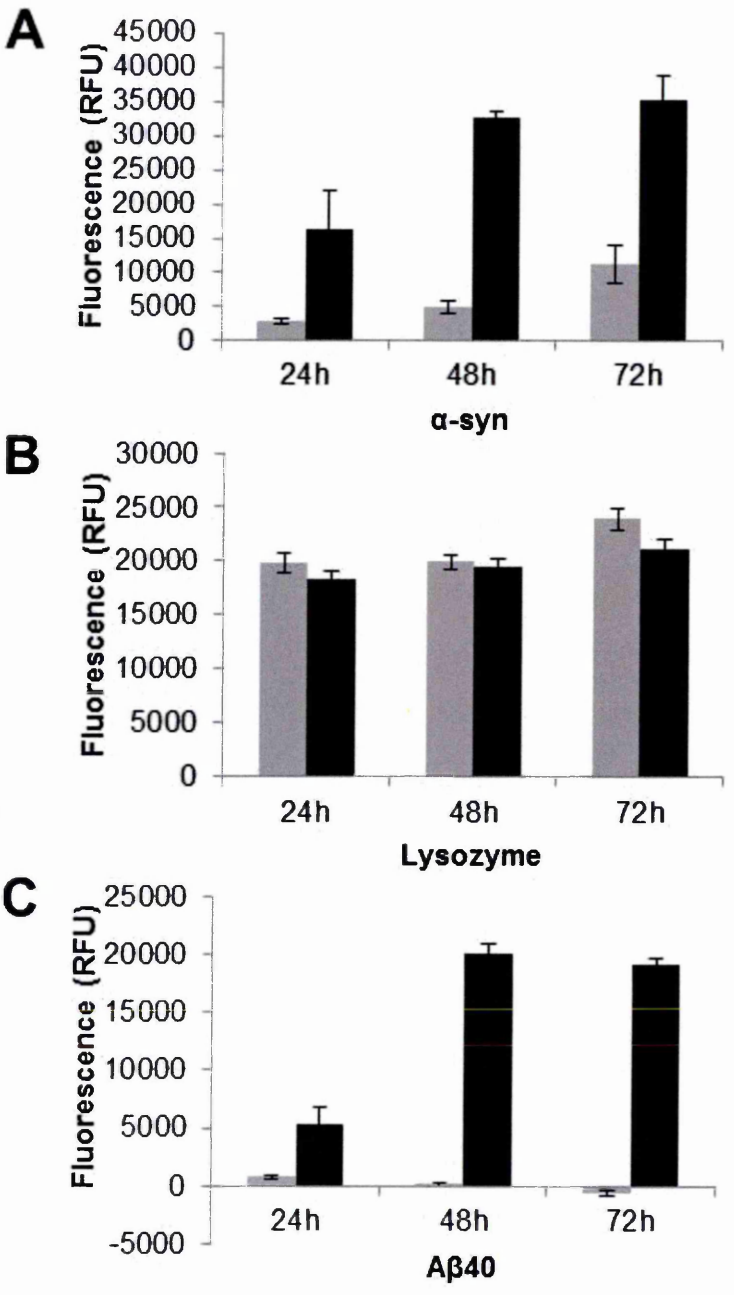

Figure 3.14. Cell membrane integrity and cytotoxic effects caused by amyloid fibrils. SH-SY5Y cells ($2x10^4$/well) were incubated with fragmented and full length fibrils; (A) α-syn (7 μM) and (B) Aβ40 (10 μM) and (C) Lysozyme (10 μM) and fluorescence was recorded over 72 hours (520_{Em}/ 485_{Ex}). Full length fibrils (light grey bars) and fragmented fibrils (dark grey bars) (n=6, SE).

3.3.4. TIRE: Protein: lipid interactions

The TIRE method has recently been adapted to enable the study of protein and peptide interactions at natively derived cellular membranes, utilising electrostatic deposition of cells using the LS method. Figure 3.15 illustrates the process of deposition via LS method, and the monitoring of the water surface pressure upon the addition of cells. The compression of water by barriers shows a linear rise of surface pressure demonstrating the formation of a two dimensional solid phase layer. The subsequent removal of cells by electrostatic adherence to the gold slide can be seen by the 'dips' in the isotherm trace. After cell deposition the surface pressure recovers (20 mN/m) by closing of the barriers allowing reproducible deposition of cells onto gold slides.

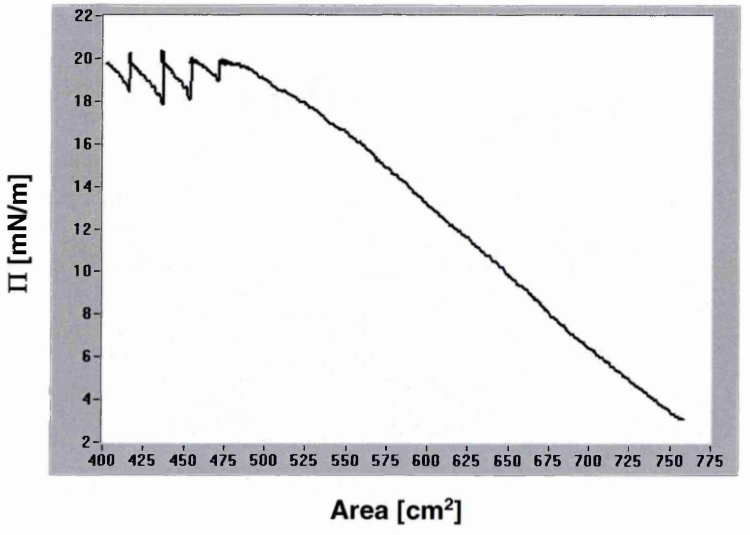

Figure 3.15. Pressure-Area isotherm during LS deposition. Cell deposition on the water sub-phase increases the surface pressure (Π) during barrier compression, once target pressure is reached (20 mN/m) a gold slide is lowered and the removal of cells occurs via horizontal dipping.

The protein: lipid interaction of amyloid fibrils at SH-SY5Y cell membranes was detected using the TIRE method. Each fibril sample was injected into the TIRE cell and incubated for 30 min. Three cell washes (~900 μL) were performed in 1 x PBS buffer (pH 8.0) after protein adsorption, and a single spectroscopic scan was subsequently performed. Fig 3.16 shows a typical set of TIRE Ψ(λ) and Δ(λ) spectra recorded after a spectroscopic scan in 1x PBS of bare gold and Cauchy layer (Fig.3.16 A) and after completion of amyloid protein incubation (Fig. 3.16 B and C). The variable parameter using TIRE was *d* of the adsorbed layer; Cauchy, all other parameters were fixed including the RI (*n*). Experimental data was evaluated by fitting TIRE spectra to the model system using the software provided by J.A. Woollam Ltd (J.A. Woollam 2002) (described in Chapter 1, Fig. 1.8). TIRE analysis focuses on Δ(λ) spectra as it is more sensitive to changes of thickness than Ψ(λ) spectra (Nabok *et al.,* 2005). The four layer model (described in Chapter 1, Table 1.2) was used for TIRE measurements, and the values of *d* and thickness increment (Δd (nm)) were recorded after each spectroscopic scan in steady-state conditions.

The Δ(λ) spectra show protein: lipid binding reactions; a shift of Δ to a higher wavelength (to the right) is associated with an increase in *d*, and a shift to a lower wavelength (to the left) is associated with a decrease in *d*. The magnified Δ(λ) spectra of 3.16 (B) show a negative shift of Δ(λ) to the left of the Cauchy layer (blue line) upon sequential protein incubations of fragmented α-syn fibrils. Fig. 3.16 (C) shows minimal changes to the Δ(λ) position, with 100 μg (pink line) showing an increase in Δ(λ) distinctly to the right. The backward shift seen in Fig. 3.16 (B) is a result of incubation with

fragmented fibrils recording a decrease in membrane thickness. The full length fibrils on the other hand demonstrate a reduced membrane interaction as a result of the negligible shift of wavelength after each protein adsorption (Fig 3.16 (C)).

Figure 3.16. TIRE spectra, multiple spectroscopic scans upon protein adsorption. (A) Typical spectra for the ellipsometric angles $\Psi(\lambda)$ (green curves) and $\Delta(\lambda)$ (red/blue curves). A spectroscopic scan was performed on initial bare Au layer incubated in 0.1 M Cys-HCl before (blue Δ curve) and after cell deposition by LS (red Δ curve) showing an increase in wavelength and thickness. (B) and (C) spectra show an example of sequential injections of α-syn fibrillar material over a concentration range and the changes in $\Delta(\lambda)$ after 30 min incubations (Appendix I and II for Lysozyme and Aβ40 examples of spectroscopic scans).

A

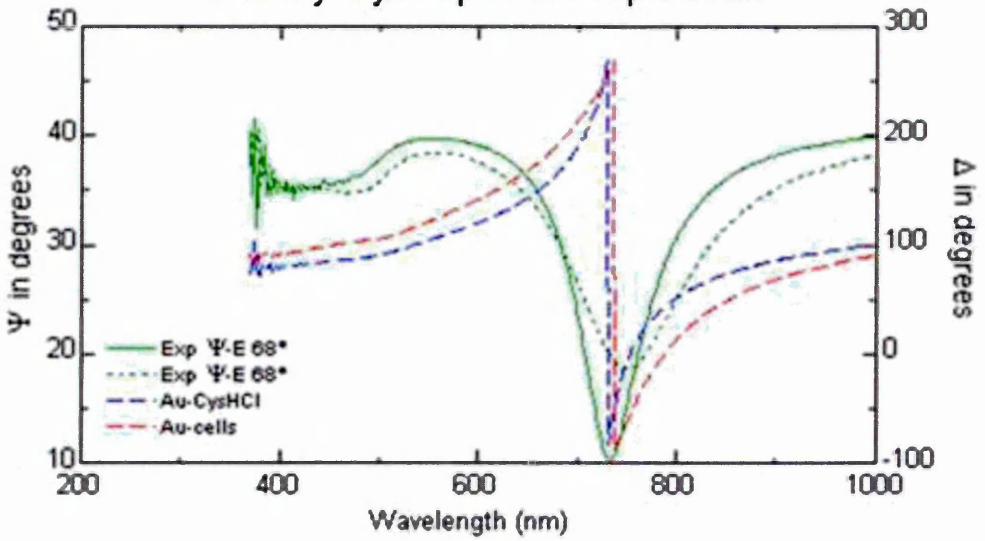
Cauchy layer spectroscopic scan
Ψ in degrees
Δ in degrees
Wavelength (nm)
Exp Ψ-E 68°
Exp Ψ-E 68°
Au-CysHCl
Au-cells

B

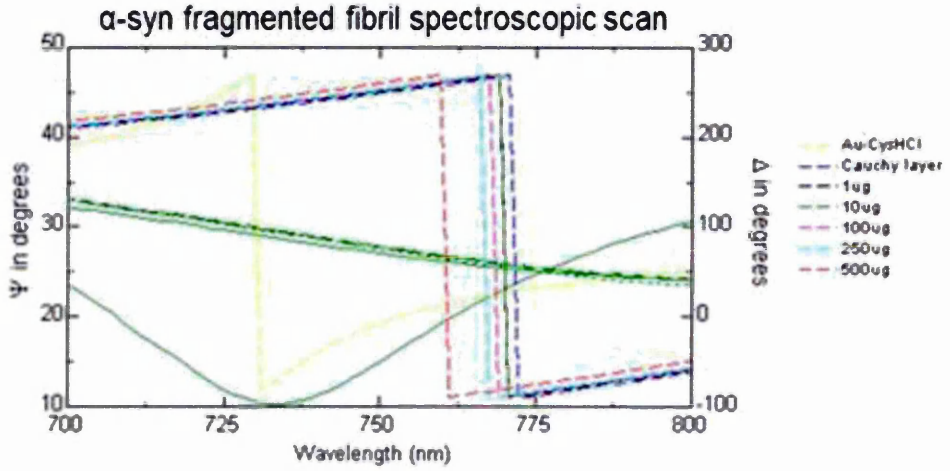
α-syn fragmented fibril spectroscopic scan
Ψ in degrees
Δ in degrees
Wavelength (nm)
Au-CysHCl
Cauchy layer
1ug
10ug
100ug
250ug
500ug

C

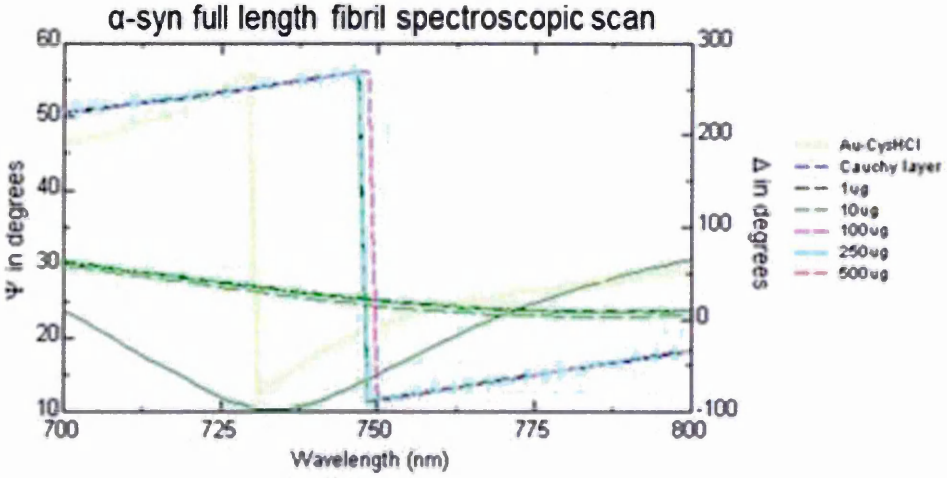
α-syn full length fibril spectroscopic scan
Ψ in degrees
Δ in degrees
Wavelength (nm)
Au-CysHCl
Cauchy layer
1ug
10ug
100ug
250ug
500ug

Figure 3.17 demonstrates the minimal change (averaged 0.07 nm) in thin film thickness over sequential buffer washes (3 x cell volume/ wash), highlighting the stability of the deposited cell membrane.

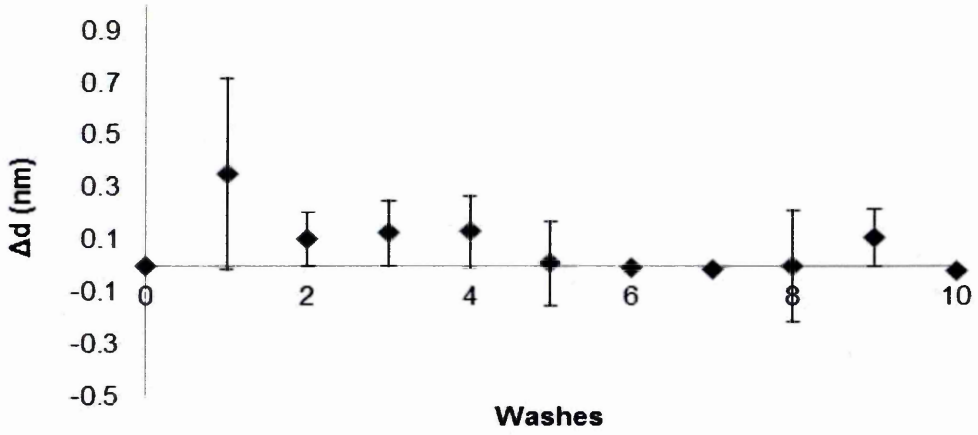

Figure 3.17. Multiple thin-film buffer washes. Monitoring thin film stability during repeated buffer injections (900 µL 1 x PBS/ buffer wash) (n=2, SE).

The obtained changes in effective *d* of the deposited membrane were recorded using the four layer model and interpreted into graphical representation, by the incremental changes in thickness (Δd (nm)) after each concentration, (n=3, SE). Fibrils were sequentially injected over the sensor surface leading to a communicative increase in total deposited fibril material. The concentration of the fibrils injected was taken relative to the monomer from which the fibrils were prepared, ensuring that protein samples are identical in their analysis.

A small loss of material at the TIRE surface can be observed following the addition of full length fibrils prepared from all three proteins between 1-10 µg/ml (Fig. 3.18 A-C), with losses of between -0.5 – 1.8 nm being observed.

The incubation of full length α-syn fibrils initially causes the highest loss of deposited material (-1.8 nm) and recovers to ~0.3 nm at 100 μg/mL (Fig. 3.18 A) after which plateaus around -0.5 nm unlike α-syn fragmented counterparts (Fig. 3.18 D) which continually loses deposited material after each injection. Full length lysozyme (Fig. 3.18 B) and Aβ40 (Fig. 3.18 C) over the concentration range show minimal changes in thickness suggesting reduced membrane disruption, causing a minor loss of up to -0.5 nm overall, compared to -0.8 to -1.0 nm caused by its fragmented counterparts at equivalent concentrations (Fig. 3.18 E and F). The TIRE data shows that at low initial concentrations full length fibrils are disrupting the membrane resulting in a loss of material (Fig. 3.18 A-C) however as the total concentration of the fibrils increases there is some recovery of the total thickness, presumably as the full length fibrils accumulate on the surface. This accumulation could occur via aggregative fibril-fibril interactions which limits their disruptive membrane interaction, or as a result of the saturation of available lipid binding sites causing the plateau in the fibril-membrane interaction as the last of the available binding sites is filled.

Fragmented fibrils display an increased ability when compared to full length fibrils to bind to and disrupt natively derived membranes. These fragmented fibrils are short in length when compared to full length fibrils, as observed by AFM (Fig. 3.9 A-C) and as a result have an increased number of fibril ends. Initial low concentrations between 1-10 μg/mL for fragmented fibrils of α-syn (Fig. 3.18 D) result in a loss of material at the membrane (-1.5 to -2 nm), which is indicative of their cytotoxicity effects (Fig. 3.12 and 3.14). Lysozyme fragmented fibrils exhibit an initial increase in membrane thickness between

1-10 μg/mL reaching ~0.9 nm (Fig. 3.18 ii E), whereas Aβ40 displays a loss of material at 1 μg/mL of ~0.3 nm followed by a slight gain in thickness between 5-10 μg/mL (Fig. 3.18 F). However, after 10 μg/mL both fragmented Lysozyme and Aβ40 fibrils show a noticeable loss of material; ~ -1.0 nm.

These observations demonstrate an accumulation of fragmented fibrillar material at the membranes surface similar to that seen by their full length counterparts, however, upon reaching a critical point results in the loss of material from its surface presumably via membrane disruption, even though additional fibrillar material is being added. The concentration range over which this effect of increasing then decreasing thickness is observed is protein specific, however the pattern of activity is common to all types studied. Fragmented α-syn fibrils display a clear concentration dependent effect (Fig. 3.18 D), causing a substantial loss of membrane thickness of up to -5 nm at 500 μg/mL compared to -1.5 nm by their full length counterparts at its lowest concentration of 1 μg/mL. Whilst fragmented Aβ40 causes its greatest loss of membrane at 20 μg/mL (-0.8 nm) and lysozyme fibrils reach around -1.0 nm at 35 μg/mL. Overall, TIRE data of fragmented fibrils demonstrate enhanced membrane disruption by fibril-membrane association in which material is lost following increased injections (Fig. 3.18 D, E & F). This activity correlates with the enhanced ability to induce dye release from synthetic LUVs (Fig. 3.12) and decrease in cell viability assays (Fig. 3.14).

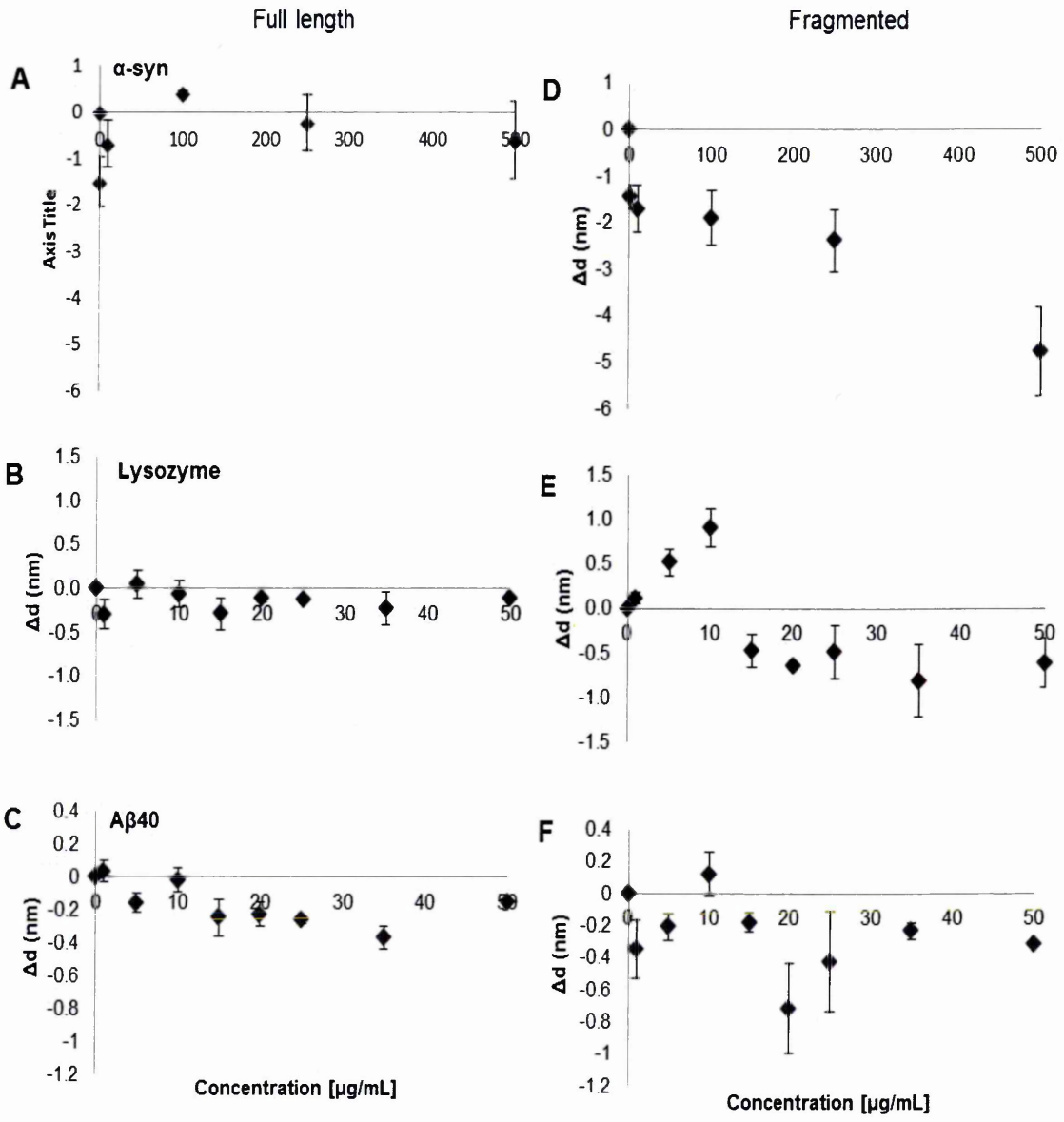

Figure 3.18. Incremental changes of membrane thickness by TIRE. SH-SY5Y cell membranes were deposited by LS method and amyloid fibrils interactions were measured. (A+D) α-syn, (B+E) lysozyme and (C+F) Aβ40. Membrane thickness measured by change in Δd (nm) versus fibril concentration (n=3, SE).

3.4. Discussion

The extent of fibril formation and gross morphology has been shown as protein specific, whereby the generic fibril epitope is present in all three amyloid proteins, but individual differences in protein load causes variances in levels of antibody binding and ThT intensities (Fig. 3.9). These observations support the consensus that the relationship between primary structure and propensity to form fibrils is driven by the interactions between polypeptide chains, whereby amino acid sequence can increase or decrease the rate of protein aggregation, affecting structural details of grown fibrils (Fandrich *et al.,* 2002 and Babenko *et al.,* 2013). Therefore, fundamentally it is the composition and sequence of a peptide or protein that affects its propensity to form amyloid structures (Stefani *et al.,* 2003).

Many proteins are capable of forming amyloid fibrils including α-syn, Aβ40 and lysozyme, with each proteins amyloid formation being associated with a disease-state; Parkinson's disease, Alzheimer's disease and hereditary systemic amyloidosis respectively. Their fibrillar interaction at cellular membranes is likely to be governed by electrostatic and hydrophobic interactions, as reported by Tofoleanu *et al.*, (2012) in the case of Aβ, whose electrostatic interaction between charged peptide residues and lipid head groups modulated Aβ-membrane binding. Furthermore, the hydrophobicity of fibril ends has been suggested as a common property which can cause dramatic distortions in lipid membranes affecting cell viability (Milanesi *et al.*, 2012). Thus proposing a direct relationship between the number of fibrils

ends and membrane binding and/or subsequent disruption, causing the loss of material. This effect is elicited by fibrils from all three studied proteins, demonstrating an enhanced fibril-membrane interaction by fragmented species in particular; resulting in increased cytotoxicity supported by lipid models and cell viability assays (Fig. 3.12 and Fig. 3.14).

The human-derived neuroblastoma cell line, SH-SY5Y is currently used in *in vitro* models for neuron function and differentiation studies in PD. Therefore, the deposition of whole cells by LS method (Fig. 3.15) enabled the *in situ* characterisation of subsequent protein: lipid interactions in an *in vivo* -like model of PD. The combination of LS with electrostatic deposition avoids the use of *in vitro* model lipid bilayers and also fixative methods, which can complicate determining biological changes, due to cellular effects like ischemia within tissue sections (Nakamura 2013). In addition to the novel deposition of native cells the biophysical technique; TIRE, coupled with the fluid cell system with a fixed volume capacity has enabled the detection of native protein interactions *in situ*, identifying a generic mode of action for which three different amyloid proteins elicit at lipid membranes.

The major finding of this work is the characterisation of the interaction of both full length and fragmented amyloid fibrils with natively derived membranes, and the correlation of cytotoxicity via membrane disruption. Our data of fibril-membrane disruption and cytotoxic effects associated with fragmented fibrils complement published findings, where short fragmented fibrils present a generic mechanism of action by which fibril associated cytotoxicity is enhanced. This interaction is dependent on the length of the fibrils in question with a decrease in length and a subsequent increase in fibril end

number, resulting in disruption and loss of natively derived lipid material derived from whole SH-SY5Y neuronal cells in an *in vivo* model (Fig. 3.18). Our findings correlate to published work by Xue *et al.,* (2009) who demonstrated using *in vitro* synthetic lipids, that fibril length correlates with the ability to disrupt membranes and subsequently reduces cell viability. Using FTIR spectroscopy they confirmed that no significant structural perturbations occurred upon generation of fragmented fibrils and that only the physical attribute altered was length. This observation is in accord with our own AFM images (Fig. 3.9) that show a change in length of the aggregated material. Carboxyfluorescein encapsulated liposome dye release assays (Fig. 3.11 & 3.12) showed that fibril fragmentation enhanced the ability to disrupt liposome membranes over full length fibrils; which was also seen by Xue *et al.*, (2009). Hence the results presented here are comparable to those previously reported *in vitro*. These observations highlight the importance of fibril length and the associated membrane disruption abilities. A direct result of membrane disruption *in vivo* would lead to a loss in cell viability; and this hypothesis was investigated using CellTox Green (Promega). This relatively novel assay has been recently used to help identify and characterise potential therapeutic agents in treating a parasitic disease, which alters cell membrane structure resulting in apoptosis (Suleman *et al.,* 2014). Our results using CellTox demonstrated that fragmented fibrils caused a loss of membrane integrity upon incubation with SH-SY5Y cells, resulting in cytotoxic effects (Fig. 3.14). This effect is much greater than their longer full length counterparts. These results are in agreement with Xue *et al.,* (2009) MTT assay; where fragmented fibrils

exhibited a higher cytotoxic effect to SH-SY5Y cells resulting in decreased cell viability. However, our data demonstrates the potential mode of action, with CellTox assay results suggesting that the loss of cell viability is due to direct fibril-membrane interaction, causing a physical disruption of membranes and subsequent cell death. This would be an additional mechanism of action to that proposed by the internalization of the fragmented cells due to their reduced size (Jakhira *et al.,* 2014). It has also been demonstrated using liposomes and cryo-EM that the fibril interaction is via the fibril end, penetrating the lipid membrane and causing subsequent removal or blebbing (Milanesi *et al.,* 2012). Further to these observations our novel TIRE biophysical data utilising natively derived cellular membranes from a model neuronal cell line; SH-SY5Y, has indicated a generic mechanism of membrane disruption by three amyloid proteins, with fragmented fibrils resulting in an increased loss of material presumably by the same blebbing mechanism observed by cryo-EM.

In conclusion, we provide additional mechanistic insight into how fibrils interact with natively derived membranes by applying TIRE, showing an overall cytotoxic effect caused by amyloid fibrils and in particular fragmented fibrils causing enhanced cell toxicity by stripping material from membranes.

3.5. Summary

I. Findings from TIRE data demonstrated that fragmented fibrils from all three proteins were able to cause enhanced membrane disruption using the model cell line SH-SY5Y, compared to their full length counterparts.

II. Using *in vitro* assays including artificial membranes in dye release assays and a cell viability assay in cultured SH-SY5Y cells, fragmented fibrils corroborated the generic effect seen using TIRE, and displayed increased membrane disruption and cytotoxicity effects than full length fibrils.

4.1. Introduction

4.1.1. Protein targeting

The proper localisation of proteins to their specific subcellular location is essential for sustaining order and organisation in all cells (Akopian *et al.*, 2013). Therefore a major question is how a cell regulates the trafficking of thousands of different proteins, each with specific functions and selective targets. Physicochemical properties such as internal signal sequences and transmembrane domains help mediate the delivery of proteins (Dhanoa *et al.,* 2010), dictating their targeting via either a post-translational mechanism whose preprotein is fully synthesised and released into the cytosol before delivery, or via co-translational mechanism whose nascent polypeptide is still attached to the ribosome upon organelle targeting (Zimmerman *et al.,* 2011). The study of membrane associated events is vital for numerous cellular processes, but observing their interactions is complicated by the technical issues posed by their lipid environments. This results in utilising various biochemical and biophysical methodologies to study such interactions, but which is hindered by problems regarding the purification of the proteins and correct folding to maintain activity (Kriechbaumer *et al.*, 2012 (A)). Therefore, the development of techniques to investigate how proteins interact with native membranes is vital, working towards a greater understanding of diseases and the development of new therapeutics.

4.1.2. Chloroplasts (CP) and protein targeting pathways

One of the destinations for proteins is the chloroplast (CP), these are highly specialised organelles performing essential functions in green tissues of plants such as; photosynthesis - converting energy into food and oxygen vital for the survival of all living organisms, and nitrogen and amino acid metabolism. They evolved like mitochondria through an endosymbiotic event from once free living prokaryotic cells, followed by the relocation of most endosymbiotic genes from the progenitor organelle to the host cell nucleus, leaving CPs with only ~100 protein encoding genes important for photosynthesis and other CP functions. This resulted in the development of complex mechanisms to transport ~3000 proteins into the CP and thus requiring stringent and specific import processes (Jarvis *et al.,* 2001 and Schewenkert *et al.,* 2011). The CP is composed of six distinct sub-organellar compartments: three membranes consisting of a membrane bilayer which is separated by two envelope membranes (outer and inner membrane), and internal thylakoid membranes creating three aqueous compartments, containing the intermembrane space of the bilayer, the stroma and thylakoid lumen spaces (Fig. 4.1) (Jarvis *et al.,* 2008).

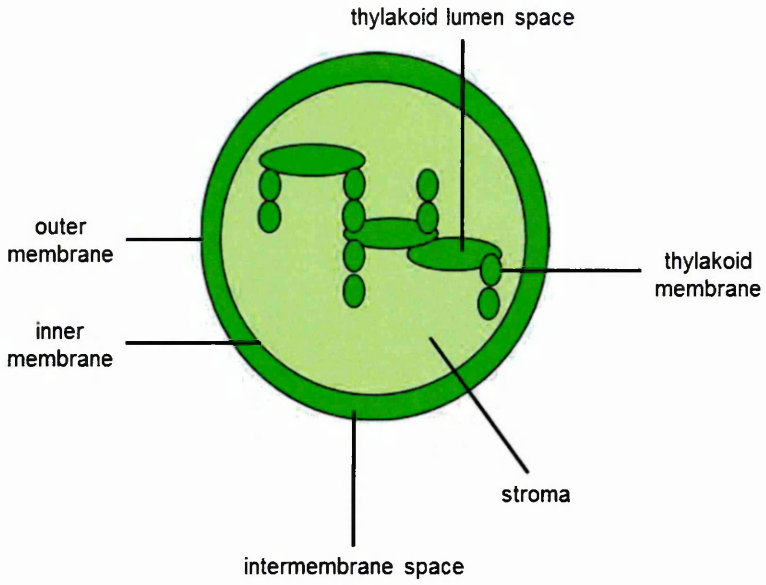

Figure 4.1. The sub-compartments of the chloroplast. The CP is composed of six distinct sub-organellar compartments.

The structural intricacy within the CP poses several obstacles to the plant cell regarding the targeting of preproteins, including specificity of targeting, transport across the outer and inner envelope membrane, and finally correct targeting and assembly within the CP. Significant mistargeting of preproteins would likely present cytotoxicity problems (Jarvis *et al.,* 2001 and 2008). Phylogenetic evidence has shown that a combination of protein import machinery derived from pre-existing cyanobacterial proteins, with the addition of novel subunits such as; surface receptor proteins and cytosolic factors known as chaperones, has helped to provide specificity and directionality of protein transport into CPs (Jarvis *et al.,* 2001).

The machinery proposed to be responsible for the import of the majority of plastids proteins is the translocon at the outer chloroplast (TOC) envelope. This is responsible for the recognition and translocation of the preprotein

through to the translocon at the inner envelope of the CP (TOC-TIC system) (Cline *et al.,* 2008), the TIC complex then targets the translocated preprotein to the stroma. The selectivity of proteins to their target destinations is governed by following distinct pathways according to their particular targeting sequences. For the endoplasmic reticulum (ER) protein targeting is mostly by a co-translational mechanism, employing N-terminal transmembrane segments or cleavable signal sequences such as the signal recognition particle (SRP) (Mandon *et al.*, 2007). The association of the SRP to a hydrophobic sequence within the nascent polypeptide chain enables the delivery of membrane and secretory proteins to the Sec61 protein channel whilst it's still attached to the translating ribosome. Binding to the SRP receptor on the ER membrane causes the hydrophobic signal peptide to be cleaved in an energy dependent manner (Colombo *et al.,* 2009 and Akopian *et al.*, 2013). In contrast, CP protein import is predominantly a post-translational process, due to the co-translational pathway not being accessible to a large group of membrane proteins which are classified as tail-anchored proteins (TA protein) (Colombo *et al.,* 2009).

4.1.3. Post-translational targeting and tail-anchored proteins.

Protein import into CP's occurs post-translationally, and is a highly complex process utilised by TA proteins. TA proteins are a class of integral membrane proteins that contain a single hydrophobic transmembrane domain (TMD) at their C-terminus. TA proteins do not harbour a cleavable signal sequence at

the N-terminal as used in co-translational targeting (Lee *et al.,* 2014), instead they depend on signal sequences in the C-terminal and TMD for membrane targeting information (Borgese *et al.,* 2011). This is due to the close proximity of a TA protein's TMD to its C-terminus causing it to be still inside the ribosome tunnel when the termination codon is reached, therefore making the TA protein unavailable to SRP binding during translation. As a result, membrane insertion of a newly synthesised TA protein occurs post-translationally (Abell *et al.,* 2011) making the structure and targeting of these TA proteins a model system to study.

TA proteins function in a wide range of cellular processes and at a variety of intracellular membranes, including the regulation of apoptosis, trafficking in the secretory pathway and protein translocation (Borgese *et al.*, 2003 and Abell *et al.,* 2011). Examples of TA proteins include the soluble *N*-ethylmaleimide-sensitive factor attachment protein receptors (SNAREs) which mediate fusion of cellular transport vesicles with cell membranes; also Toc34 is a member of the outer membrane translocon complex in CPs which mediates protein import. The functions of these proteins are inextricably linked to their localisation, and therefore raises the question of how is organelle targeting specificity achieved? (Borgese 2003).

Many TA proteins have been identified in mammalian and yeast model systems, but our understanding of plant TA proteins is rudimentary, due to only a few authentic plant TA proteins have been identified and investigated (Dhanoa *et al.,* 2010) these include; Toc33 and Toc34 in *Arabidopisis thaliana* (Lee *et al.,* 2014, Qbadou *et al.,* 2003). Therefore, bioinformatic searches have been utilised to identify putative TA proteins encoded by the

Arabidopsis thaliana genome (Pedrazzini *et al.,* (2009) and Kriechbaumer *et al.,* (2009)). A large-scale bioinformatics search was performed entailing a number of features of TA proteins which were combined to predict their localisation. Kriechbaumer *et al.,* (2009) specified algorithms parameters requiring: a C-terminus of 30 residues maximum, a TMD within the C-terminus of 50 residues, the specific absence of additional TMDs, and lack of secretory signal peptides or N-terminal signal sequences. Kriechbaumer *et al.,* (2009) successfully assigned 130 TA proteins including 29 associated with plastids, which there is currently limited data for. The predictions correlated well with the SUBA database (SUB-cellular location database for *Arabidopsis* proteins) and the proteins identified - in particular the plastidial TA proteins are now valuable tools for understanding post-translational protein targeting, and may help reveal further information on the selectivity of these proteins to their targeted organelles. Dhanoa *et al.,* (2010) recently undertook a comparative analysis of the requirements for the targeting and insertion mechanisms of three plastid TA proteins; Toc33, Toc34 involved in the import of transit peptide-containing precursors to CP, and the novel outer envelope protein 9 (OEP9) as identified by Kriechbaumer *et al,.* (2009). Results demonstrated that there were at least two distinct sorting pathways for TA outer envelope proteins, mediated by the nature of molecular targeting signals, and the membrane protein and lipid components involved. It was established that the C-terminus and TMD sequences for OEP9 were necessary and sufficient for CP targeting, whereas the targeting of Toc33 and Toc34 depended on almost the entire protein sequence, with additional targeting signals in the N-terminus GTPase (Dhanoa *et al.,* 2010).

Figure 4.2 shows the post-translational targeting of TA proteins to peroxisomes, mitochondria, CPs or the ER, following synthesis on free polyribosomes in the cytosol. From the ER, TA proteins are also targeted to internal organelles within the endomembrane system via vesicular trafficking. Based primarily on studies of TA protein, their biogenesis in yeasts and mammals (reviewed in Borgese *et al.,* 2003, 2007 and High and Abell 2004) shows selective targeting of nascent TA proteins from the cytosol to peroxisomes, mitochondria, CP or ER, and depends on the TA protein following one or more distinct pathways. Due to the post-translational targeting and highly hydrophobic nature of TA membrane proteins, it is logical to propose that their targeting to the outer CP envelope would utilise cytosolic factors; like chaperones, to ensure their safe arrival at the organelles target surface in an import-competent, unfolded state (Jarvis *et al.,* 2008).

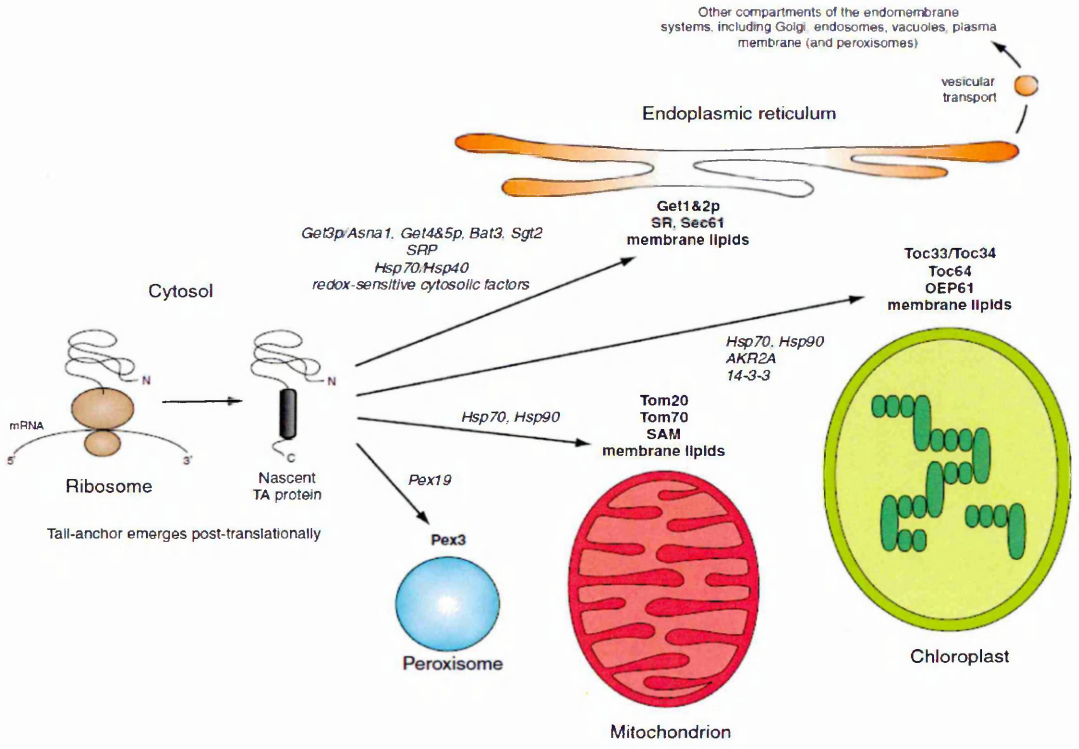

Figure 4.2. Known and predicted targeting pathways for plant TA proteins. TA protein targeting post-translationally to various organelles externally or internally. Each of these pathways is mediated by specific cytosolic chaperones and targeting factors (*italicized*) and/or cognate membrane-bound receptor and insertion machineries (**bold**) (Abell and Mullen 2011).

4.1.4. Cytosolic cofactors: Molecular Chaperones

Molecular chaperones have well established functions as heat shock proteins (Hsp) helping cells deal with cellular stresses, such as high temperature, changes in pH and the stabilisation of protein structures

working to prevent the aggregation and/or the degradation of misfolded proteins (Kriechbaumer *et al.*, 2011). The post-translational targeting of proteins to organelles like mitochondria are well established, and these pathways commonly depend upon cytosolic cofactors in an energy dependent manner, acting to maintain the preproteins in its unfolded state which ensures competent translocation into or across the organellar membrane (Abell *et al.,* 2007). Abell *et al.,* (2007) identified novel interactions between a model TA protein; Sec61β, and two cytosolic chaperones Hsp40 and Heat shock constitutively expressed 70 (Hsc), demonstrating its targeting to the ER in an SRP independent manner via chaperone-mediated targeting. Therefore, proposing a chaperone-mediated route distinctive from the well-established SRP-dependent pathway in co-translational protein targeting.

Three chaperone mediated pathways have been documented so far for ER-targeted TA proteins: one mediated by SRP in a post-translational manner, another by Hsc70 and Hsp40 chaperones and last by a novel ATPase (known as the 'guided entry for tail anchored proteins' (Get) pathway in yeast and the transmembrane recognition-complex (TRC) in mammal systems), acting as a chaperone binding at the TMD of a nascent ER destined TA protein, and directing its subsequent insertion into the ER membrane (Borgese *et al.,* 2011 and Stefanovic *et al.,* 2007). Although the Get/TRC pathway using cytosolic cofactors has been well characterised in mammalian and yeast systems, it has not yet been investigated in detail in plants.

4.1.5. Chaperones & plant TA protein targeting

An example of a molecular chaperone that is involved in protein targeting to all organelles is Hsp70 (Zimmermann 1998; Artigues *et al.*, 2002; Soll, 2002; Abell *et al.*, 2007; Kriechbaumer *et al.*, 2012 (A)). Cytosolic chaperones such as Hsp70 can be constitutively expressed (Hsc) or stress-induced (Hsp) depending on cellular environmental conditions. A common structural feature of the Hsp70 family is an amino terminal ATPase and a carboxy-terminal substrate binding domain; composed of a β-sandwich subdomain and a α-helical lid segment (Fig 4.3). They act through cycles of substrate binding and release, governed by adensosine triphosphate (ATP) binding and hydrolysis (Vabulas *et al.,* 2010 and Young *et al.,* 2003).

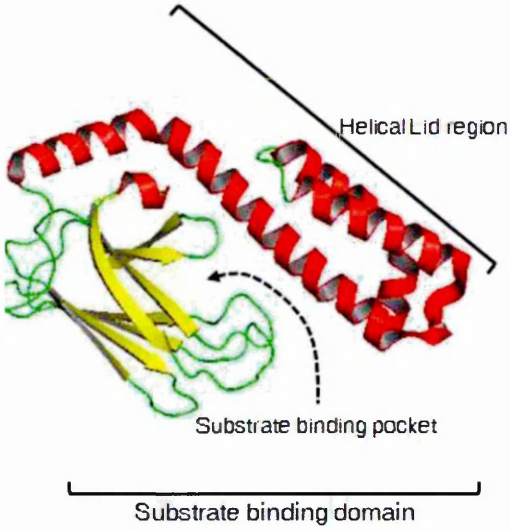

Figure 4.3. The structural features of molecular chaperone; Hsp70. Depicting a β-sheet sandwich substrate binding pocket and α-helical 'lid' region. When an Hsp70 protein is ATP bound, the lid is open and peptides bind and release, and when ADP bound, the lid is closed and peptides are tightly bound to the substrate binding domain (HSPIR 2014).

The chaperone mediated pathways have led to numerous studies focussing on characterising protein interactions between CP-targeted TA proteins and chaperones, and identifying chaperone-like receptors at the CP membrane which act as preprotein recognition/binding sites for subsequent protein import (Qbadou *et al.,* 2006, Von L'Oeffelholz *et al.,* (2011) and Kriechbaumer *et al.,* 2011). Although some propose that chaperones may be unlikely to achieve protein targeting alone, they do provide differential binding of family members to targeting sequences, which can potentially offer a mechanism for achieving specificity of binding. A study by Kriechbaumer *et al.,* (2012 (B)) established the role of cytosolic factors with regards to efficiency and targeting specificity using import competent CP and TA proteins as a model system. The level of targeting of the TA protein; Toc33 (a component of the CP translocase) was found to be specific for CP membranes in the absence of chaperones, but upon addition of the chaperone, Hsp90, saw a ~2 fold increase in targeting efficiency. Over all findings revealed that cytosolic factors like Hsp70 and Hsp90 do not play a major role in determining the specificity of targeting, but upon their addition can increase the efficiency of targeting by ~50 %.

Chaperone receptors have been well studied, revealing a consistent feature of a clamp-type tetratricopeptide repeat (TPR) domain (Fig 4.4), which is highly specific to binding chaperones (Qbadou *et al.,* 2006 and Schwenkert *et al.,* 2011); containing basic residues promoting its interaction with the carboxylate groups of chaperones, such as Hsp70 and Hsp90 at their C-terminus end (Kriechbaumer *et al.,* 2011).

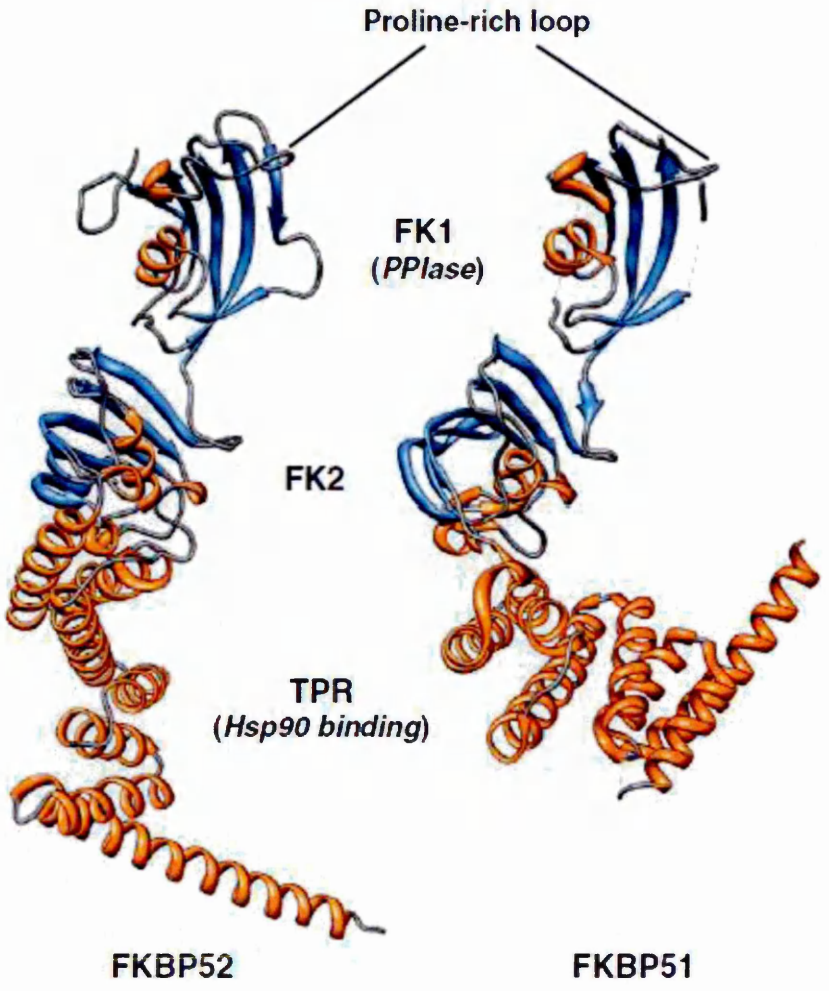

Figure 4.4. Structural TPR motif enabling protein-protein interactions. Crystallographic structures of two human steroid hormone receptors; FKBP52 and FKBP51, which bind the molecular chaperone Hsp90 via a C-terminal tetratricopeptide repeat (TPR) domain whose structural motif acts a binding scaffold and binds to the EEVD motif in the extreme C-terminus of Hsp90 (Storer *et al.,* 2011).

Figure 4.5 shows the proposed pathways for newly synthesised preproteins in the presence of cytosolic chaperones, and their roles in facilitating protein targeting to the CP surface (Paila *et al.,* 2013). Individual TPR domains have previously been shown to selectively discriminate between the two chaperones; Hsp70 and Hsp90. For example the Hsp70/90 organising protein (HOP) containing three TPR domains, have all been shown to present different binding affinities for Hsp70 and Hsp90 (Schmid *et al.,* 2012). The plastidial chaperone receptor Toc64 has been localised at the outer envelope membrane, and also features three TPR domains (Sohrt and Soll 2000) similar to the motifs present in Hsp70 and Hsp90. Qbadou *et al.,* (2006) demonstrated that the C-terminal TPR clamp domain of Toc64 mediated the docking of Hsp90-associated pre-proteins, whilst showing low efficiency binding with Hsp70, suggesting a preference of chaperone binding by the receptor; Toc64.

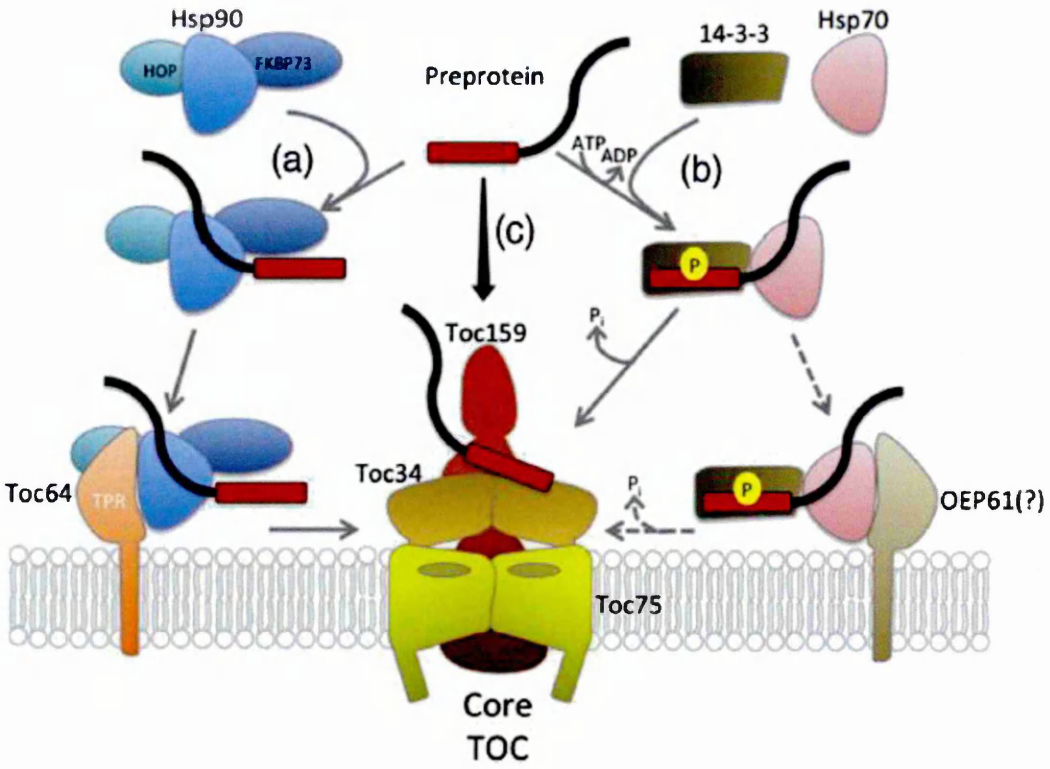

Figure 4.5. The cytosolic chaperone systems and their role in targeting of preproteins to the core TOC complex. Three pathways have been proposed: (a) Hsp90 along with co-chaperones bind preproteins and dock at the outer envelope membrane via an interaction with the exposed TPR domain of Toc64, which then delivers the preprotein to the core TOC complex. (b) Hsp70 binds the newly synthesised preproteins binding to exposed TPR domains of the outer envelope protein 61 kDa (OEP61), proposed to facilitate preprotein transfer to the core TOC complex. Finally (c) is the direct binding of cytoplasmic preprotein to Toc34 and Toc159 receptors at the TOC core complex (Paila *et al.,* 2013).

Von L'Oeffelholz *et al.,* (2011) identified an uncharacterised protein in *Arabidopsis thaliana* localised at the outer envelope of the CP membrane; OEP61, containing a TPR clamp domain at its N-terminus and a single TMD

at its C-terminus. Thus OEP61 shared common features with the TA plant chaperone receptor Toc64, possibly providing an additional cytosolic binding site at the CP outer membrane. Binding assays showed that OEP61 specifically interacted with the chaperone; Hsp70 via the TPR domain, and was capable of binding selectively to CP precursor complexes, including some TA proteins - suggesting this receptor may have complementary function with Toc64 to facilitate TA protein targeting (Abell *et al.,* 2011). Recent research by Schweiger *et al.,* (2012) and Schweiger and Schwenkert (2013) have proposed that although the plant specific protein AtTPR7 (aka OEP61- named by Von L'Oeffelholz *et al.,*) does function as a chaperone docking protein, it can bind both chaperones; Hsp70 and Hsp90, albeit with different affinities, and its localisation resides in the ER membrane. AtTPR7 was identified as an interaction partner of *Arabidopsis* Sec63 homologue; AtERdj2, a component of the ER Sec translocon, suggesting it (OEP61) plays a role in post-translational import into the ER. Although the role of OEP61/AtTPR7 has still not been properly defined, the receptor may act at both membranes (possibly under different conditions) as a cytosolic binding site within the post-translational import of TA proteins.

Recent studies by Kriechbaumer *et al.,* (2011, 2012 (A)) have utilised the novel spectroscopic technique; total internal reflection ellipsometry (TIRE) to study the binding of molecular chaperones to recombinant protein receptors, and at natively derived CP membranes respectively. Establishing OEP61 as a CP receptor which shows preferential binding to the molecular chaperone, Hsp70, but requiring further work to consolidate this finding.

4.2. Aims of Model II - protein: protein interactions

I. To employ the TIRE method for the detection of molecular chaperone binding to receptor deficient CP membranes, deposited by LS method.

II. To assess the binding of TA proteins with CP membranes and evaluate binding interactions of cytosolic co-factors; molecular chaperones Hsp70 and Hsp90, with TA proteins *in vitro* using radiolabelled proteins.

III. The phenotypic analysis of receptor deficient CP membranes of *Arabidopsis thaliana* plants by RNA tissue extraction and electron microscopy.

4.3. Results

4.3.1. TIRE & Knock out (KO) mutant chloroplast targeting

The novel CP receptor, OEP61, was identified by Von L'Offelholz *et al.,* (2011) by gene sequence analysis. The receptor was shown to be capable of binding selectively to CP precursor complexes, including some TA proteins, and has been associated with protein import showing a strong affinity for the molecular chaperone, Hsp70. Previous work by Kriechbaumer *et al.*, (2011) employed TIRE to measure molecular chaperone binding to soluble recombinant chaperone receptor proteins, Toc64 and OEP61, lacking their transmembrane domain (TMD). Using TIRE, a clear discrimination between specific and non-specific binding of chaperone proteins and their isoforms to a particular receptor was established, with Toc64 showing higher affinity for Hsp90, and OEP61 for Hsp70. Further work was performed utilising the novel method of LS to deposit natively derived CP membranes from pea plants. Kriechbaumer *et al.,* (2012 (A)) repeated chaperone incubation with native CP membranes and obtained binding properties which were consistent with previous data showing receptor dependent binding (Kriechbaumer *et al.,* 2011). It is assumed that chaperones must be binding to OEP61 and Toc64, as these are the only known CP examples of TPR clamp receptors at the outer CP membrane. However, it has not differentiated between cognate receptor- chaperone binding *in situ*, and it cannot be excluded that chaperones may be binding to undiscovered CP receptors. Hence, it is necessary to test for additional chaperone-receptor

interactions by comparing chaperone binding for wild-type (WT) *Arabidopsis* CP's and CP's derived from OEP61 and Toc64 knock-out (KO) mutants using TIRE.

Figure 4.6 illustrates a typical isotherm showing cell deposition via LS method and the monitoring of the water surface pressure upon the addition of cells. The compression of water by barriers shows a linear rise of surface pressure demonstrating the formation of a two dimensional solid phase layer. The subsequent removal of cells by electrostatic adherence to the gold slide can be seen by the 'dips' in the isotherm trace, which then recovers to its target pressure by further closing of the barriers, allowing reproducible deposition of cells onto gold slides.

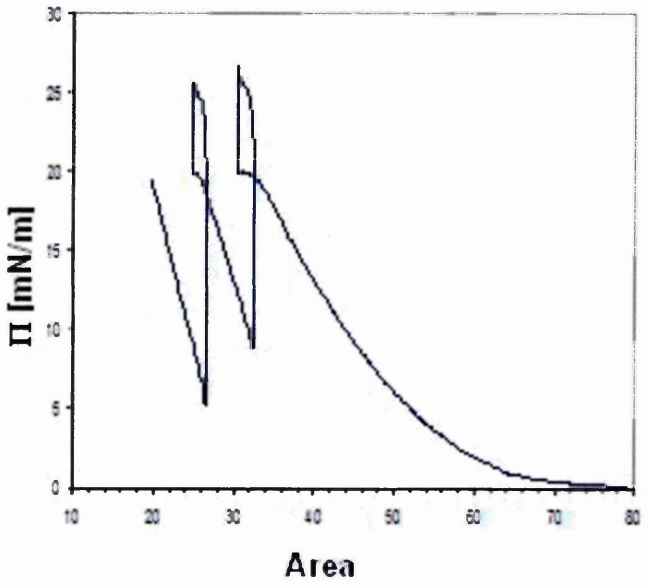

Figure 4.6. Pressure-Area isotherm during LS deposition. A typical pressure-area isotherm of LS CP deposition, the cells on the water sub-phase during barrier compression changes the surface pressure (Π), once target pressure is reached (20 mN/m) the gold slide is lowered and the removal of cells occurs via horizontal dipping.

To define the contribution of each receptor to chaperone binding, *Arabidopsis thaliana* CPs deficient of either the OEP61 or Toc64 receptor were deposited using LS method (Fig. 4.6) Chaperone binding was subsequently measured using TIRE method (Chapter 1, Fig. 1.8) and the four-layer model (Chapter 1, Table 1.2) where a single spectroscopic scan was used for fitting TIRE data (as described in Chapter 3), plotting an increase in layer thickness (Δd (nm)) against increasing protein concentrations.

Figure 4.7 (A and B) shows WT CP (diamond) binding to respective chaperones; Hsp70 and Hsp90, displaying a concentration dependent effect from 0.001-100 μg/ml. Truncated chaperones (Hsp70-C, Hsp90-C) lack a C-terminal heptapeptide (PKIEEVD for Hsp70) or pentapeptide (MEEVD for Hsp90), which are responsible for specific binding to the TPR domain of receptors at the CP membrane (Kriechbaumer *et al.,* 2012 (A)). As a result of truncation, binding is considerably decreased in Fig. 4.7 (A and B) from 2.5-3.0 nm (WT - diamond) to < 0.6 nm (triangle), with a loss of concentration dependence as seen for WT CP. This confirms that binding is due to a specific interaction between TPR domains of receptors and the C-termini of chaperones, ruling out non-specific chaperone activity.

To test whether the targeting of each chaperone is specific to a particular membrane receptor, the full-length chaperone was incubated with CPs deficient of a specific chaperone receptor, and monitored utilising TIRE. This was achieved via the deposition of natively derived KO CP membranes: KO oep61 (square) or KO toc64 (circle) respectively. (Mutant CPs: triple KO

Toc64 was provided by the Jarvis group, published by Aronsson *et al.,* 2007, and OEP61 KO by T-DNA insertion provided by the Abell group, SHU).

The incubation of each chaperone with the KO CP which retained its proposed cognate receptor (Fig. 4.7 A, circle: Toc64-Hsp70, and B, square: OEP61-Hsp90) showed protein binding of > 2.0 nm, displaying a positive concentration dependence similar to WT CP binding. However, when each chaperone is incubated with its KO CP lacking its proposed cognate receptor, target binding is noticeably reduced. Upon OEP61 receptor removal, Hsp70 binding is dramatically decreased from ~2.5 nm to <0.2 nm (square). This is also seen for Hsp90, whereby the removal of Toc64 receptor results in loss of Hsp90 binding from 3.0 nm to ~1.0 nm (circle) at its highest concentration (100 μg/ml). Therefore, the detection of specific binding of proteins to their cognate receptors has been shown using TIRE, and demonstrates that there are no other receptors that make a substantial contribution to binding of Hsp70 and Hsp90 at the CP outer membrane.

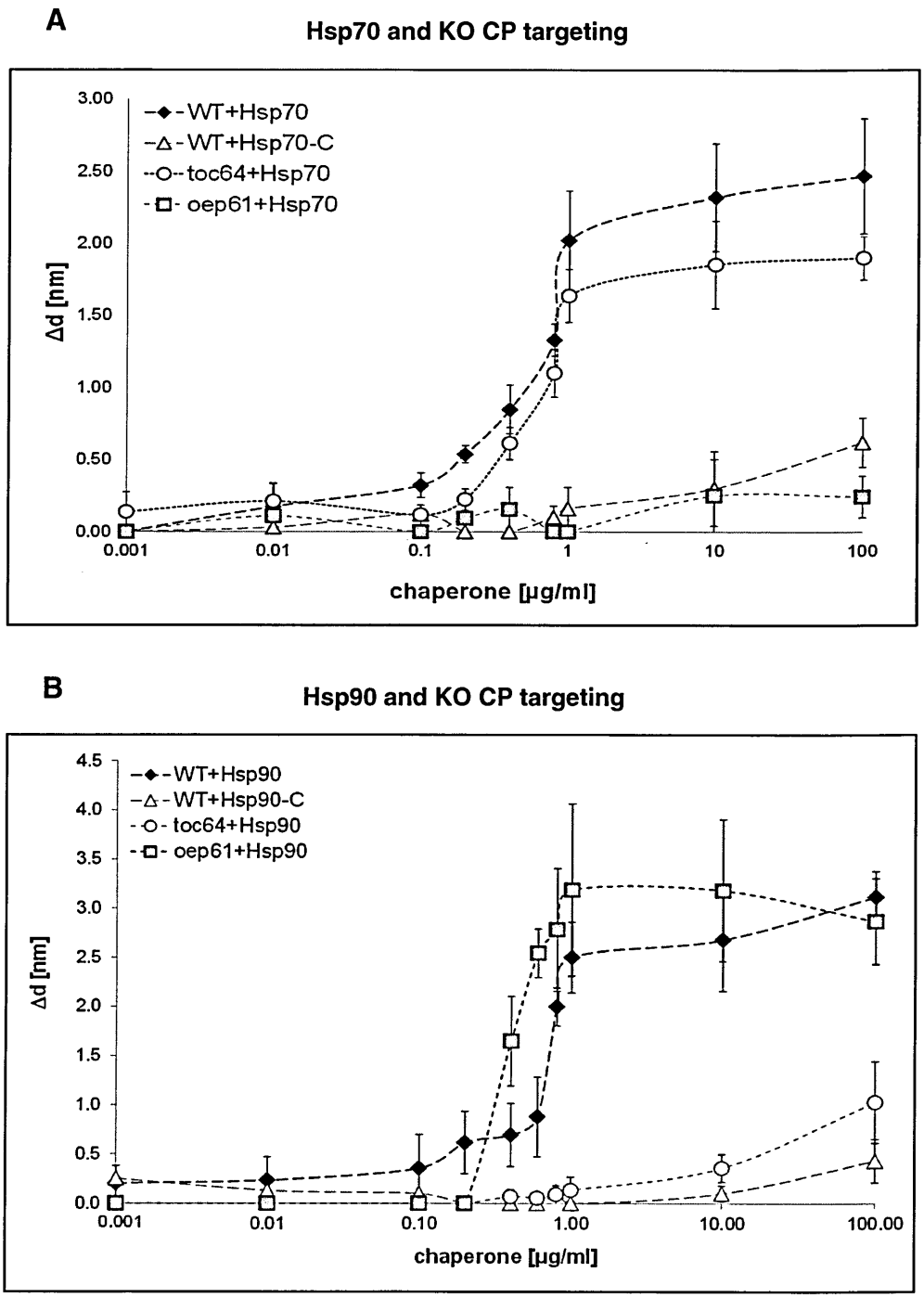

Figure 4.7. TIRE & chaperone binding at KO CP membrane: TIRE data illustrates the change in binding (Δd, nm) as a result of chaperone concentration (µg/ml). WT CP (diamond), WT CP and truncated chaperone (triangle), KO Toc64 (circle) and KO OEP61 (square). TIRE binding of the chaperone Hsp70 (A) and Hsp90 (B), to WT and KO CP membranes (n= 3, SE).

4.3.2. Protein targeting and molecular chaperones as cytosolic co-factors

Chaperones are able to bind specifically to receptors at the outer CP envelope (Kriechbaumer *et al.,* 2012 (A)), whose functional role is to maintain and stabilise pre-proteins as they are directed to their target membranes, and may also increase targeting efficiency. TA proteins are a class of integral membrane proteins that contain a single hydrophobic TMD close to the C-terminus. The proximity of the TMD and C-terminus means that the hydrophobic preprotein tail emerges from the ribosome only after termination of translation, and is therefore a model system for post-translational targeting (Borgese *et al.,* 2007).

Possible targeting pathways of chaperones and TA proteins are shown in Figure 4.8, including the direct binding of TA protein to the translocon complex (Toc75, Toc34 and Toc159) at the CP membrane, or a combination of TA-binding with chaperones and subsequent chaperone receptors, followed by protein insertion/ translocation.

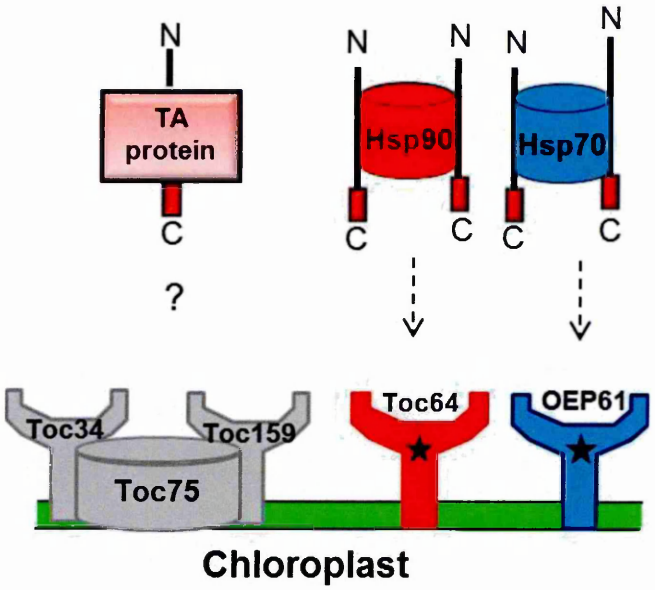

Figure 4.8 Schematic of post-translational targeting model for TA proteins. A proposed targeting model of TA protein binding at the outer CP envelope, unaccompanied or in the presence of cytosolic co-factors; Hsp70 and Hsp90. The specificity of TA protein binding is unknown (?), chaperones are hypothesised to increase targeting efficiency via their cognate receptors at the outer CP envelope; Hsp90 to Toc64, and Hsp70 to OEP61 (dotted arrows). Therefore, TA protein may bind directly to the translocon channel (Toc75, Toc34 and Toc159), or they may initially bind to chaperones and their cognate receptors for protein docking, followed by translocation via the translocon channel.

Protein targeting was tested using a defined cell free system comprising radiolabeled nascent proteins and purified CP organelles. To synchronise the targeting environment, translated proteins were generated without a stop codon, thereby locking the protein on the ribosome, which was subjected to centrifugation to separate the RNC from other cytosolic components of the

lysate. The purified RNC was resuspended in a physiological buffer and, once the targeting assay was assembled, was released from the ribosome by puromycin treatment. After incubation with organelles and cytosolic factors, the organelles were separated by centrifugation, washed and subjected to analysis after phosphor exposure to measure protein-CP binding. Kriechbaumer *et al.,* (2012 (B)) demonstrated that upon release of the nascent chain, free ribosomes that remained within the sample did not contribute significantly to targeting efficiency, and therefore could be assumed not to have any impact on subsequent binding assays.

Two TA proteins were selected from the TA plastids identified by a bioinformatics screen performed by Kriechbaumer *et al.,* (2009): TA At1g17780.1 (TA17) and TA At3g63160.1 (TA63). The gene sequences for each TA protein (including the T7 promoter region) were amplified by PCR to attain DNA transcripts. The PCR products were of expected size for TA17 and TA63 at 570bp and 210bp respectively, with no contaminating artefacts (Fig 4.9 a). DNA transcripts were then used as templates in transcription for the production of RNA, producing expected product sizes (Fig 4.9 b).

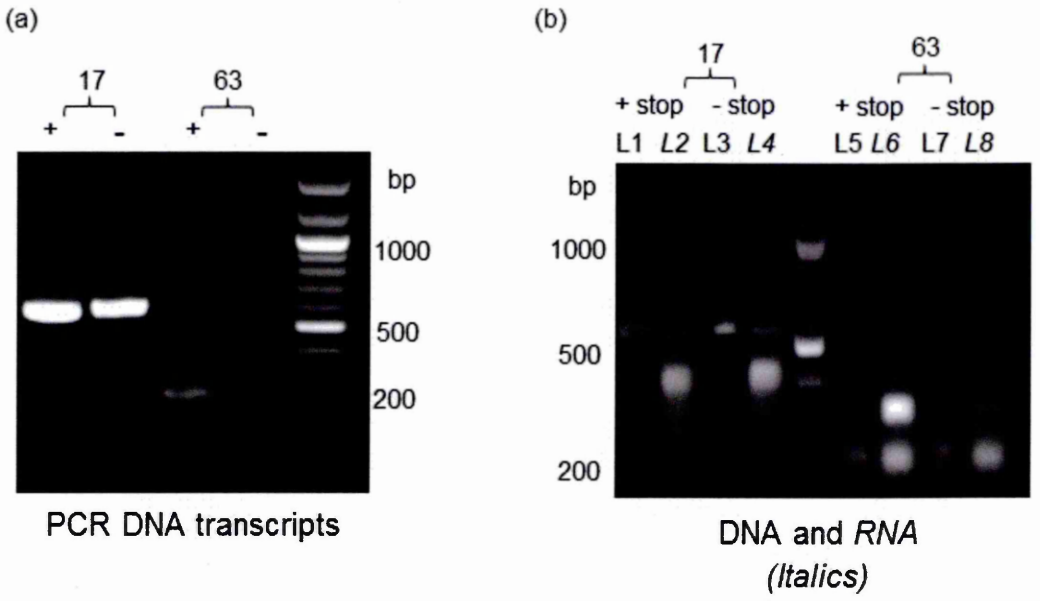

Figure 4.9. Tail anchored protein gene isolation by PCR. (a) Using gene specific primers the T7 promoter and gene sequence for proteins of interest (+/- STOP codon) were isolated and amplified using PCR. (b) DNA template from PCR underwent transcription where it was transcribed into mRNA by T7 RNA polymerase.

Protein translations were performed in wheat germ extract with RNA transcripts of TA17 and TA63 using Easy Tag Express ^{35}S-radiolabel. Translated proteins were of expected size, TA17 (21 800 M_r) and TA63 (7400 M_r) and were visualised on SDS-PAGE after exposure on phosphor plates (Fig 4.10). Protein bands of interest were corrected against background, and run alongside a molecular weight marker (GE Healthcare, CFA626).

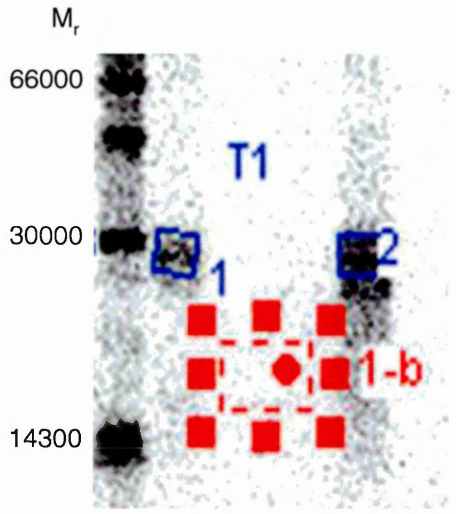

Figure 4.10. Radiolabelled CP binding assay of TA17. The exposed acrylamide gel (16%) is an example of a binding assay for the TA protein; At1g17 (21,800 M_r). Band (1) denotes centrifuged CP membrane with bound TA protein, and band (2) as unbound TA protein in supernatant. Bands were corrected against background noise (red box) (total density light unit (DLU)/ mm^2) to quantify band intensity and data recorded for graphical representation (Appendix III for At3g63 phosphor gel).

Intact pea CPs were purified, subjected to liquid nitrogen freezing and stored at minus 80 °C. As a result of snap freezing and storage at sub-zero temperatures the membrane protein translocation machinery of CPs is irreversibly impaired (Heber 1967 and Santaurius 1971), ensuring that subsequent assays measured protein membrane binding events only. A light microscope was used to check membrane intactness which can show that the CP's retained their normal shape and size after isolation; however, their true integrity could not be determined but was not relevant at this stage. An initial targeting assay was assembled consisting of CP and TA protein only,

which demonstrated the binding of TA proteins at CP membranes with a high amount of ^{35}S-labelled protein remaining in the bound CP fraction (Fig 4.11). After incubation, the CP membrane was washed to remove non-specifically bound protein using the zwitterionic buffer – HEPES (50 mM) and relatively physiological pH 8.0. The mild buffer wash and subsequent CP binding of TA protein signifies a peripheral association of proteins with the CP outer envelope; however, it cannot be established as a specific interaction at the membrane.

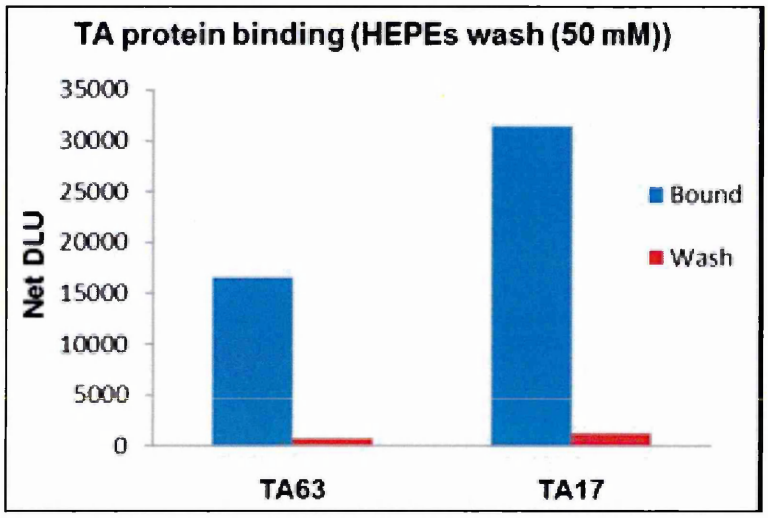

Figure 4.11. Total protein bound for TA17 and TA63 in a standard CP binding assay. Total radiolabelled proteins bound with CP before and after a buffer wash (50 mM HEPES pH 8.0) (single measurements).

Chaperones such as Hsp70 have three major functional domains including an N-terminal ATPase domain which binds ATP and hydrolyses it to adenososine diphosphate (ADP). This drives a conformational change in its two other domains, the substrate binding domain and C-terminal domain. The C-terminal domain is synonymous of a 'lid' for the substrate domain, which is open in the presence of ATP, and closed when ADP bound (Mayer

et al., 2005). ATP dependence was tested for the chaperone; Hsp70, which was incubated with both TA proteins with and without the addition of ATP (1 mM). Fig. 4.12 shows that Hsp70 alone with TA protein shows a reduction in membrane binding (~50 % for TA 17 and ~20 % for TA63). The addition of ATP shows a slight increase in TA protein binding, between 10-20%, suggesting that ATP may be affecting Hsp70 activity which correlates to its structural architecture, whereby the presence of ATP aids the chaperones capability of substrate binding; however, overall Hsp70 cannot be seen to promote TA protein targeting, either in the presence or absence of ATP.

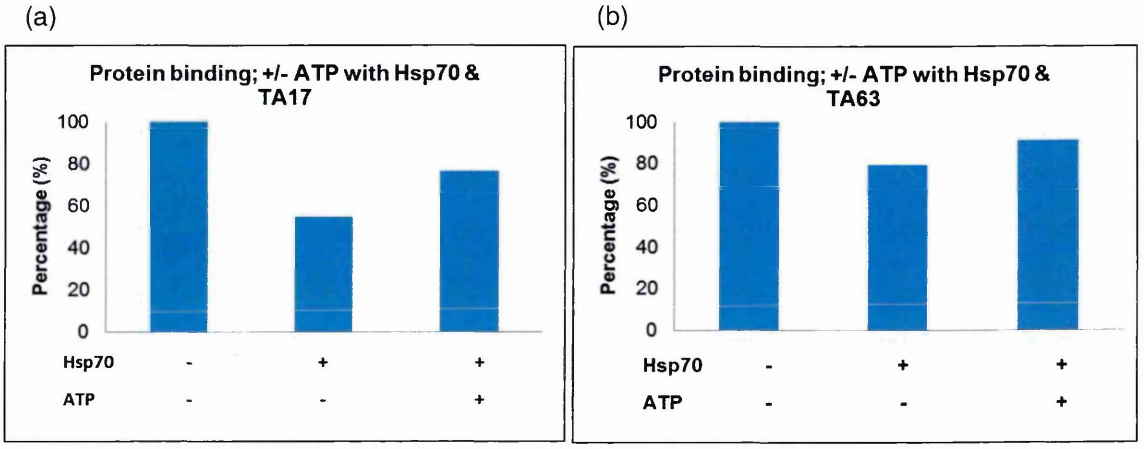

Figure 4.12. Protein binding of TA17 (a) and TA63 (b) upon addition of ATP with chaperone; Hsp70. TA proteins ±1 mM ATP with chaperone; Hsp70 (2 µM). Percentage binding normalised to standard binding condition; CP and TA protein only (single measurements).

Substrate binding was repeated for Hsp90 with ATP (1 mM) for each TA protein, and binding analysed. Figure 4.13 shows TA17 binding with Hsp90 achieving ~60% of TA protein bound compared to TA17 without Hsp90. This

was repeated for the TA63 which showed little or no change to TA63 protein binding, in the presence of Hsp90.

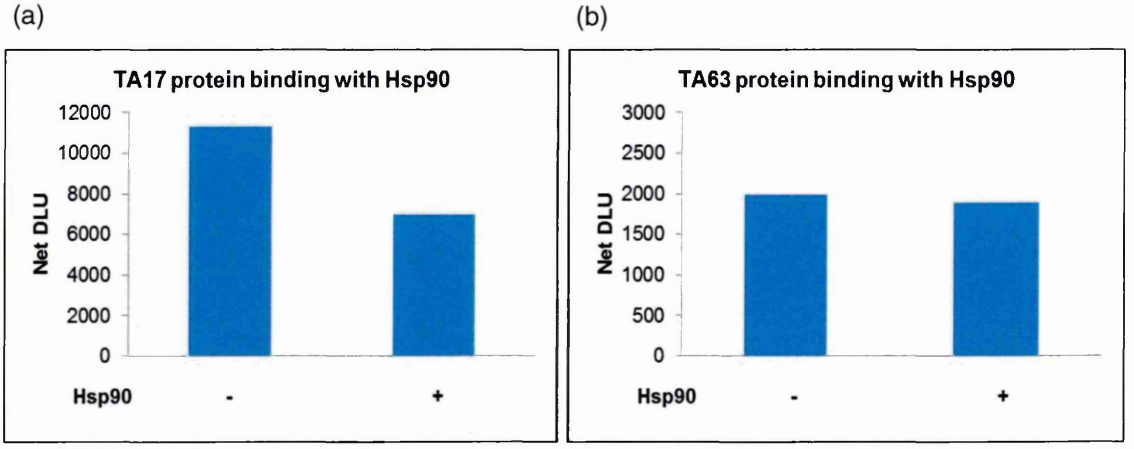

Figure 4.13. The addition of molecular chaperones shows minimal effects to TA protein binding at CP membrane. Showing bound protein for (a) TA17 and (b) TA63 with chaperone, Hsp90 (1mM ATP) (single measurements).

Based on Figs. 4.12 and 4.13 the chaperones may be interacting with TA proteins, but are not enhancing their targeting efficiency to the CP. This suggests that the chaperones could be performing their core functions of binding aggregated or misfolded proteins. This in turn reduces the hydrophobic interaction of the complex at the CP membrane, and causes an overall reduction in free TA protein available to bind non-specifically to the CP.

The proposal that chaperones may be performing their core function was investigated by comparing the amount of bound and unbound protein after

incubation with or without chaperones. From Fig. 4.14, the difference between TA protein in bound and unbound fractions in the presence of chaperones, results in equal or higher levels of TA protein in the unbound fraction, compared to CP only. This supports findings that in the presence of chaperones, the TA protein may be interacting with chaperones but does not necessarily promote their membrane binding.

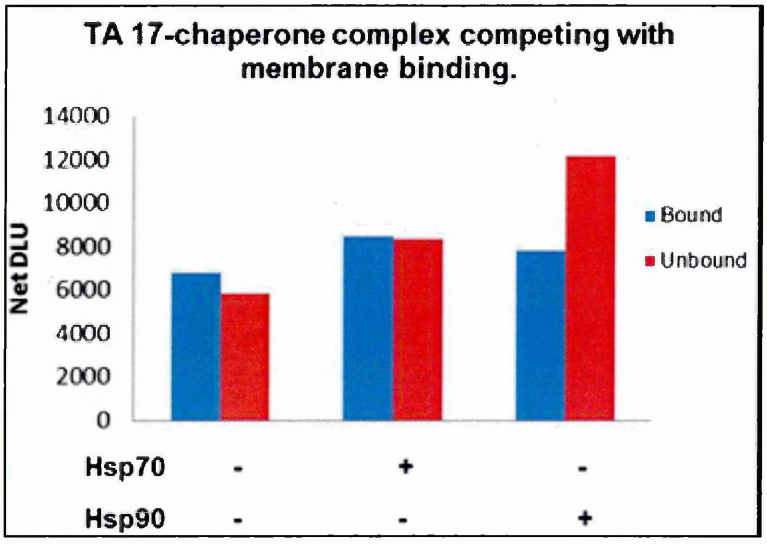

Figure 4.14. Comparison of bound and unbound radiolabelled TA17 in the presence of molecular chaperones. The levels of CP bound and unbound TA protein is compared after its incubation with molecular chaperones; Hsp70 or Hsp90 (single measurements).

The small glutathione-rich tetratricopeptide repeat-containing protein alpha (SGTA) is known to mediate interactions with the C-termini of molecular chaperones, Hsp70 and Hsp90 due to its TPR repeat domain (Buchanan *et al.,* 2007). Therefore, SGTA was used as a competitive inhibitor of CP receptors for TA protein binding assays. Upon incubation of TA protein and

Hsp70 with SGTA it can be seen that there is a decrease in the total protein bound with CP membranes (Fig. 4.15), suggesting that the addition of SGTA has provided an alternative binding partner for the chaperone. However, it cannot be ruled out that SGTA may be associating with the TA protein, which has been reported amongst its interactions with a range of other hydrophobic polypeptides (Leznicki *et al.,* 2012).

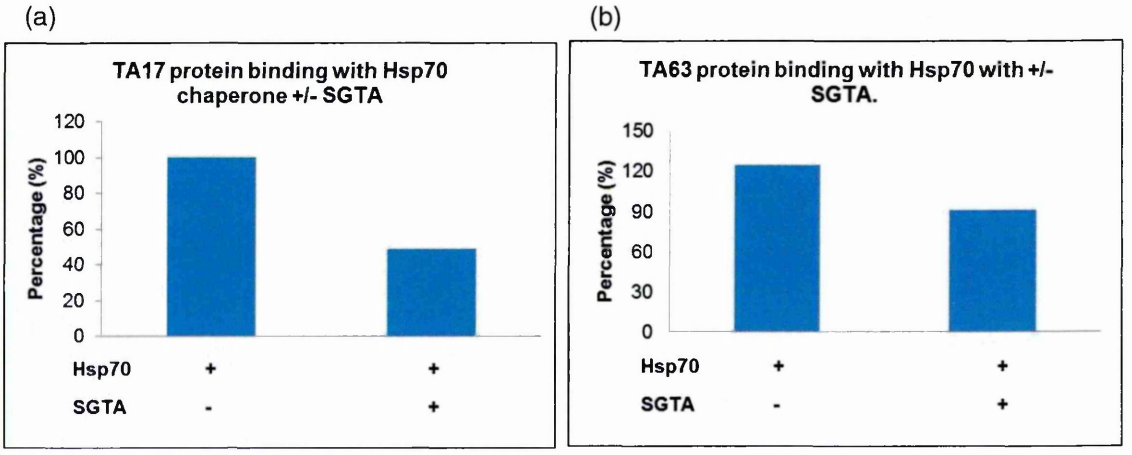

Figure 4.15. TA protein binding with Hsp70 and competitive inhibitor; SGTA. TA proteins: (a) TA17 and (b) TA63, were incubated with Hsp70 and with the addition of the competitive inhibitor; SGTA. Percentage was determined by normalising protein binding to WT CP and TA protein only (single measurements).

To test whether the effect of SGTA was due to non-specific binding, SGTA was subsequently incubated with each TA protein only. In Fig. 4.16 it can be seen that this resulted in decreased bound TA protein in the presence of SGTA, suggesting that there is a direct association between SGTA and

substrate protein. This direct binding to TA protein may account for the effect observed in Fig 4.15.

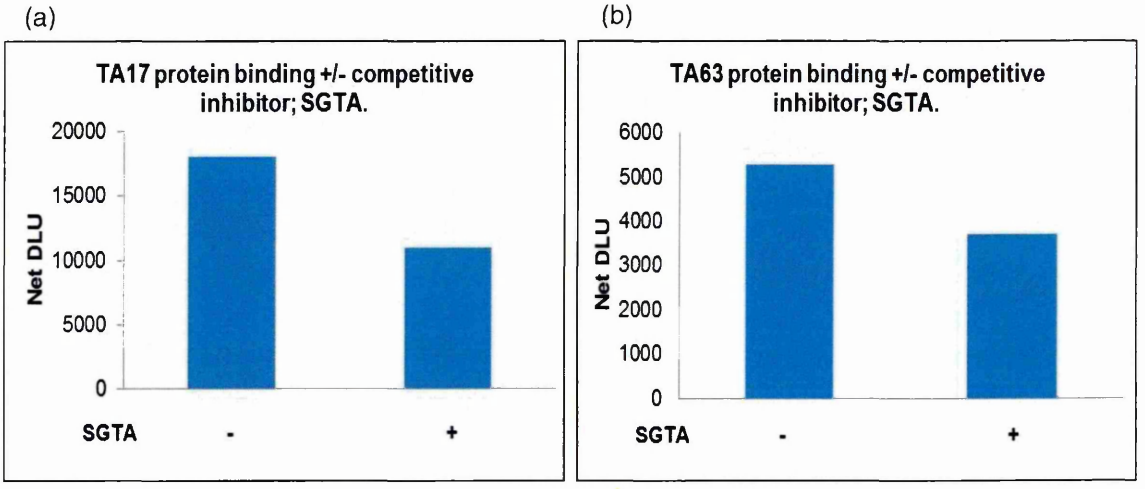

Figure 4.16. SGTA independently associates with TA proteins. TA protein binding ± SGTA (2 μM) (single measurements).

The outer envelope of the CP membrane contains receptors for substrate binding and subsequent translocation events, included amongst these are two receptors that have been shown to preferentially bind the chaperones Hsp70 and Hsp90; OEP61 and Toc64 respectively (Fig. 4.7) (Von L'Oeffelholz, *et al.,* 2011, Kriechbaumer *et al.,* 2011 and 2012 (A) and Qbadou *et al.,* 2006). Treatment of CPs with non-specific protease treatment would result in the removal of the majority of outer envelope receptors. Thermolysin, a metalloprotease was selected as it digests only those proteins with exposed cytosolic domains (Cline *et al.,* 1984). Protease treated CPs were subsequently incubated with TA17 with each chaperone (Fig. 4.17). It can be seen that upon protease treatment there is a ~60 % loss of bound TA protein compared to untreated CP without chaperones present.

Upon the addition of both chaperones there is also a noticeable loss of TA17 bound protein; around ≥90 % when compared to untreated CP in the presence of chaperone. The results show that the removal of outer envelope proteins by thermolysin treatment caused a comparable loss of TA bound protein with and without chaperones. From Fig. 4.17, the addition of chaperones decreases non-specific binding of TA protein to the CP membrane (lanes 3 and 5 compared to lane 1), and are only able to deliver TA proteins if their receptors are present (lane 4 vs 3 and lane 6 vs 5 for Hsp70 and Hsp90 respectively). The chaperone-independent binding of TA protein to the CP membrane comprises of protein-dependent and protein-independent aspects (comparing lanes 1 and 2); however, it is not possible to identify what is responsible for the protein-dependent interaction.

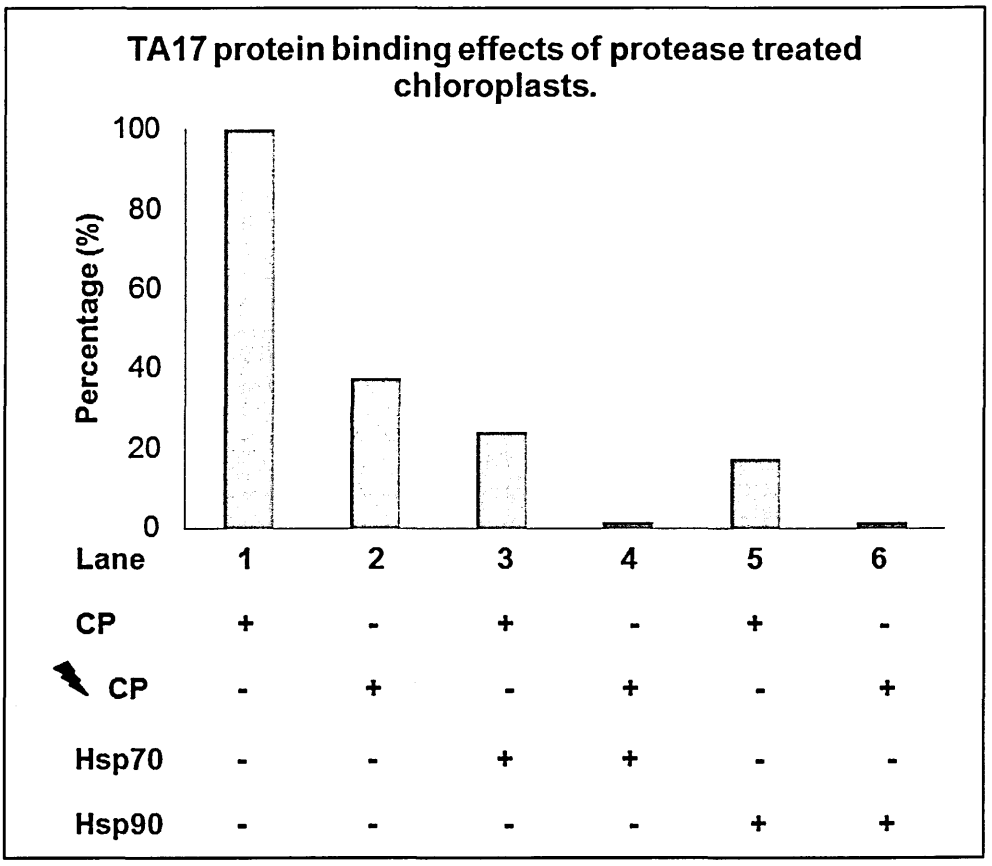

Figure 4.17. The effects of protease treated CP and TA protein binding. CPs were pre-treated with thermolysin (40 U/mL) (lightning bolt) and the reaction stopped with EDTA (10 mM). Standard binding assay was performed with the incubation of untreated or treated CP with TA-17 ± chaperones.

4.3.3. Characterising the OEP61 KO mutant; GabiKat, using gene expression analysis.

Recent work published by Kriechbaumer *et al.,* (2011 and 2012 (A)) have shown chaperones (Hsp70 and Hsp90) binding to proteins at the CP membrane, but was unable to show the contribution of protein binding by their cognate receptors, OEP61 and Toc64, or whether any other additional receptors are involved. Therefore, to define the contribution of each receptor to chaperone binding, KO chloroplasts deficient of either OEP61 or Toc64 receptors (by T-DNA insertion) were deposited using LS method and chaperone binding was measured by TIRE (Fig 4.7).

Using the clone number for OEP61 (At5g21990) from the ABRC (Arabidopsis Biological Resource Center) and the GABI-kat 'simple search' tool, successful detection hits for T-DNA insertions were identified (the triple KO mutant of Toc64 was provided by Jarvis group, as published in 2007, OEP61 KO by B.Abell group, SHU). Gene deletion was achieved by the introduction of T-DNA insertions into the genes sequence, causing the knock-out (KO) of the gene of interest, *Arabidopsis thaliana* seeds were subsequently purchased from Gabi-Kat and grown, followed by the harvest of leaves and seeds from mature plants (performed by V.Kriechbaumer, Abell Group SHU). T-DNA insertions can be used as mutagens to create a loss of function mutation in plants, and acts a marker for subsequent identification. Therefore, the aim of this work was to analyse gene expression to confirm the successful gene KO of OEP61, which was used in TIRE analysis (Fig

4.7), by utilising RT-PCR after RNA extraction from gene deficient CP seedlings.

Wild-type (WT) CP and triple KO Toc64 were used as a positive control to compare the level of gene expression of the KO OEP61 mutant (denoted as 'GK' during PCR analysis). Primers were designed to amplify selected regions of the OEP61 gene sequence separately, consisting of three different primer sets (Chapter 2 Table 2.6.) to identify the location of the T-DNA insertion.

Total RNA was extracted from 100 mg of leaf tissue and was analysed on agarose gel as seen in Fig. 4.18 (i), showing the RNA was intact and free of contaminating artefacts. cDNA synthesis was performed using total RNA for each line which were to be used as templates for PCR amplification of OEP61 full-length cDNA. Initial cDNA synthesis for each RNA type was performed using three gene specific primers: actin, OEP61 (1) and OEP61 (2) (forward primer only) and cDNA was synthesised (Fig 4.18 (ii)), cDNA synthesis was subsequently repeated using only a single specific gene primer: OEP61 (2) (Fig. 4.18 (iii)). By using a single gene specific primer during cDNA synthesis it enabled sensitive downstream RT-PCR amplification for that particular gene sequence.

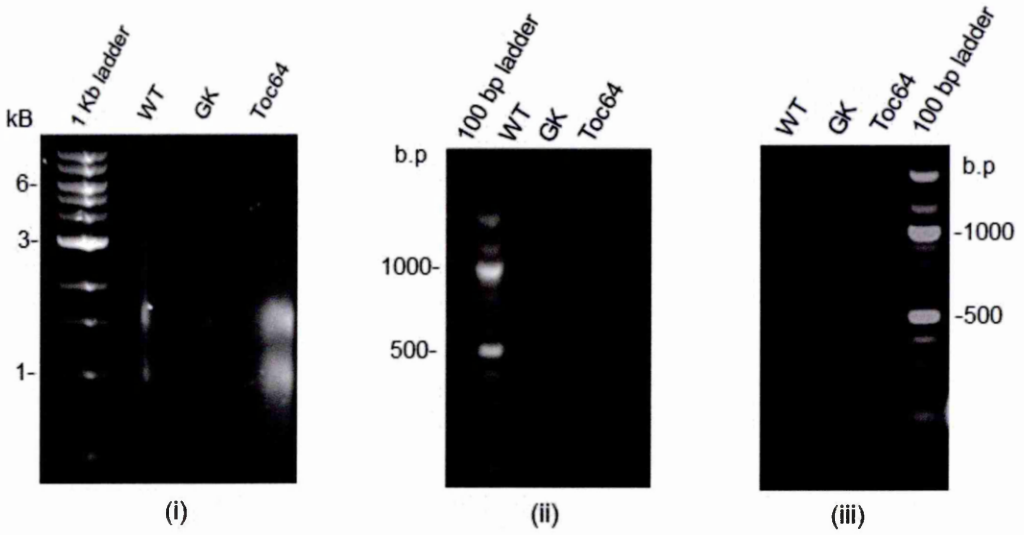

Figure 4.18. RNA isolation and cDNA synthesis. (i) Extracted CP RNA (1 µg) loaded onto a 1% (w/v) TAE agarose gel. (ii) Complementary DNA synthesis from 1 µg total RNA for each genotype was performed using Protoscript II First strand synthesis kit (NEB) using gene specific primers; OEP61(1) For, OEP61 (2) Rev, actin For and toc64 For primers. (iii) cDNA synthesis performed using one specific gene primer of OEP61: Forward primer of OEP61(2).

The constitutively expressed gene actin was employed as a housekeeping gene, representing a standard protein that is regularly expressed throughout the cell reflecting normal cellular functions. Upon RNA extraction and subsequent RT-PCR, actin was confirmed present in all three lines, with WT and Toc64 displaying similar levels of actin, and GK showed a slightly lower level for actin, meaning that the cDNA yield is similar for WT and Toc64 (Fig. 4.19). The agarose gel was repeated with all three samples to check the cDNA yield of actin (specifically for GK line) and confirmed similar yield for cDNA across all three lines (shown in Fig 4.21).

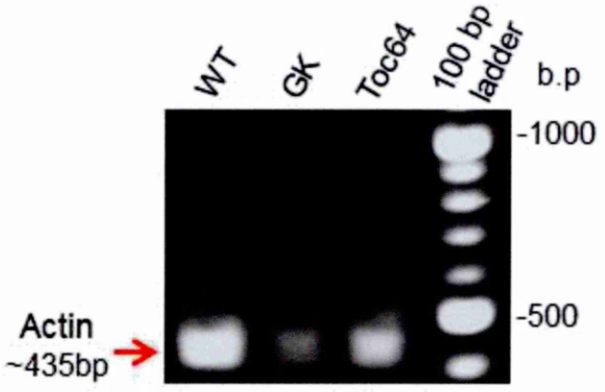

Figure 4.19. Gene specific primers and cDNA synthesis. Agarose gel (1% w/v) showing gene specific RT-PCR products from isolated RNA of CPs derived from leaf tissue. The cDNA yield for the housekeeping gene; actin (435 bp) is compared in all three lines.

To analyse the OEP61 KO mutant, three sets of primers were utilised, two of which aimed to amplify the entire gene in two halves; OEP61(1) and OEP61(2), and the third set were an intron specific primer previously described by Von L'Oeffeleholz *et al.,* (2011). The OEP61(1) primer pair resulted in numerous unspecific bands and did not yield the expected product (828 bp) in any of the genotypes, including after genomic DNA clean-up (Qiagen) and was therefore omitted from results. Fig. 4.18 (i) shows a predominant band at 1000 bp using OEP61 (2) cDNA, which was characteristic of genomic DNA (gDNA) contamination. Therefore RNA samples were subjected to gDNA removal using the gDNA Wipeout buffer from Qiagen and PCR was repeated. Primers designed specifically to the second half of the gene sequence of OEP61 (2) (851-1663 bp) was successful in amplifying the PCR product as expected (813 bp) after

genomic DNA removal (Fig 4.20 ii), whilst including a few faint unspecific bands suggesting a lack of primer specificity remained. From figure 4.18 the expected product size (813 bp) for the OEP61 transcript can be visualised for WT and Toc64 lines, however, the GK KO band is undetectable suggesting that the OEP61 transcript has been disrupted.

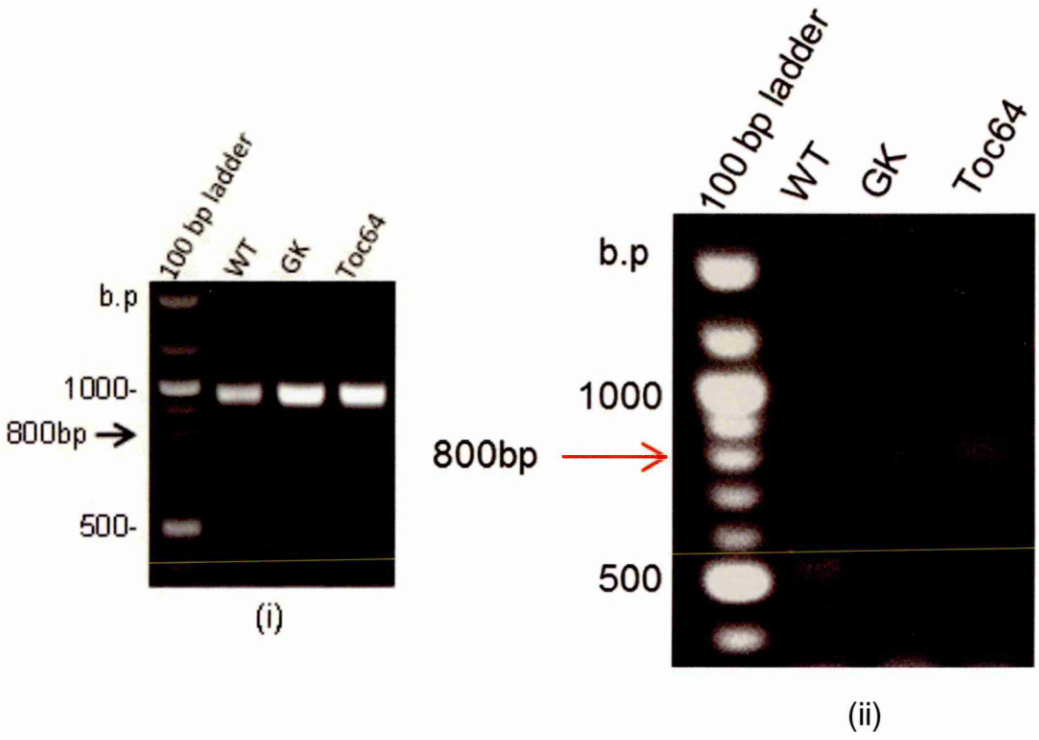

Figure 4.20. Proposed T-DNA insertion of GabiKat located in second half of OEP61 gene sequence. Gene specific cDNA synthesis amplifying the second half of OEP61 (OEP61(2)). (i) gDNA contamination at 1000 bp, (ii) after gDNA removal treatment and PCR was repeated and revealed a band running slightly above ~800bp which correlates to the expected product size of 813 bp for OEP61 (2) with GK band absent.

As a result of the deficient band for OEP61 in the latter half of its gene sequence (851 -1663 bp) shown in Fig. 4.20 (ii), and without the first set of primers yielding a product which spanned the first 850 bp of OEP61 due to technical issues, the intron spanning primers designed by Von L'Offelholz *et al.*, (2011) were utilised. The third set of primers flank an intron sequence within OEP61, and therefore will only produce a product in cDNA as a result of intron splicing. The primers are designed towards the middle of the OEP61 sequence, and yield a product of ~166 bp as shown in Fig. 4.21.

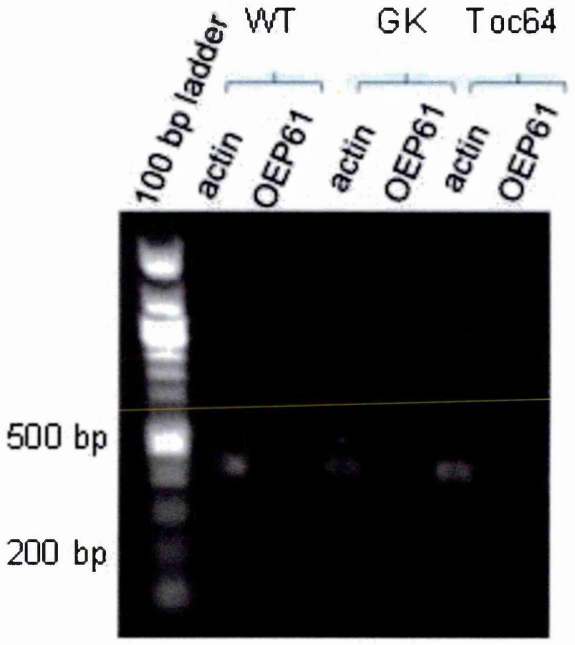

Fig 4.21. PCR using an intron exclusive specific primer of OEP61. OEP61 intron exclusive specific primers yield a product of ~166 bp, and repeat PCR for the housekeeping gene; actin, yielding similar cDNA bands at 435 bp.

Figure 4.20 (ii) suggests that the OEP61 KO mutant is effective, and that the T-DNA insertion site is toward the latter half of the OEP61 sequence as shown in the proposed schematic (Fig. 4.22). The partial disruption of the OEP61 gene sequence could result in the proteins expression but in a truncated form, which is deficient of its C-termini anchor and therefore would not be membrane inserted. However, the soluble form of the protein lacking its TMD could still be present and actively disrupting protein targeting as seen by Von L'Offelholz *et al.,* (2011).

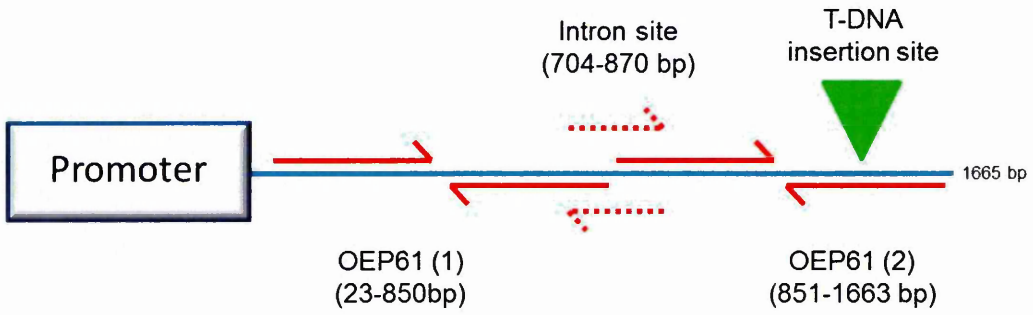

Figure 4.22. Schematic of the proposed location for the T-DNA insertion of the mutant GabiKat (KO of OEP61). Using gene specific RT-PCR it is proposed that there has been a disruption to the latter half of the OEP61 sequence as a result of T-DNA insertion.

4.3.4. Ultra-Structural study of the OEP61 KO mutant; GabiKat.

If OEP61 plays a role within protein import then phenotypic variations might be expected as a result of the KO mutation, which would affect normal CP functions and/or development. Therefore, EM was performed on 8 day old Arabidopsis leaves, specifically to analyse CP organelles. The abundant and relatively large organelles (typically 1-5 μM in diameter) can be readily analysed by EM. The complex structure of the CP is particularly sensitive to developmental changes, environmental effects and genetic alterations, therefore making EM a powerful tool in monitoring the effects of such vicissitudes (Hyman and Jarvis, 2011). No visible defects of the plant leaves; KO OEP61 (GK), were found when directly compared to the wild-type (WT) plant or KO Toc64 (Fig. 4.23) at a superficial level, *i.e.* leaf morphology or colour. However, the size of leaves varied in particular GK leaves were seen to be smaller than WT and Toc64.

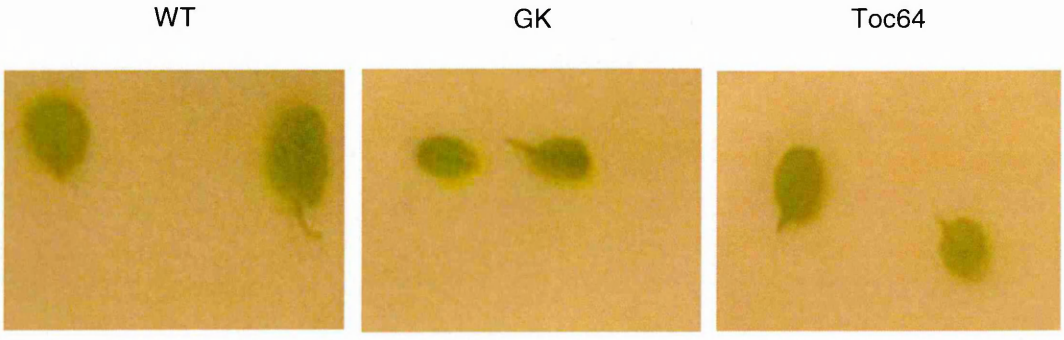

Figure 4.23. 8 day old *Arabidopsis Thaliana* leaves. Wild-type (WT), KO OEP61 (GK) and KO Toc64.

Subsequently, the organelle CPs were inspected for any abnormal features using ImageJ (Image processing and analysis in Java, National institutes of Health), including measurements of the surface area, width and length of ≥10 samples of chloroplasts, which were quantified and compiled into figures for direct comparison against one another.

The 8 day old *Arabidopsis thaliana* leaves from WT, KO OEP61 (GK) and KO Toc64 were harvested and subjected to EM analysis. The quantification of morphological differences of ≥10 electron micrographs per genotype (Fig. 4.24) considered the length, width and surface area of all CPs. There were no prominent variations in CP cross-sectional area or size, with organelles surface area between 11-12 μm^2, length ~6 μm^2 and widths ~2-3 μm^2. This suggests that all three genotype CPs are similar in all aspects with regards to morphology, and confirming that there were no external factors affecting organelle maturation for example, developmental stages of growth and subsequent leaf size. Therefore attention was focused at the organellar and molecular levels for any abnormalities.

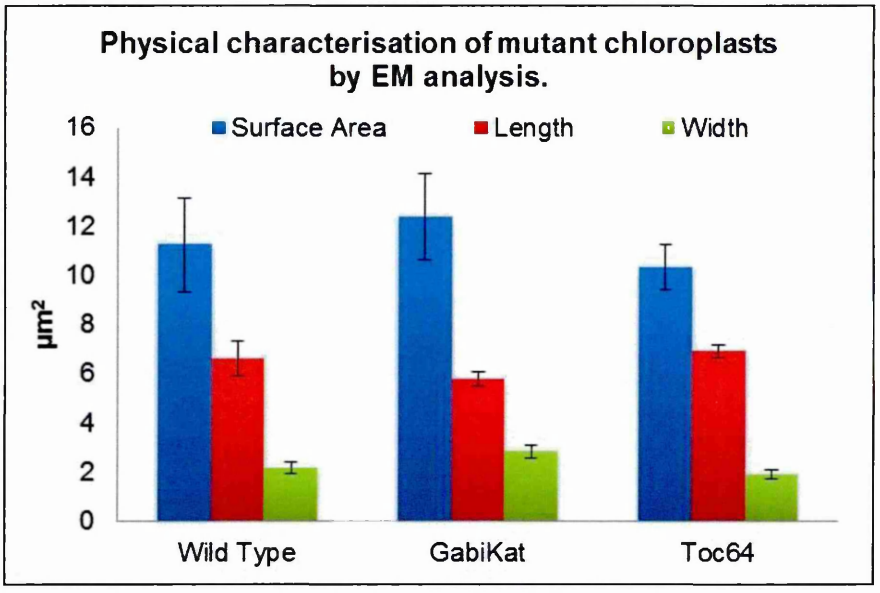

Figure 4.24. Quantification of chloroplast electron micrographs. The length, width and membrane circumference were measured and used to calculate cross-sectional area using. Scale bar 1-2 µM were used and magnification differences accounted for in data interpretation using ImageJ (n=10, SE).

As a result of similar morphologies with regards to analysed measurements of CPs for WT, GabiKat and Toc64 the micrographs were manually evaluated for any qualitative differences. Figure 4.25 shows that WT and KO Toc64 CP present a typical internal structure, with striated stacking of thylakoid membranes into grana stacks and organised lamellae links. However, OEP61 KO (GK) displays an atypical intracellular arrangement, whose thylakoid membranes present a network of densely aggregated granum and disorganised lamellae, covering the entire intracellular space of the organelle, which was visualised in all EM micrographs. Results indicate that the OEP61 KO has caused a radical disruption of internal CP membranes.

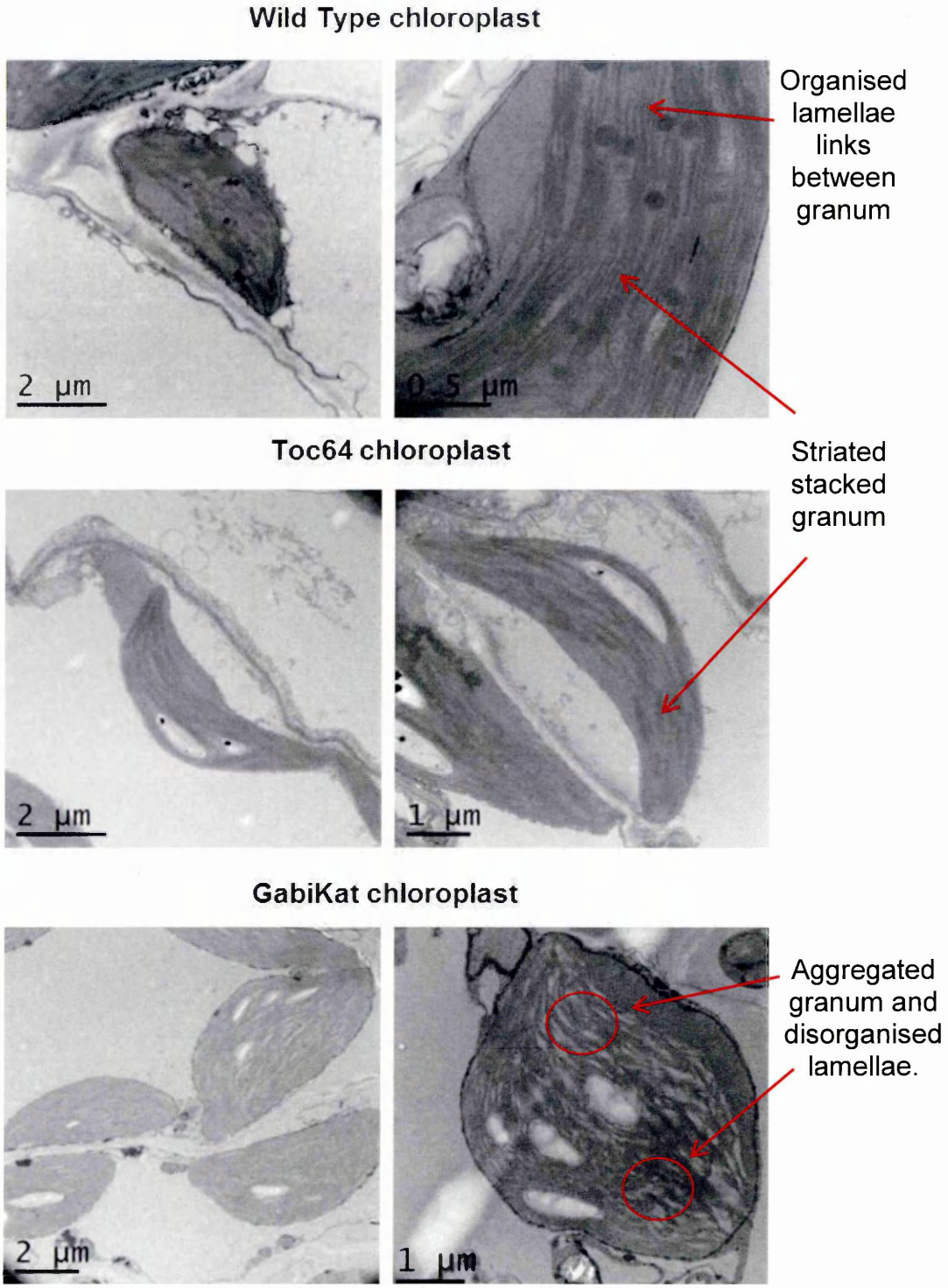

Figure 4.25. EM analysis reveals intracellular structural compositions of chloroplasts. Representative transmission electron micrographs of WT, Toc64 and GabiKat (OEP61 KO) CPs, at least 10 whole CPs micrographs from each genotype were analysed (images shown are selected from these). Highlighted in red emphasises normal and abnormal features of CPs.

4.4. Discussion

4.4.1. TIRE & KO mutant chloroplast targeting

To explore the receptor specificity binding of chaperones Hsp70 and Hsp90 to OEP61 and Toc64 at the outer CP membrane, the optical method TIRE was used. Mutant CP and proteins were obtained and prepared by V.Kriechbaumer (post-doctoral researcher, SHU) and LS deposition and TIRE were performed collaboratively. TIRE is 10 times more sensitive than conventional SPR (Nabok *et al.*, 2008) which is advantageous due to the low abundance of some receptor proteins at chloroplast membranes, ranging between 0.1 ng/µg to 0.5 ng/µg (Vojta *et al.,* 2004). TIRE has not only differentiated between specific and non-specific binding of proteins to individual CP receptors by gene deletion (Fig. 4.7), but has also identified between binding of similar isoforms (e.g. Hsp70 and Hsp70-C) targeting to specific CP receptors. The data supports the targeting of chaperones Hsp90 and Hsp70 to published work, which have identified that chaperones bind with high affinity to a specific receptor; Toc64 and OEP61, respectively (Qbadou *et al.,* 2006 and Kriechbaumer *et al.*, 2012 (A)). Studies by Schweiger *et al.,* (2012) have located the OEP61 receptor (AtTPR7) to the ER and alternatively found varying degrees of binding of chaperones (Hsp90 and Hsp70) to both receptors; Toc64 and OEP61 according to different isoforms (Schweiger *et al.,* 2013); nevertheless, OEP61 retained a stronger affinity towards Hsp70 - in line with previous results by Von L'Offelholz *et al.,*

(2011). It has also been recently shown using *in vitro* isothermal titration calorimetry and *in silico* simulation studies, that the TPR domain of Toc64 binds with 1:1 stoichiometry in similar micromolar affinity to both Hsp70 and Hsp90, suggesting that the receptor does not discriminate between the chaperones (Panigrahi *et al.,* 2013). However, TIRE provides an *in vivo* like model utilising natively derived membranes and measuring real-time protein adsorption *in situ*. Our findings corroborate that chaperone binding favours a particular receptor which has been supported by chaperone truncation – also shown by Panigrahi *et al.,* (2013) noting a profound decrease in affinity after mutations of the C-termini protein motif. In conclusion, by using CP isolated from OEP61 and Toc64 KO lines, whereby their binding specificity is ultimately compromised, it has demonstrated that OEP61 and Toc64 are the sole significant chaperone receptors at the outer CP membrane.

4.4.2. Protein targeting and molecular chaperones as cytosolic co-factors

The contact between the TPR domains of membrane docking proteins and cytosolic preproteins (such as; TA proteins), can occur directly or indirectly utilising chaperones bound to the preproteins acting as scaffold proteins (Schweiger *et al.,* 2013). The results from *in vitro* pulldown assays using TA membrane proteins as a model system for post-translational targeting, demonstrated substantial non-specific binding at the CP membrane. One consequence of nascent protein chain release into an uncrowded

environment (lysate free) is non-specific binding, due to the hydrophobicity of TA domains. TA proteins are therefore not exposed to other cytosolic proteins in which they may aggregate with, alternatively, it cannot be discounted that self-aggregation may occur; where upon the primary function of molecular chaperones would ensue to protect the pre-protein from such interactions, and prevent self-aggregation (Ellis *et al.,* 2006). In the presence of chaperones with or without the addition of ATP, TA- binding was noticeably reduced (Fig 4.12 and 4.13) which was also seen in the presence of the competitive inhibitor, SGTA (Fig. 4.15 and 4.16). Such interactions can be attributed to the hydrophobicity of TA proteins, rich in hydroxylated residues and deficient in acidic residues (Flores-Perez and Jarvis 2013), resulting in non-specific interactions with other proteins (Leznicki *et al.*, 2012) and reducing the overall free TA protein available to bind at the CP membrane, as seen in Fig. 4.14, with a substantial presence of TA protein in the chaperone unbound supernatant.

Effects of organelle freezing have been proposed to irreversibly impair translocation machinery of CP (Heber 1967 and Santaurius 1971) interfering and/or inhibiting the sequential binding of chaperone receptors with bound pre-proteins, and subsequent association with the translocon complex. Kriechbaumer *et al.,* (2012 (B)) utilised import competent CPs to study protein import, using a variety of CP membrane proteins. Kriechbaumer *et al.,* (2012 (B)) showed that CP targeting efficiency was enhanced in the presence of chaperones (Hsp70 and Hsp90) which could not be replicated here, and could be related to CP preparations by freezing. Furthermore,

import competency of CP was confirmed by membrane insertion of Tic22 - an intermembrane space protein, which was established after thermolysin treatment did not result in protein degradation (Kriechbaumer *et al.,* 2012 (B)). Therefore, it is feasible that the freeze-thaw of CP membranes has possibly compromised the ability of pre-protein binding due to the incompetent state of the CP organelle, although the main issue is most likely due to the aggregation of TA proteins.

Studies using protease-treatment have been utilised to probe the surfaces of cells, organelles and isolated membranes in order to gain information on localization of membrane proteins, or removing proteins adsorbed or bound to the surface of membrane-bound structures (Cline *et al.,* 1984). Figure 4.17 shows that protease treatment by thermolysin results in an overall reduction in non-specific binding of TA proteins, with or without the addition of chaperones. Different protease types have been shown to identify varied extents of protein involvement in targeting (Hoffman *et al.,* 2005). An outer membrane protein targeted specifically to the CP membrane in pea known as OEP14, was previously reported not to require proteins at the surface of the CP for insertion due to a lack of sensitivity to CP pre-treatment with thermolysin. However, subsequent studies found reduced protein insertion in CPs treated with the protease; trypsin, identifying that OEP14 does indeed require at least one protein; Toc75, for its insertion into the outer membrane. Therefore, trypsin is an alternative protease which has access to not only exposed cytosolic domain proteins but also protein within the intermembrane space, thus revealing protein involvements in outer membrane targeting that

thermolysin has not (Hoffman *et al.,* 2005). In this situation thermolysin treatment has been able to establish that the non-specific binding of TA protein is not only affected by the loss of outer CP chaperone receptors, but possibly by additional unidentified CP proteins that may contribute to not only the non-specific binding of TA protein, but also to the loss of specific TA-binding upon protease treatment, in which case trypsin could be used in the future.

Overall the data has shown that the non-specific interactions by TA proteins have dominated targeting assays, preventing the detailed analysis of specific membrane binding. It has shown that chaperones interact with TA protein but do not necessarily promote protein targeting, proposing that the chaperones may be binding aggregated or misfolded proteins, which in turn reduces the hydrophobic interaction of the complex at the membrane, and the total free amount of TA protein to bind at the CP membrane.

The proposed targeting model in Fig. 4.26 reiterates that non-specific binding dominated TA protein binding, and when in the presence of cytosolic co-factors; Hsp70 and Hsp90, they may interact but not necessarily enhance targeting efficiency via cognate chaperone receptors.

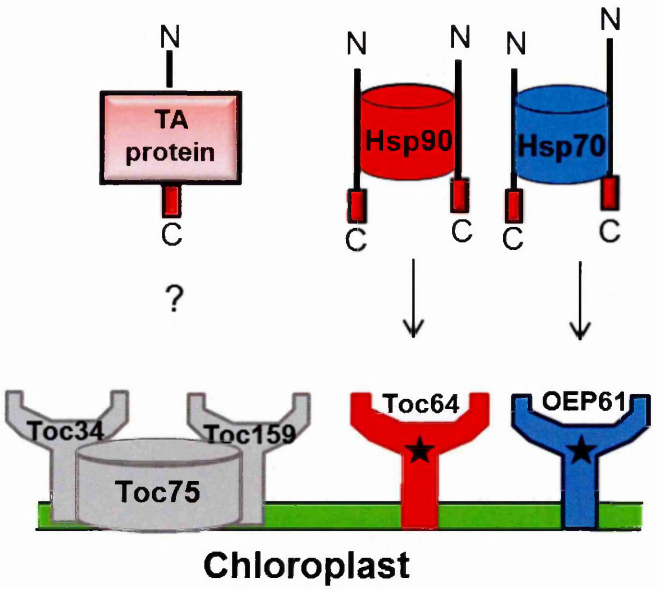

Figure 4.26. Schematic appended from post-translational targeting model. The non-specific binding of TA protein has been signified by question mark (?) and specific binding to chaperone cognate receptors by directional arrows.

4.4.3. Characterising the OEP61 KO mutant; GabiKat, using gene expression analysis.

Cellular processes can be disrupted, compromised or completely abolished by genetic mutations; therefore, the study of mutant genes is a powerful tool for linking a gene sequence to a phenotype from which the biological function can be ascertained (Radhadmony *et al.,* 2005). The use of insertional mutagenesis was achieved using the T-DNA of *Agrobacterium tumefaciens,* which was used as mutagens to create a loss of function mutation in the OEP61 gene of the *Arabidopisis* plant. The advantage of using T-DNA is that it not only disrupts the expression of the gene into which it is inserted, but it

can also act as a marker for subsequent identification of the mutation by PCR-based strategies (Radhadmony *et al.,* 2005). The use of sequence specific primers has enabled prediction of the location of the T-DNA insertion of the OEP61 KO mutant (Figure 4.20 ii). Two primers (omitting OEP61 (1)) were utilised to span specific sections of the genes sequence, and upon amplification of each section by PCR a product was detected. Interestingly, OEP61 (2) did not yield a detectable band between 851-1663 bp, whereas intron primers covering 704-870 bp did, proposing that the T-DNA insertion site of the KO mutant has disrupted the latter half of the OEP61 gene - after 870 bp (Fig 4.22). Therefore, OEP61 protein expression may result in a truncated form of the protein defect of its C-terminus. Von L'Offelholz *et al.,* (2011) reported that soluble OEP61 lacking its C-terminus (containing a single TMD), inhibited CP targeting impairing its ability to co-ordinate the transfer of precursor proteins to the translocase. Therefore, this suggests that the KO mutant should be tested for phenotypic variances as a result of the loss of its membrane anchor. In addition, genome sequencing could be performed to pinpoint the exact location of the T-DNA insertion to confirm it is in the latter half of the genes sequence, alternatively protein expression could be investigated by immunoblot although sensitivity issues may prevent detailed analysis.

4.4.4. Ultra-Structural study of the OEP61 KO mutant; GabiKat.

Based on the analysis of the CP mutant; GK, the abnormal stacking and distribution of thylakoid membranes visualised using EM, has been

associated as a result of the KO mutation of the gene; OEP61 (Fig. 4.25). Thylakoids are exclusively linked to organisms carrying out oxygenic photosynthesis, with membrane biogenesis involving a combination of lipid, protein and pigment synthesis, along with their transport and integration in to functional membrane-integral complexes (Vothknecht *et al.,* 2012). The extent of effects caused by KO mutants can vary, depending on the functional importance of the gene at hand. Vital proteins such as the vesicle-inducing protein in plastids (Vipp1) have been shown to be involved in the formation of vesicles leading to thylakoid biogenesis. Subsequent Vipp1 T-DNA mutant plants revealed normal sized CP by EM analysis, but of which contained few internal membranes demonstrating severe distortion and diffuse distribution inside the organelle, which correlated with their reduced functional capacity for oxygenic photosynthesis (Kroll *et al.,* 2001).

On the other hand, Aronsson *et al.,* (2007) attempted to define the role of Toc64 - proposed to mediate the docking of Hsp90-associated preproteins at the outer CP membrane (Qbadou *et al.,* 2006). This was achieved by the generation of single, double and triple *Arabidopsis* KO mutants. Results showed that the inactivation of Toc64 did not have any serious consequences to CP biogenesis or plant development, demonstrating that Toc64 was not essential for the efficient import of proteins into CP's in Arabidopsis. However, it could be proposed that protein import by OEP61 is analogous to Toc64 (Abell *et al.,* 2011), therefore, a double KO of both genes could cause significant phenotypic effects. The proposed function for OEP61 is the cognate receptor for the molecular chaperone Hsp70, whose binding transfers bound precursor proteins to the core translocase (Von

L'Oeffelholz *et al.,* 2011). Therefore, defects in protein expression - as a result of a KO mutation may result in loss of protein import, some of which may be important for thylakoid structure. However, with regards to the intracellular abnormality noted in Fig. 4.25, it is possible that more than one gene may have been mutated as a result of the KO mutagenesis, which could be affecting thylakoid membrane stacking; or alternatively, it may be an indirect effect of the KO mutation. Therefore it would be beneficial to perform further analytical investigation, for example focussing on protein content to identify and quantify proteins which are present (or missing) and compare this against WT CP, or alternatively produce a second independent KO line to confirm that the phenotype is the same.

4.5. Summary

I. Findings from TIRE identified that OEP61 and Toc64 are the sole significant chaperone receptors at the outer CP membrane, and favourably bind to molecular chaperones; Hsp70 and Hsp90 respectively.

II. As a result of dominant non-specific interactions and protein aggregation, the binding of TA protein was inconclusive. Chaperone-independent binding of TA protein to the CP membranes is comprised of protein-dependent and protein-independent factors. Although, protease treatment of CP displayed some specificity of targeting when comparing TA17 binding with or without chaperones, suggesting that TA proteins may be binding to unidentified CP membrane proteins.

III. Gene expression analysis confirmed that the KO mutant is effective, which could result in a truncated form of the OEP61 protein, lacking its membrane anchor. EM analysis subsequently identified abnormal intracellular stacking of the thylakoid membranes, which could be a downstream effect and therefore further tests are required to rule out alternative explanations.

5.1. Conclusion

The data presented in this thesis outlines a novel methodology that has been developed using LS deposition, resulting in the ability to deposit natively derived membranes as a thin film on a gold coated sensor surface. Coupled with the optical technique of TIRE, this has enabled the detection and identification of protein: lipid and protein: protein interactions at these natively derived membranes. Two models were investigated, model I studied protein: lipid interaction and model II protein: protein interaction. The data has provided insights into the binding of amyloid fibrils with human neuronal whole cells, and protein targeting of molecular chaperones at outer envelope CP membranes, highlighting the versatility of TIRE.

TIRE analysis regarding model I (Chapter 3) has established methods to observe protein: lipid interactions and was used to further characterise the mode of action by which amyloid fibrils bind to lipid membranes. It has been demonstrated that fibril length correlates with the ability to disrupt membranes and to reduce cell viability, where the fragmentation of fibrils resulted in a reduction in fibril length and a rise in the number of fibril ends, thereby identifying key features proposed to contribute to their ability to bind and disrupt lipid membranes. TIRE data demonstrated that fragmented fibrils are able to cause enhanced membrane disruption using the model cell line SH-SY5Y. This was demonstrated for three amyloid proteins (Fig. 3.18), including α-syn which is implicated in the neurodegenerative disease, PD. Supporting experiments were performed, and whose results were

corroborated successfully *in vitro*. Using artificial membranes in dye release assay (Fig. 3.12) results showed that fragmented fibrils caused an increased dye release in comparison to their full length counterparts for all three proteins. A cell viability assay focussing on membrane integrity using cultured SH-SY5Y cells displayed increased cytotoxicity and loss of cell viability as a result of fragmented fibril incubation for α-syn and Aβ40 (Fig. 3.14). Concluding overall that fragmented fibrils caused increased cytotoxic effects as a result of direct membrane disruption.

Regarding model II (Chapter 4), TIRE was successfully applied to observe the binding of a specific chaperone protein to a cognate receptor from natively derived chloroplast membranes. The deposition of native CP membrane had been subjected to KO gene mutations (Fig. 4.7) and the data support published work which proposes that chaperones Hsp70 and Hsp90 bind to a cognate CP receptor. Furthermore, it has provided evidence that OEP61 and Toc64 are the predominant chaperone receptors to reside at the outer CP membrane.

As a result of the identification of chaperone cognate receptors, further studies utilising *in vitro* pulldown assays looked to explore the role of chaperones as cytosolic co-factors in the post-translational targeting of TA proteins. The results demonstrated that much of the binding of TA protein at the CP is non-specific. In the presence of Hsp70 and Hsp90, the binding of TA proteins was shown to be comprised of protein dependent (e.g. aggregation) (Fig. 4.14) and independent (binding of other proteins, SGTA) interactions (Fig. 4.16). For the most part, chaperones did not directly result

in promoting TA targeting efficiency, but may have acted to reduce their non-specific binding.

Supporting experiments using RT-PCR analysis and EM were performed to confirm the KO gene mutation of OEP61 (GK) and identify any intracellular effects to the CP organelle. RT-PCR results identified that the T-DNA insertion is located to the latter end of the OEP61 gene sequence, which could result in the production of a truncated form of the protein lacking its C-terminus (Fig. 4.20 ii and Fig. 4.22). Subsequent EM analysis of OEP61 KO mutant from young *Arabidopsis thaliana* leaves, presented uncharacteristic thylakoid membranes within CP organelles compared to WT CP (Fig. 4.25). From these results it is suggested that defects in protein expression may be a result of the KO mutation, causing a loss of protein function and therefore loss of protein import, which may indirectly affect thylakoid structure.

The label free, fast and real-time measurements of TIRE taking place *in situ,* enable the sensitive detection of direct changes at a sensors surface, in terms of thin film thickness and consequently protein adsorption. Importantly, models I and II have highlighted the versatility of TIRE, using the LS method for the deposition of native cell membranes which has enabled the study of protein interactions *in situ* using plant organelles and mammalian cells. The LS films required no selective chemistry for cell attachment, unlike other biophysical methods such as, SPR, which can obscure and lower sensitivity to native protein binding. TIRE and LS combined provide a method for the sensitive detection and quantification of protein interactions at natively derived cell membranes.

5.2. Future Work

5.2.1. Instrumental advancements

The potential applications of TIRE include the vast screening of compounds for new pharmaceuticals. At present the use of the TIRE instrument requires a large amount of manual input, and hence critical functions need to be streamlined to make it more user-friendly. A recommendation to the instrumental set-up of TIRE would entail the automation of sample injection, to provide greater precision and reproducibility during sample delivery and consumption, minimising waste of valuable sample. This could be achieved by building a motorised injection pump, consisting of a small stage to hold the sample syringe which is then decompressed by the automated pump to release the sample. This would ensure that the flow rate is controlled and reproducible for every sample analysed.

5.2.2. TIRE and LS method as a tool in biology

The analysis of protein/ ligand interactions at native cell membranes using TIRE demonstrates the versatility of the method, encouraging its application to be utilised further in other areas of research, such as biopharmaceuticals. For example, the use of nanoparticles (NP) in medicine has seen an unprecedented growth of research, including applications such as drug

delivery. The use of NP requires stringent testing to overcome challenges such as specificity of target delivery and toxicity effects caused by NPs, some of which include membrane lysis (Goodman *et al.,* 2004). Using TIRE, the possibility to deposit native cells from target organelles and measure the specificity of NP binding, which can include the analysis of their functionalization and the monitoring of toxicity; such as membrane disruption, could enable the development of increased safety and biocompatibility of NP in drug delivery for new medicines (Jong *et al.,* 2008).

TIRE with LS may also provide an alternative method for the development of *in vivo* disease models, aiming to reduce the number of animals used for pre-clinical and neuroprotective studies, such as mice/rat and primates. The development of PD models *in vivo* use three main neurotoxins; 6HD, rotenone (a natural pesticide extracted from root vegetables) and MPTP to induce PD-like symptoms. The administration is usually by systemic injection; however 6HD crosses the blood brain barrier poorly and is injected directly into the brain by either free-hand or by stereotaxic means (Bove *et al.,* 2005). The induction of PD-symptoms are not wholly representative of the sporadic nature of PD in humans, and thus the administration of drugs for efficacy testing may be insufficient to assess the neuroprotective properties of such treatments. Therefore, using the TIRE method could enable the ability to assess the structure of membrane proteins and ligand binding in their native environment and enable the screening of possible targets and drug binding, using dynamic scans to derive kinetic binding affinities which could potentially be used as therapeutic agents in treating diseases like PD.

In conclusion, TIRE could have a wider implication in the screening of compounds in new pharmaceuticals, providing an *in vivo* model utilising natively derived organelles and cell membranes as therapeutic targets.

5.2.3. Further developments of Model I

The work presented in Model I illustrates that a reduction in fibril length results in enhanced membrane disruption and loss of cell viability. Therefore, controlling fibril length would be therapeutically beneficial. Molecular chaperones have been described in chapter 4 as playing a pivotal role in protein homeostasis in cells, by reducing the misfolding and aggregation of proteins. It is thus feasible that chaperones may diminish the cytotoxic effects of fibrils at cellular membranes, especially for fragmented fibrils by a method of unfolding, refolding and stabilisation of non-toxic structures (Fig. 5.1). Preliminary work was carried out funded by an external grant (Dr Hadwen Trust) to use TIRE as an *in vivo* method to study protein: lipid interactions of amyloid fibrils in the presence of molecular chaperones, using LS method to deposit native cells from the neuronal cell line SH-SY5Y, with future proposals to study organelles such as mitochondria implicated in PD models (Nakamura *2*013). In particular the family of heat shock chaperones such as the constitutively expressed Hsc70 was shown to act as an anti-aggregation barrier, whereby it binds to and coats α-syn fibrils, resulting in a reduced cellular toxic effect compared to 'naked' fibrils (Pemberton *et al.,* 2011).

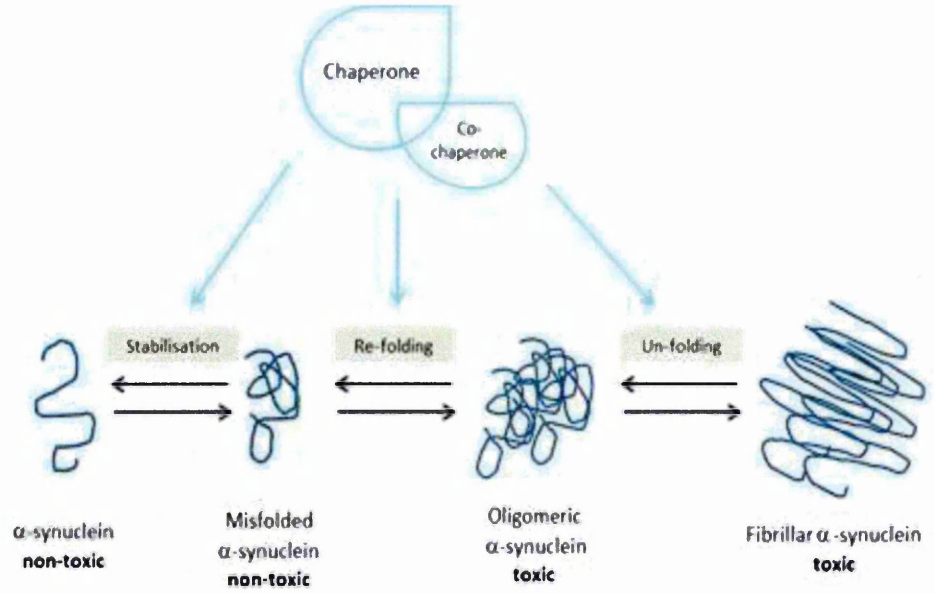

Figure 5.1 A schematic proposal of the therapeutic effects upon addition of molecular chaperones with α-syn aggregates. The molecular chaperone Hsp70 is predicted to unfold toxic species and refold into non-toxic species whilst stabilising the structures.

Initial data from *in vitro* experiments using the CellTox™ assay indicated that the addition of Hsp70 to full length and fragmented fibrils reduced cell death when incubated with SH-SY5Y cells. This is proposed to be achieved by the stabilisation of a non-toxic fibrillar intermediate reducing the fibril-lipid interaction at membranes (Appendix IV). Future work utilising TIRE will enable *in situ* analysis of amyloid protein: lipid interactions in the presence of molecular chaperone, Hsp70 to support *in vitro* results.

5.2.4. Further developments of Model II

Further work is necessary to characterise the role of molecular chaperones as cytosolic co-factors in the post-translational targeting of tail-anchored membrane proteins. The *in vitro* pulldown assays highlighted the lack of sensitivity to distinguish between specific and non-specific CP binding of TA proteins, whereas TIRE has excelled in its sensitivity to distinguish between similar binding affinities (Kriechbaumer *et al.,* 2011). Therefore, TIRE is recommended to be used for the detection of chaperone binding to KO mutant CPs with the addition of recombinant TA protein. Preliminary expression of soluble recombinant TA proteins was performed in *E. coli* following a published protocol for the expression of tail-anchored membrane proteins; Leznicki *et al.,* (2010). However, technical difficulties with regards to protein solubility issues prevented the production of the required concentration of soluble protein. Several aspects of the protein expression method were explored to overcome solubility issues, including growth temperatures, growth medium (Luria-Broth and auto-induction media) and timescales of protein induction.

With regards to the KO mutant by T-DNA insertion, it would be beneficial to generate a second independent KO line using the GabiKat website, to identify an alternative OEP61 T-DNA insertion site. This would confirm that the phenotype observed is a result of OEP61 loss or disruption, rather than by a second mutation in another gene that could have caused the abnormal thylakoid stacking (Fig. 4.25). Further analytical methods could be utilised to

study the ultra-structural abnormality seen in GK chloroplasts. Ferro *et al.*, (2003) use subcellular proteomic analysis (Liquid chromatography mass spectrometry, LC-MS/MS) and applied various extraction procedures to provide an in-depth analysis of chloroplast envelope membrane proteins. Their separation and subsequent analysis by LC-MS/MS enabled the identification of more than 100 envelope proteins, including components of the protein import machinery. Furthermore, the high abundance of a range of proteins within the plant proteome for instance; Rubisco, which can yield up to 40% of total protein content, could mask low-abundant proteins and hinder their detection (Bindschedler and Cramer 2011). Thus the removal of such proteins can be achieved by selective precipitation for which plant specific protocols have been published (Thiellement *et al.*, 2007). Therefore, functional proteomics would enable the analysis of proteins present in mutant (GK) and WT chloroplast, providing more specific information with regards to irregularities in protein levels and thus their expression, distinguishing whether the abnormal thylakoid membranes is due to the OEP61 KO or an upstream effect.

Overall, the method of TIRE coupled with LS was shown to be a versatile tool in biosensing, and was successfully used as an analytical tool for probing and quantifying protein interactions *in situ*. The future potential of TIRE within the biomedical and pharmaceutical setting has been highlighted, and could be used to explore a range of diverse membranes that have poised complications for other approaches.

Appendices

Appendix I

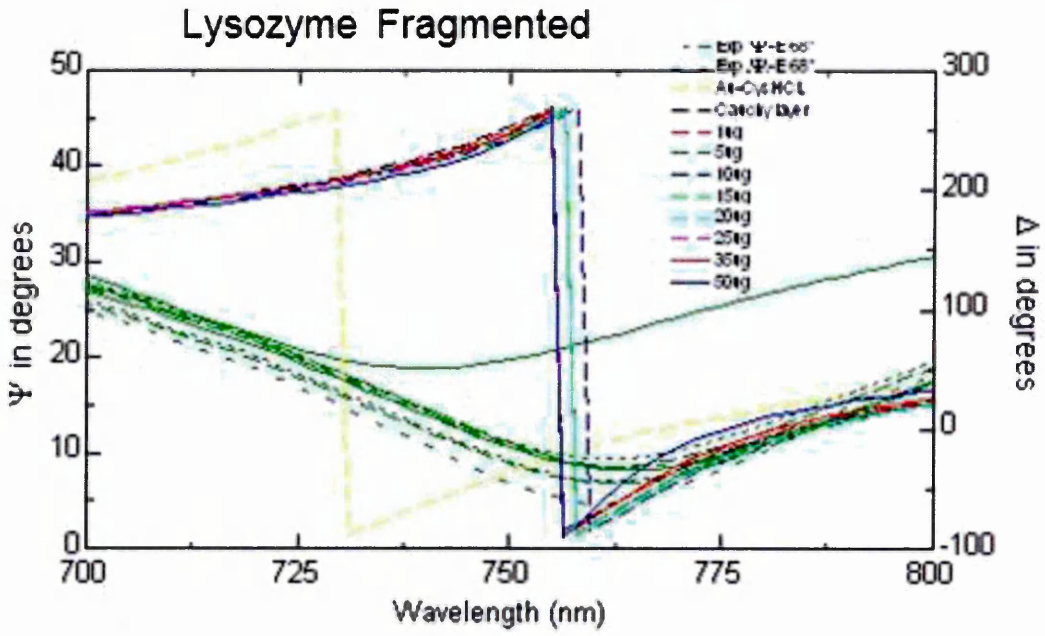

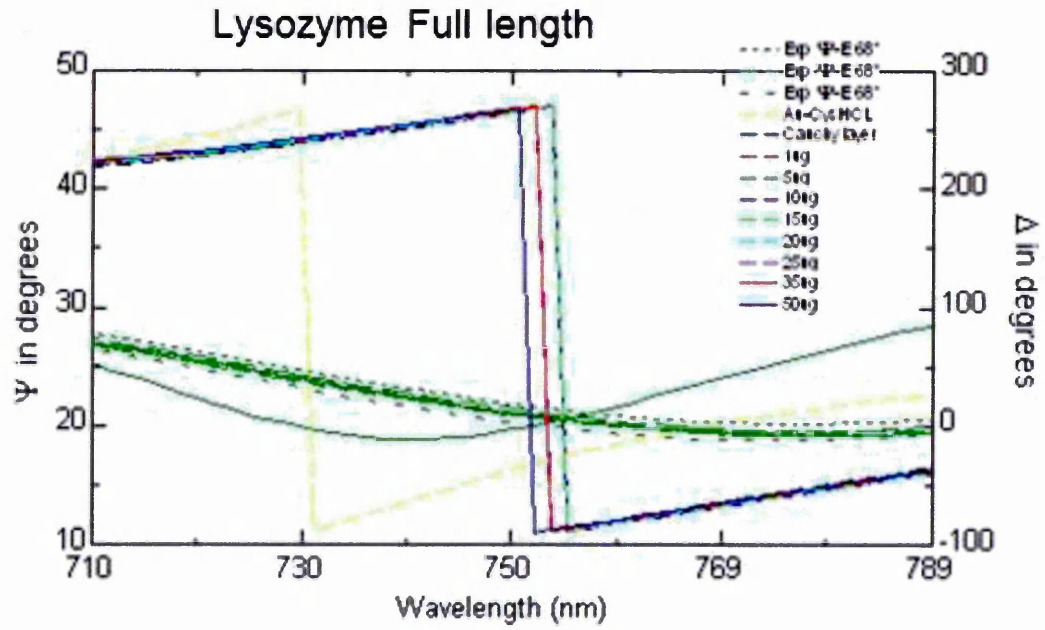

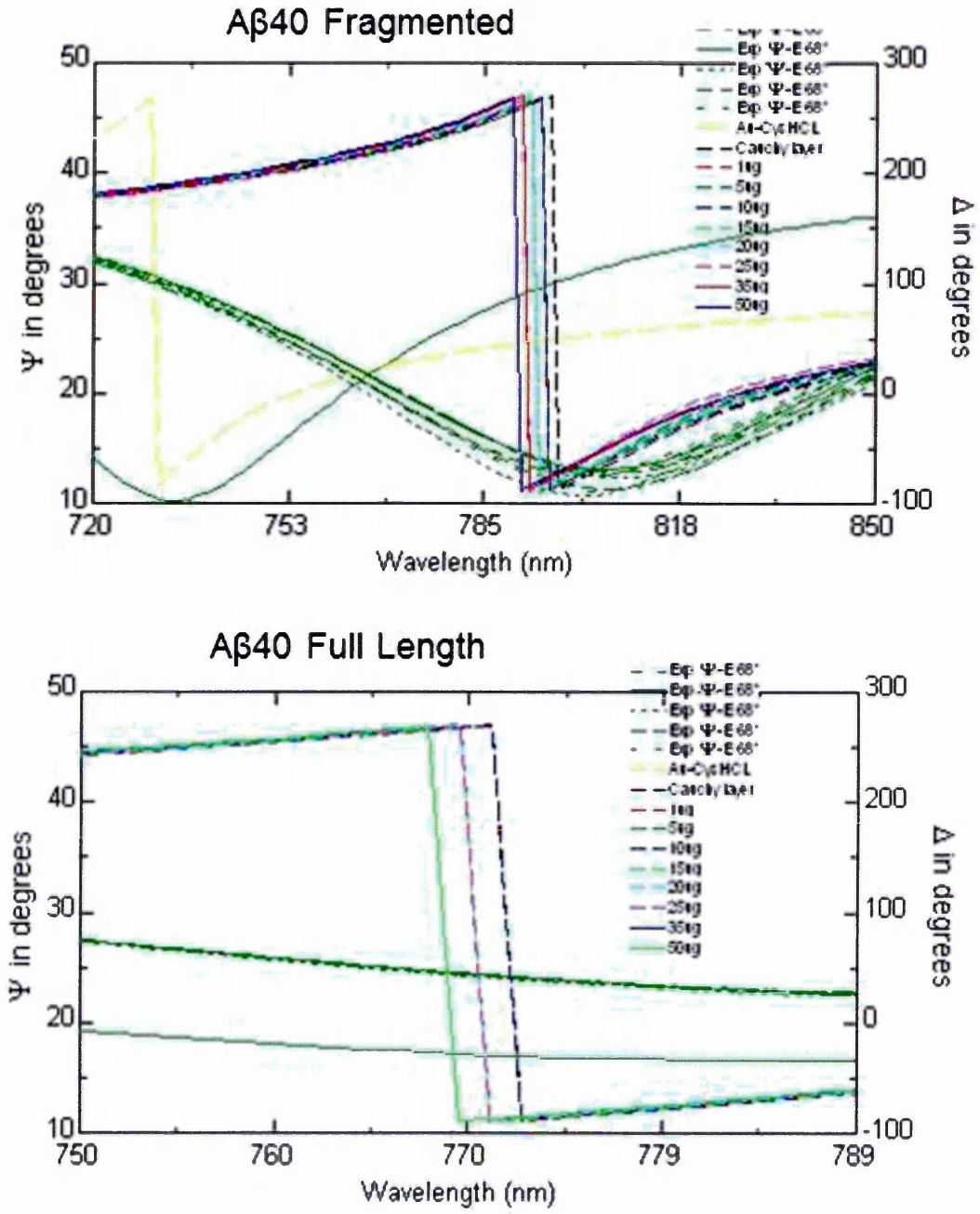

Appendix I and II: TIRE Spectroscopic scans of sequential incubations of Lysozyme and Aβ40 fibrils with SH-SY5Y cells deposited using LS.

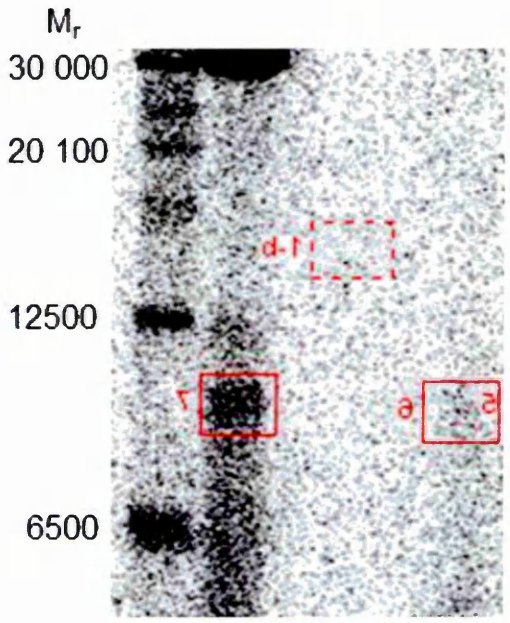

Phosphor exposed SDS-PAGE gel of a standard binding assay with TA protein, ^{35}S-At3g63 M_r 7400. Bands were corrected against background noise (red box) (total density light unit (DLU)/ mm^2) to quantify band intensity and data recorded for graphical representation (left red box bound TA protein, right red box unbound supernatant).

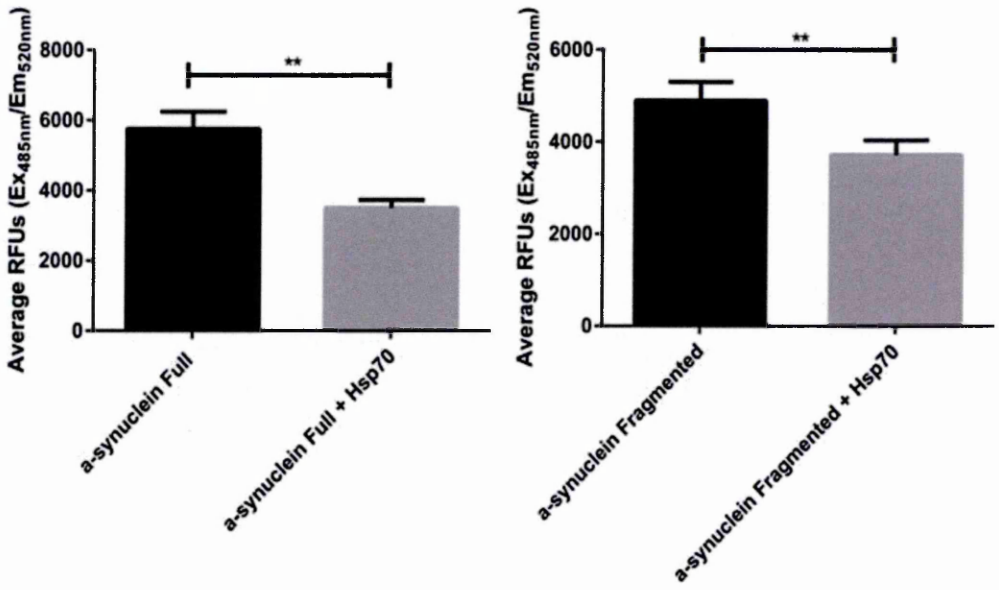

Appendix IV. CellTox™ Average RFUs after Addition of Fibrils and Hsp70. Amyloid α-syn (7 μM) and Hsp70 (0.7 μM) with celltox dye after 24h. Full length α-syn ± Hsp70 and fragmented fibril ± Hsp70, p-values generated were 0.0087 and 0.022 respectively (using the Mann-Whitney Test), indicating there was significant difference in regards to the decrease in number of dead cells when the chaperone was added to fibril solutions (Performed collaboratively with SHU student; Teresa Whitely, under Dr Hadwen Grant funding).

References

Abell, B. M. & Mullen, R. T. (2011). Tail-anchored membrane proteins: exploring the complex diversity of tail-anchored-protein targeting in plant cells. Plant Cell Reports, **30**, 137-151.

Abell, B. M., Rabu, C., Leznicki, P., Young, J. C. & High, S. (2007). Post-translational integration of tail-anchored proteins is facilitated by defined molecular chaperones. Journal of Cell Science, **120**, 1743-1751.

Abell, B. M., Pool, M. R., Schlenker, O., Sinning, I. & High, S. (2004). Signal recognition particle mediates post-translational targeting in eukaryotes. The EMBO Journal, **23**, 2755-2764.

Akopian, D., Shen, K., Zhang, X. & Shan, S. O. (2013). Signal recognition particle: an essential protein-targeting machine. Annual Review of Biochemistry, **82**, 693-721.

Arnau, J., Lauritzen, C., Petersen, G. E. & Pedersen, J. (2006). Current strategies for the use of affinity tags and tag removal for the purification of recombinant proteins. Protein Expression and Purification, **48**, 1-13.

Aronsson, H., Boij, P., Patel, R., Wardle, A., Topel, M. & Jarvis, P. (2007). Toc64/OEP64 is not essential for the efficient import of proteins into chloroplasts in Arabidopsis thaliana. The Plant Journal: for Cell and Molecular Biology, **52**, 53-68.

Arslan Yildiz, A., Kang, C. & Sinner, E. K. (2013). Biomimetic membrane platform containing hERG potassium channel and its application to drug screening. The Analyst, **138**, 2007-2012.

Artigues, A., Iriarte, A. & Martinez-Carrion, M. (2002). Binding to chaperones allows import of a purified mitochondrial precursor into mitochondria. The Journal of Biological Chemistry, **277**, 25047-25055.

Arwin, H. (2001). Is ellipsometry suitable for sensor applications? Sensors and Actuators A: Physical, **92**, 43-51.

Arwin, H. (2000). Ellipsometry on thin organic layers of biological interest: Characterization and applications. Thin Solid Films, **377-378**, 48-56.

Babenko, V. & Dzwolak, W. (2013). Amino acid sequence determinants in self-assembly of insulin chiral amyloid superstructures: Role of C-terminus of B-chain in association of fibrils. FEBS letters, **587**, 625-630.

Bemporad, F. & Chiti, F. (2012). Protein Misfolded Oligomers: Experimental Approaches, Mechanism of Formation, and Structure-Toxicity Relationships. Chemistry & Biology, **19**, 315-327.

Berggard, T., Linse, S. & James, P. (2007). Methods for the detection and analysis of protein-protein interactions. Proteomics, **7**, 2833-2842.

Biancalana, M. & Koide, S. (2010). Molecular mechanism of Thioflavin-T binding to amyloid fibrils. Biochimica et Biophysica Acta (BBA) - Proteins and Proteomics, **1804**, 1405-1412.

Biehle, S. J., Carrozzella, J., Shukla, R., Popplewell, J., Swann, M., Freeman, N. & Clark, J. F. (2004). Apolipoprotein E isoprotein-specific interactions with tissue plasminogen activator. Biochimica et Biophysica Acta (BBA) - Molecular Basis of Disease, **1689**, 244-251.

Bindschedler, L. V. & Cramer, R. (2011). Quantitative plant proteomics. Proteomics, **11**, 756-775.

Blodgett, K. B. (1935). **Films Built by Depositing Successive Monomolecular Layers on a Solid Surface**. Journal of the American Chemical Society, **57**, 1007-1022.

Blodgett, K. B. (1934). **Monomolecular films of fatty acids on glass.** Journal of the American Chemical Society, **56**, 495-495.

Booth, D. R., Sunde, M., Bellotti, V., Robinson, C. V., Hutchinson, W. L., Fraser, P. E., Hawkins, P. N., Dobson, C. M., Radford, S. E., Blake, C. C. & Pepys, M. B. (1997). Instability, unfolding and aggregation of human lysozyme variants underlying amyloid fibrillogenesis. Nature, **385**, 787-793.

Borgese, N. & Fasana, E. (2011). Targeting pathways of C-tail-anchored proteins. Biochimica et Biophysica Acta, **1808**, 937-946.

Borgese, N., Colombo, S. & Pedrazzini, E. (2003). The tale of tail-anchored proteins: coming from the cytosol and looking for a membrane. The Journal of Cell Biology, **161**, 1013-1019.

Borgese, N., Brambillasca, S. & Colombo, S. (2007). How tails guide tail-anchored proteins to their destinations. Current Opinion in Cell Biology, **19**, 368-375.

BovÃc, J., Prou, D., Perier, C. & Przedborski, S. (2005). Toxin-Induced Models of Parkinson's Disease. Neurotherapeutics, **2**, 484-494.

Breydo, L., Wu, J. W. & Uversky, V. N. (2012). α-Synuclein misfolding and Parkinson's disease. Biochimica et Biophysica Acta (BBA) - Molecular Basis of Disease, **1822**, 261-285.

Briand, E., Zach, M., Svedhem, S., Kasemo, B. & Petronis, S. (2010). Combined QCM-D and EIS study of supported lipid bilayer formation and interaction with pore-forming peptides. The Analyst, **135**, 343-350.

Bucciantini, M., Giannoni, E., Chiti, F., Baroni, F., Formigli, L., Zurdo, J., Taddei, N., Ramponi, G., Dobson, C. M. & Stefani, M. (2002). Inherent toxicity of aggregates implies a common mechanism for protein misfolding diseases. Nature, **416**, 507-511.

Buchanan, G., Ricciardelli, C., Harris, J. M., Prescott, J., Yu, Z. C., Jia, L., Butler, L. M., Marshall, V. R., Scher, H. I., Gerald, W. L., Coetzee, G. A. & Tilley, W. D. (2007). Control of androgen receptor signaling in prostate

cancer by the cochaperone small glutamine rich tetratricopeptide repeat containing protein alpha. Cancer Research, **67**, 10087-10096.

Chamberlain, A. K., MacPhee, C. E., Zurdo, J., Morozova-Roche, L. A., Hill, H. A., Dobson, C. M. & Davis, J. J. (2000). Ultrastructural organization of amyloid fibrils by atomic force microscopy. Biophysical Journal, **79**, 3282-3293.

Ciccotosto, G. D., Tew, D., Curtain, C. C., Smith, D., Carrington, D., Masters, C. L., Bush, A. I., Cherny, R. A., Cappai, R. & Barnham, K. J. (2004). Enhanced toxicity and cellular binding of a modified amyloid beta peptide with a methionine to valine substitution. The Journal of Biological Chemistry, **279**, 42528-42534.

Cline, K., Werner-Washburne, M., Andrews, J. & Keegstra, K. (1984). Thermolysin is a suitable protease for probing the surface of intact pea chloroplasts. Plant Physiology, **75**, 675-678.

Cline, K. & Dabney-Smith, C. (2008). Plastid protein import and sorting: different paths to the same compartments. Current Opinion in Plant Biology, **11**, 585-592.

Colombo, S. F., Longhi, R. & Borgese, N. (2009). The role of cytosolic proteins in the insertion of tail-anchored proteins into phospholipid bilayers. Journal of Cell Science, **122**, 2383-2392.

Conway, K. A., Harper, J. D. & Lansbury, P. T. (1998). Accelerated in vitro fibril formation by a mutant alpha-synuclein linked to early-onset Parkinson disease. Nature medicine, **4**, 1318-1320.

Cooper, M. A. & Singleton, V. T. (2007). A survey of the 2001 to 2005 quartz crystal microbalance biosensor literature: applications of acoustic physics to the analysis of biomolecular interactions. Journal of Molecular Recognition, **20**, 154-184.

Cretich, M., Damin, F. & Chiari, M. (2014). Protein microarray technology: how far off is routine diagnostics? The Analyst, **139**, 528-542.

Daghestani, H. N. & Day, B. W. (2010). Theory and applications of surface plasmon resonance, resonant mirror, resonant waveguide grating, and dual polarization interferometry biosensors. Sensors (Basel, Switzerland), **10**, 9630-9646.

Danzer, K. M., Krebs, S. K., Wolff, M., Birk, G. & Hengerer, B. (2009). Seeding induced by alpha-synuclein oligomers provides evidence for spreading of alpha-synuclein pathology. Journal of Neurochemistry, **111**, 192-203.

Danzer, K. M., Haasen, D., Karow, A. R., Moussaud, S., Habeck, M., Giese, A., Kretzschmar, H., Hengerer, B. & Kostka, M. (2007). Different species of alpha-synuclein oligomers induce calcium influx and seeding. The Journal of neuroscience : the official journal of the Society for Neuroscience, **27**, 9220-9232.

Davidson, W. S., Jonas, A., Clayton, D. F. & George, J. M. (1998). Stabilization of alpha-synuclein secondary structure upon binding to synthetic membranes. The Journal of Biological Chemistry, **273**, 9443-9449.

De Jong, W. H. & Borm, P. J. (2008). Drug delivery and nanoparticles: Applications and hazards. International Journal of Nanomedicine, **3**, 133-149.

Dev, K. K., Hofele, K., Barbieri, S., Buchman, V. L. & van der Putten, H. (2003). Part II: α-synuclein and its molecular pathophysiological role in neurodegenerative disease. Neuropharmacology, **45**, 14-44.

Dhanoa, P. K., Richardson, L. G., Smith, M. D., Gidda, S. K., Henderson, M. P., Andrews, D. W. & Mullen, R. T. (2010). Distinct pathways mediate the sorting of tail-anchored proteins to the plastid outer envelope. PLoS One, **5**, e10098.

Dixon, M. C. (2008). Quartz Crystal Microbalance with Dissipation Monitoring: Enabling Real-Time Characterization of Biological Materials and Their Interactions. Journal of Biomolecular Techniques: JBT, **19**, 151-158.

Eanes, E. D. & Glenner, G. G. (1968). X-ray diffraction studies on amyloid filaments. The journal of Histochemistry and Cytochemistry : Official Journal of the Histochemistry Society, **16**, 673-677.

Edvardsson, M., Svedhem, S., Wang, G., Richter, R., Rodahl, M. & Kasemo, B. (2009). QCM-D and reflectometry instrument: applications to supported lipid structures and their biomolecular interactions. Analytical Chemistry, **81**, 349-361.

Eisenberg, D. & Jucker, M. (2012). The amyloid state of proteins in human diseases. Cell, **148**, 1188-1203.

Ellis, R. J. & Minton, A. P. (2006). Protein aggregation in crowded environments. Biological Chemistry, **387**, 485-497.

Engel, M. F., Khemtemourian, L., Kleijer, C. C., Meeldijk, H. J., Jacobs, J., Verkleij, A. J., de Kruijff, B., Killian, J. A. & Hoppener, J. W. (2008). Membrane damage by human islet amyloid polypeptide through fibril growth at the membrane. Proceedings of the National Academy of Sciences of the United States of America, **105**, 6033-6038.

Eriksson, H. M., Persson, K., Zhang, S. & Wieslander, Å. (2009). High-yield expression and purification of a monotopic membrane glycosyltransferase. Protein Expression and Purification, **66**, 143-148.

Fan, X., White, I. M., Shopova, S. I., Zhu, H., Suter, J. D. & Sun, Y. (2008). Sensitive optical biosensors for unlabeled targets: A review. Analytica Chimica Acta, **620**, 8-26.

Fändrich, M. & Dobson, C. M. (2002). The behaviour of polyamino acids reveals an inverse side chain effect in amyloid structure formation. The EMBO Journal, **21**, 5682-5690.

Finot, E., Markey, L., Hane, F., Amrein, M. & Leonenko, Z. (2013). Combined atomic force microscopy and spectroscopic ellipsometry applied to the analysis of lipid-protein thin films. Colloids and surfaces.B, Biointerfaces, **104**, 289-293.

Flores-Pérez, Ú. & Jarvis, P. (2013). Molecular chaperone involvement in chloroplast protein import. Biochimica et Biophysica Acta (BBA) - Molecular Cell Research, **1833**, 332-340.

Fodero-Tavoletti, M. T., Villemagne, V. L., Rowe, C. C., Masters, C. L., Barnham, K. J. & Cappai, R. (2011). Amyloid-β: The seeds of darkness. The International Journal of Biochemistry & Cell Biology, **43**, 1247-1251.

Fredenburg, R. A., Rospigliosi, C., Meray, R. K., Kessler, J. C., Lashuel, H. A., Eliezer, D. & Lansbury, P. T.,Jr. (2007). The impact of the E46K mutation on the properties of alpha-synuclein in its monomeric and oligomeric states. Biochemistry, **46**, 7107-7118.

Gallea, J. I. & Celej, M. S. (2014). Structural Insights into Amyloid Oligomers of the Parkinson Disease-related Protein alpha-Synuclein. The Journal of Biological Chemistry, **289**, 26733-26742.

Gengler. Régis Yves Norbert. 2010. A modified langmuir Schaefer Method for the creation of Functional thin films. PhD thesis, University of Groningen.

Gharibyan, A. L., Zamotin, V., Yanamandra, K., Moskaleva, O. S., Margulis, B. A., Kostanyan, I. A. & Morozova-Roche, L. A. (2007). Lysozyme Amyloid Oligomers and Fibrils Induce Cellular Death via Different Apoptotic/Necrotic Pathways. Journal of Molecular Biology, **365**, 1337-1349.

Giehm, L., Svergun, D. I., Otzen, D. E. & Vestergaard, B. (2011). Low-resolution structure of a vesicle disrupting α-synuclein oligomer that accumulates during fibrillation. Proceedings of the National Academy of Sciences of the United States of America, **108**, 3246-3251.

Glabe, C. G. (2006). Common mechanisms of amyloid oligomer pathogenesis in degenerative disease. Neurobiology of Aging, **27**, 570-575.

GonzÃ¡lez-Maeso, J. (2010). Anxious interactions. Nature Neuroscience, **13**, 524-526.

Gonzalez, M. W. & Kann, M. G. (2012). Chapter 4: Protein interactions and disease. PLoS One Computational Biology, **8**, e1002819.

Goodman, C. M., McCusker, C. D., Yilmaz, T. & Rotello, V. M. (2004). Toxicity of gold nanoparticles functionalized with cationic and anionic side chains. Bioconjugate Chemistry, **15**, 897-900.

Greenwald, J. & Riek, R. (2010). Biology of amyloid: structure, function, and regulation. Structure (London, England : 1993), **18**, 1244-1260.

Heat Shock Protein Information Resource. (2014). The Hsp70 machines. http://pdslab.biochem.iisc.ernet.in/hspir/hsp70.php.

Heber, U. (1967). Freezing Injury and Uncoupling of Phosphorylation from Electron Transport in Chloroplasts. **42**, 1343-1350.

Herczenik, E. & Gebbink, M. F. (2008). Molecular and cellular aspects of protein misfolding and disease. FASEB journal : official publication of the Federation of American Societies for Experimental Biology, **22**, 2115-2133.

Hill, S. E., Miti, T., Richmond, T. & Muschol, M. (2011). Spatial extent of charge repulsion regulates assembly pathways for lysozyme amyloid fibrils. PloS One, **6**, e18171.

Hofmann, N. R. & Theg, S. M. (2005). Chloroplast outer membrane protein targeting and insertion. Trends in Plant Science, **10**, 450-457.

Hyman, S. & Jarvis, R. P. (2011). Studying Arabidopsis chloroplast structural organisation using transmission electron microscopy. Methods in Molecular Biology (Clifton, N.J.), **774**, 113-132.

Jakhria, T., Hellewell, A. L., Porter, M. Y., Jackson, M. P., Tipping, K. W., Xue, W. F., Radford, S. E. & Hewitt, E. W. (2014). Beta$_2$-Microglobulin Amyloid Fibrils Are Nanoparticles That Disrupt Lysosomal Membrane Protein Trafficking and Inhibit Protein Degradation by Lysosomes. The Journal of Biological Chemistry, **289**, 35781-35794.

Jarvis, P. (2008). Targeting of nucleus-encoded proteins to chloroplasts in plants. The New Phytologist, **179**, 257-285.

Jarvis, P. & Soll, J. (2001). Toc, Tic, and chloroplast protein import. Biochimica et Biophysica Acta, **1541**, 64-79.

Jellinger, K. A. (2011). Interaction between alpha-synuclein and other proteins in neurodegenerative disorders. The Scientific World Journal, **11**, 1893-1907.

Kang, L., Wu, K. P., Vendruscolo, M. & Baum, J. (2011). The A53T Mutation is Key in Defining the Differences in the Aggregation Kinetics of Human and Mouse Î±-synuclein. Journal of the American Chemical Society, **133**, 13465-13470.

Kastorna, A., Trusova, V., Gorbenko, G. & Kinnunen, P. (2012). Membrane effects of lysozyme amyloid fibrils. Chemistry and Physics of Lipids, **165**, 331-337.

Kayed, R., Head, E., Thompson, J. L., McIntire, T. M., Milton, S. C., Cotman, C. W. & Glabe, C. G. (2003). Common structure of soluble amyloid oligomers implies common mechanism of pathogenesis. Science (New York, N.Y.), **300**, 486-489.

Kayed, R., Head, E., Sarsoza, F., Saing, T., Cotman, C. W., Necula, M., Margol, L., Wu, J., Breydo, L., Thompson, J. L., Rasool, S., Gurlo, T., Butler, P. & Glabe, C. G. (2007). Fibril specific, conformation dependent antibodies recognize a generic epitope common to amyloid fibrils and fibrillar oligomers that is absent in prefibrillar oligomers. Molecular neurodegeneration, **2**, 18.

Kenworthy, A. K. (2001). Imaging Protein-Protein Interactions Using Fluorescence Resonance Energy Transfer Microscopy. Methods, **24**, 289-296.

Knight, J. D. & Miranker, A. D. (2004). Phospholipid catalysis of diabetic amyloid assembly. Journal of Molecular Biology, **341**, 1175-1187.

Kriechbaumer, V., Nabok, A., Mustafa, M. K., Al-Ammar, R., Tsargorodskaya, A., Smith, D. P. & Abell, B. M. (2012 (A)). Analysis of protein interactions at native chloroplast membranes by ellipsometry. PloS One, **7**, e34455.

Kriechbaumer, V. & Abell, B. M. (2012 (B)). Chloroplast envelope protein targeting fidelity is independent of cytosolic components in dual organelle assays. Frontiers in Plant Science, **3**, 148.

Kriechbaumer, V., Nabok, A., Widdowson, R., Smith, D. P. & Abell, B. M. (2012 (C)). Quantification of ligand binding to G-protein coupled receptors on cell membranes by ellipsometry. PloS One, **7**, e46221.

Kriechbaumer, V., Shaw, R., Mukherjee, J., Bowsher, C. G., Harrison, A. M. & Abell, B. M. (2009). Subcellular distribution of tail-anchored proteins in Arabidopsis. Traffic (Copenhagen, Denmark), **10**, 1753-1764.

Kriechbaumer, V., Tsargorodskaya, A., Mustafa, M. K., Vinogradova, T., Lacey, J., Smith, D. P., Abell, B. M. & Nabok, A. (2011). Study of receptor-chaperone interactions using the optical technique of spectroscopic ellipsometry. Biophysical Journal, **101**, 504-511.

Kroll, D., Meierhoff, K., Bechtold, N., Kinoshita, M., Westphal, S., Vothknecht, U. C., Soll, J. & Westhoff, P. (2001). VIPP1, a nuclear gene of Arabidopsis thaliana essential for thylakoid membrane formation. Proceedings of the National Academy of Sciences of the United States of America, **98**, 4238-4242.

Kumar, S. & Nussinov, R. (2002). Close-range electrostatic interactions in proteins. Chembiochem : a European Journal of Chemical Biology, **3**, 604-617.

Kyowa Interface Science Co. (2014). Wilhelmy plate method. http://www.face-kyowa.co.jp/english/en_science/en_theory/en_what_Surface_tension/.

Langmuir, I. & Schaefer, V. (1938). **Activities of Urease and Pepsin Monolayers**. Journal of the American Chemical Society, **60**, 1351-1360.

Lashuel, H. A., Hartley, D., Petre, B. M., Walz, T. & Lansbury, P. T.,Jr. (2002). Neurodegenerative disease: amyloid pores from pathogenic mutations. Nature, **418**, 291.

Lee, J., Kim, D. H. & Hwang, I. (2014). Specific targeting of proteins to outer envelope membranes of endosymbiotic organelles, chloroplasts, and mitochondria. Frontiers in Plant Science, **5**, 173.

Lee, J. H., Hong, C. S., Lee, S., Yang, J. E., Park, Y. I., Lee, D., Hyeon, T., Jung, S. & Paik, S. R. (2012). Radiating amyloid fibril formation on the surface of lipid membranes through unit-assembly of oligomeric species of alpha-synuclein. PloS One, **7**, e47580.

Leznicki, P. & High, S. (2012). SGTA antagonizes BAG6-mediated protein triage. Proceedings of the National Academy of Sciences of the United States of America, **109**, 19214-19219.

Leznicki, P., Clancy, A., Schwappach, B. & High, S. (2010). Bat3 promotes the membrane integration of tail-anchored proteins. Journal of Cell Science, **123**, 2170-2178.

Li, J., Uversky, V. N. & Fink, A. L. (2001). Effect of familial Parkinson's disease point mutations A30P and A53T on the structural properties, aggregation, and fibrillation of human alpha-synuclein. Biochemistry, **40**, 11604-11613.

Lloyd, D. J., Wheeler, M. C. & Gekakis, N. (2010). A Point Mutation in Sec61Î±1 Leads to Diabetes and Hepatosteatosis in Mice. Diabetes, **59**, 460-470.

Long, A. R., O'Brien, C. C., Malhotra, K., Schwall, C. T., Albert, A. D., Watts, A. & Alder, N. N. (2013). A detergent-free strategy for the reconstitution of active enzyme complexes from native biological membranes into nanoscale discs. BMC Biotechnology, **13**, 41-6750-13-41.

Lundberg, M., Wikström, S. & Johansson, M. (2003). Cell surface adherence and endocytosis of protein transduction domains. Molecular Therapy, **8**, 143-150.

Makin, O. S. & Serpell, L. C. (2005). Structures for amyloid fibrils. FEBS Journal, **272**, 5950-5961.

Mandon, E. C. & Gilmore, R. (2007). The Tail End of Membrane Insertion. Cell, **128**, 1031-1032.

Martins, I. C., Kuperstein, I., Wilkinson, H., Maes, E., Vanbrabant, M., Jonckheere, W., Van Gelder, P., Hartmann, D., D'Hooge, R., De Strooper, B., Schymkowitz, J. & Rousseau, F. (2008). Lipids revert inert Abeta amyloid fibrils to neurotoxic protofibrils that affect learning in mice. The EMBO journal, **27**, 224-233.

Marx, K. A. (2003). Quartz crystal microbalance: a useful tool for studying thin polymer films and complex biomolecular systems at the solution-surface interface. Biomacromolecules, **4**, 1099-1120.

Mashaghi, A., Swann, M., Popplewell, J., Textor, M. & Reimhult, E. (2008). Optical anisotropy of supported lipid structures probed by waveguide spectroscopy and its application to study of supported lipid bilayer formation kinetics. Analytical Chemistry, **80**, 3666-3676.

Mayer, M. P. & Bukau, B. (2005). Hsp70 chaperones: cellular functions and molecular mechanism. Cellular and Molecular Life Sciences : CMLS, **62**, 670-684.

Maynard, J. A., Lindquist, N. C., Sutherland, J. N., Lesuffleur, A., Warrington, A. E., Rodriguez, M. & Oh, S. H. (2009). Surface plasmon resonance for high-throughput ligand screening of membrane-bound proteins. Biotechnology Journal, **4**, 1542-1558.

McGillivray, D. J., Valincius, G., Vanderah, D. J., Febo-Ayala, W., Woodward, J. T., Heinrich, F., Kasianowicz, J. J. & Losche, M. (2007). Molecular-scale structural and functional characterization of sparsely tethered bilayer lipid membranes. Biointerphases, **2**, 21-33.

McGlinchey, R. P., Yap, T. L. & Lee, J. C. (2011). The yin and yang of amyloid: insights from alpha-synuclein and repeat domain of Pmel17. Physical Chemistry Chemical Physics : PCCP, **13**, 20066-20075.

Milanesi, L., Sheynis, T., Xue, W. F., Orlova, E. V., Hellewell, A. L., Jelinek, R., Hewitt, E. W., Radford, S. E. & Saibil, H. R. (2012). Direct three-dimensional visualization of membrane disruption by amyloid fibrils. Proceedings of the National Academy of Sciences of the United States of America, **109**, 20455-20460.

Mossuto, M. F., Dhulesia, A., Devlin, G., Frare, E., Kumita, J. R., de Laureto, P. P., Dumoulin, M., Fontana, A., Dobson, C. M. & Salvatella, X. (2010). The Non-Core Regions of Human Lysozyme Amyloid Fibrils Influence Cytotoxicity. Journal of Molecular Biology, **402**, 783-796.

Muronetz, V. I., Sholukh, M. & Korpela, T. (2001). Use of protein–protein interactions in affinity chromatography. Journal of Biochemical and Biophysical Methods, **49**, 29-47.

Mustafa, M. K., Nabok, A., Parkinson, D., Tothill, I. E., Salam, F. & Tsargorodskaya, A. (2010). Detection of beta-amyloid peptide (1-16) and amyloid precursor protein (APP770) using spectroscopic ellipsometry and

QCM techniques: a step forward towards Alzheimers disease diagnostics. Biosensors & Bioelectronics, **26**, 1332-1336.

Mutschler, T., Kieser, B., Frank, R. & Gauglitz, G. (2002). Characterization of thin polymer and biopolymer layers by ellipsometry and evanescent field technology. Analytical and Bioanalytical Chemistry, **374**, 658-664.

Nabok, A. V., Tsargorodskaya, A., Hassan, A. K. & Starodub, N. F. (2005). Total internal reflection ellipsometry and SPR detection of low molecular weight environmental toxins. Applied Surface Science, **246**, 381-386.

Nakamura, K. (2013). alpha-Synuclein and mitochondria: partners in crime? Neurotherapeutics : the journal of the American Society for Experimental NeuroTherapeutics, **10**, 391-399.

Nakamura, K. (2013). alpha-Synuclein and mitochondria: partners in crime? Neurotherapeutics : the journal of the American Society for Experimental NeuroTherapeutics, **10**, 391-399.

Nakamura, K., Nemani, V. M., Wallender, E. K., Kaehlcke, K., Ott, M. & Edwards, R. H. (2008). Optical reporters for the conformation of alpha-synuclein reveal a specific interaction with mitochondria. The Journal of neuroscience : the official journal of the Society for Neuroscience, **28**, 12305-12317.

Narayanan, V. & Scarlata, S. (2001). Membrane binding and self-association of alpha-synucleins. Biochemistry, **40**, 9927-9934.

Nath Radhamony, R., Mohan Prasad, A., Srinivasan,R. (2005). T-DNA insertional mutagenesis in Arabidopsis: a tool for functional genomics. Electronic Journal of Biotechnology, **8**.

Necula, M., Kayed, R., Milton, S. & Glabe, C. G. (2007). Small molecule inhibitors of aggregation indicate that amyloid beta oligomerization and

fibrillization pathways are independent and distinct. The Journal of Biological Chemistry, **282**, 10311-10324.

O'Nuallain, B. & Wetzel, R. (2002). Conformational Abs recognizing a generic amyloid fibril epitope. Proceedings of the National Academy of Sciences of the United States of America, **99**, 1485-1490.

Ouberai, M. M., Wang, J., Swann, M. J., Galvagnion, C., Guilliams, T., Dobson, C. M. & Welland, M. E. (2013). alpha-Synuclein senses lipid packing defects and induces lateral expansion of lipids leading to membrane remodeling. The Journal of Biological Chemistry, **288**, 20883-20895.

Ow, S. & Dunstan, D. (2013). The effect of concentration, temperature and stirring on hen egg white lysozyme amyloid formation. Soft Matter, 9692-9701.

Ozalp, V. C. (2012). Dual-polarization interferometry for quantification of small molecules using aptamers. Analytical and Bioanalytical Chemistry, **402**, 799-804.

Paila, Y. D., Richardson, L. G. & Schnell, D. J. (2014). New Insights into the Mechanism of Chloroplast Protein Import and Its Integration with Protein Quality Control, Organelle Biogenesis and Development. Journal of Molecular Biology.

Panigrahi, R., Adina-Zada, A., Whelan, J. & Vrielink, A. (2013). Ligand recognition by the TPR domain of the import factor Toc64 from Arabidopsis thaliana. PloS One, **8**, e83461.

Patching, S. G. (2014). Surface plasmon resonance spectroscopy for characterisation of membrane protein–ligand interactions and its potential for drug discovery. Biochimica et Biophysica Acta (BBA) - Biomembranes, **1838**, 43-55.

Pedamallu, C. S. & Posfai, J. (2010). Open source tool for prediction of genome wide protein-protein interaction network based on ortholog information. Source code for Biology and Medicine, **5**, 8-0473-5-8.

Pedrazzini, E. (2009). Tail-Anchored Proteins in Plants. Journal of Plant Biology, **52**, 88-101.

Pemberton, S., Madiona, K., Pieri, L., Kabani, M., Bousset, L. & Melki, R. (2011). Hsc70 protein interaction with soluble and fibrillar alpha-synuclein. The Journal of Biological Chemistry, **286**, 34690-34699.

Petty, M. 1996. ***Langmuir-Blodgett Films: An Introduction.*** Cambridge University Press.

Phizicky, E. M. & Fields, S. (1995). Protein-protein interactions: methods for detection and analysis. Microbiological Reviews, **59**, 94-123.

Pirc, Katja and Poklar Ulrih, Nataša. (2011). Alpha-synuclein interactions with membranes. In: *Etiology and Pathophysiology of Parkinson's Disease.*(Ed. by Prof. Abdul Qayyum Rana), pp. Chapter 5. http://www.intechopen.com/books/etiology-and-pathophysiology-of-parkinson-s-disease/alpha-synuclein-interactions-with-membranes:InTech.

Poksinski, M. & Arwin, H. (2007). Total internal reflection ellipsometry: ultrahigh sensitivity for protein adsorption on metal surfaces. Optics Letters, **32**, 1308-1310.

Poksinski, M. & Arwin, H. (2004). Protein monolayers monitored by internal reflection ellipsometry. Thin Solid Films, **455–456**, 716-721.

Qbadou, S., Becker, T., Mirus, O., Tews, I., Soll, J. & Schleiff, E. (2006). The molecular chaperone Hsp90 delivers precursor proteins to the chloroplast import receptor Toc64. The EMBO Journal, **25**, 1836-1847.

Quist, A., Doudevski, I., Lin, H., Azimova, R., Ng, D., Frangione, B., Kagan, B., Ghiso, J. & Lal, R. (2005). Amyloid ion channels: A common

structural link for protein-misfolding disease. Proceedings of the National Academy of Sciences of the United States of America, **102**, 10427-10432.

Rambaran, R. N. & Serpell, L. C. (2008). Amyloid fibrils: Abnormal protein assembly. Prion, **2**, 112-117.

Rao, V. S., Srinivas, K., Sujini, G. & Kumar, G. (2014). Protein-protein interaction detection: Methods and analysis. International Journal of Proteomics, **2014**.

Reisinger, V. & Eichacker, L. A. (2008). Solubilization of membrane protein complexes for blue native PAGE. Journal of Proteomics, **71**, 277-283.

Richard, J. P., Melikov, K., Vives, E., Ramos, C., Verbeure, B., Gait, M. J., Chernomordik, L. V. & Lebleu, B. (2003). Cell-penetrating peptides. A reevaluation of the mechanism of cellular uptake. The Journal of Biological Chemistry, **278**, 585-590.

Santarius, K. A. (1971). The effect of freezing on thylakoid membranes in the presence of organic acids. Plant Physiology, **48**, 156-162.

Schmid, A. B., Lagleder, S., Grawert, M. A., Rohl, A., Hagn, F., Wandinger, S. K., Cox, M. B., Demmer, O., Richter, K., Groll, M., Kessler, H. & Buchner, J. (2012). The architecture of functional modules in the Hsp90 co-chaperone Sti1/Hop. The EMBO Journal, **31**, 1506-1517.

Schweiger, R. & Schwenkert, S. (2013). AtTPR7 as part of the Arabidopsis Sec post-translocon. Plant Signaling & Behavior, **8**, 10.4161/psb.25286. Epub 2013 Jun 11.

Schweiger, R., Soll, J., Jung, K., Heermann, R. & Schwenkert, S. (2013). Quantification of interaction strengths between chaperones and tetratricopeptide repeat domain-containing membrane proteins. The Journal of Biological Chemistry, **288**, 30614-30625.

Schweiger, R., Muller, N. C., Schmitt, M. J., Soll, J. & Schwenkert, S. (2012). AtTPR7 is a chaperone-docking protein of the Sec translocon in Arabidopsis. Journal of Cell Science, **125**, 5196-5207.

Schwenkert, S., Soll, J. & Bolter, B. (2011). Protein import into chloroplasts--how chaperones feature into the game. Biochimica et Biophysica Acta, **1808**, 901-911.

Shammas, S. L., Waudby, C. A., Wang, S., Buell, A. K., Knowles, T. P., Ecroyd, H., Welland, M. E., Carver, J. A., Dobson, C. M. & Meehan, S. (2011). Binding of the molecular chaperone alphaB-crystallin to Abeta amyloid fibrils inhibits fibril elongation. Biophysical Journal, **101**, 1681-1689.

Shvadchak, V. V., Yushchenko, D. A., Pievo, R. & Jovin, T. M. (2011). The mode of α-synuclein binding to membranes depends on lipid composition and lipid to protein ratio. FEBS letters, **585**, 3513-3519.

Sipe, J. D. & Cohen, A. S. (2000). Review: History of the Amyloid Fibril. Journal of Structural Biology, **130**, 88-98.

Sohrt, K. & Soll, J. (2000). Toc64, a new component of the protein translocon of chloroplasts. The Journal of Cell Biology, **148**, 1213-1221.

Soll, J. (2002). Protein import into chloroplasts. Current opinion in plant biology, **5**, 529-535.

Sonesson, A. W., Callisen, T. H., Brismar, H. & Elofsson, U. M. (2007). A comparison between dual polarization interferometry (DPI) and surface plasmon resonance (SPR) for protein adsorption studies. Colloids and Surfaces B: Biointerfaces, **54**, 236-240.

Speight, R. E. & Cooper, M. A. (2012). A Survey of the 2010 Quartz Crystal Microbalance Literature. Journal of Molecular Recognition, **25**, 451-473.

Stefani, M. & Dobson, C. M. (2003). Protein aggregation and aggregate toxicity: new insights into protein folding, misfolding diseases and biological evolution. Journal of Molecular Medicine (Berlin, Germany), **81**, 678-699.

Stefani, M. (2012). Structural features and cytotoxicity of amyloid oligomers: Implications in Alzheimer's disease and other diseases with amyloid deposits. Progress in Neurobiology, **99**, 226-245.

Stefanovic, S. & Hegde, R. S. (2007). Identification of a targeting factor for posttranslational membrane protein insertion into the ER. Cell, **128**, 1147-1159.

Storer, C. L., Dickey, C. A., Galigniana, M. D., Rein, T. & Cox, M. B. (2011). FKBP51 and FKBP52 in signaling and disease. Trends in Endocrinology & Metabolism, **22**, 481-490.

Striebel, C., Brecht, A. & Gauglitz, G. (1994). Characterization of biomembranes by spectral ellipsometry, surface plasmon resonance and interferometry with regard to biosensor application. Biosensors & Bioelectronics, **9**, 139-146.

Suleman, M., Gangneux, J. P., Legentil, L., Belaz, S., Cabezas, Y., Manuel, C., Dureau, R., Sergent, O., Burel, A., Daligault, F., Ferrieres, V. & Robert-Gangneux, F. (2014). Alkyl galactofuranosides strongly interact with Leishmania donovani membrane and provide antileishmanial activity. Antimicrobial Agents and Chemotherapy, **58**, 2156-2166.

Swann, M. J., Peel, L. L., Carrington, S. & Freeman, N. J. (2004). Dual-polarization interferometry: an analytical technique to measure changes in protein structure in real time, to determine the stoichiometry of binding events, and to differentiate between specific and nonspecific interactions. Analytical Biochemistry, **329**, 190-198.

Tanaka, M., Collins, S. R., Toyama, B. H. & Weissman, J. S. (2006). The physical basis of how prion conformations determine strain phenotypes. Nature, **442**, 585-589.

Thiellement, H., Zivy, M., Damerval, C. & Méchin, V. 2007. *Plant Proteomics.* : Human Press.

Tofoleanu, F. & Buchete, N. V. (2012). Molecular interactions of Alzheimer's Abeta protofilaments with lipid membranes. Journal of Molecular Biology, **421**, 572-586.

Uversky, V. N. (2008). Amyloidogenesis of natively unfolded proteins. Current Alzheimer Research, **5**, 260-287.

Vabulas, R. M., Raychaudhuri, S., Hayer-Hartl, M. & Hartl, F. U. (2010). Protein folding in the cytoplasm and the heat shock response. Cold Spring Harbor perspectives in Biology, **2**, a004390.

van der Geer, P. (2014). Chapter Four - Analysis of Protein–Protein Interactions by Coimmunoprecipitation. Methods in Enzymology, **541**, 35-47.

Vojta, A., Alavi, M., Becker, T., Hormann, F., Kuchler, M., Soll, J., Thomson, R. & Schleiff, E. (2004). The protein translocon of the plastid envelopes. The Journal of Biological Chemistry, **279**, 21401-21405.

von Loeffelholz, O., Kriechbaumer, V., Ewan, R. A., Jonczyk, R., Lehmann, S., Young, J. C. & Abell, B. M. (2011). OEP61 is a chaperone receptor at the plastid outer envelope. The Biochemical Journal, **438**, 143-153.

Vothknecht, U. C., Otters, S., Hennig, R. & Schneider, D. (2012). Vipp1: a very important protein in plastids?! Journal of Experimental Botany, **63**, 1699-1712.

Wang, W., Yang, Y., Wang, S., Nagaraj, V. J., Liu, Q., Wu, J. & Tao, N. (2012). Label-free measuring and mapping of binding kinetics of membrane proteins in single living cells. Nature Chemistry, **4**, 846-853.

Wegener, J., Janshoff, A. & Steinem, C. (2001). The quartz crystal microbalance as a novel means to study cell-substrate interactions in situ. Cell Biochemistry and Biophysics, **34**, 121-151.

Wong, P. T., Schauerte, J. A., Wisser, K. C., Ding, H., Lee, E. L., Steel, D. G. & Gafni, A. (2009). Amyloid-β Membrane Binding and Permeabilization are Distinct Processes Influenced Separately by Membrane Charge and Fluidity. Journal of Molecular Biology, **386**, 81-96.

Woollam, J. A. (2002). Guide to using WVASE32. ftp://iristor.vub.ac.be/patio/SURF/pub/DATAtransit%20SURF-INTERNVUB/oscars/WVASE/WVASE_Manual.pdf.

Xu, K., Ouberai, M. M. & Welland, M. E. (2013). A comprehensive study of lysozyme adsorption using dual polarization interferometry and quartz crystal microbalance with dissipation. Biomaterials, **34**, 1461-1470.

Xue, W. F., Hellewell, A. L., Gosal, W. S., Homans, S. W., Hewitt, E. W. & Radford, S. E. (2009). Fibril fragmentation enhances amyloid cytotoxicity. The Journal of Biological Chemistry, **284**, 34272-34282.

Yoshiike, Y., Minai, R., Matsuo, Y., Chen, Y. R., Kimura, T. & Takashima, A. (2008). Amyloid oligomer conformation in a group of natively folded proteins. PloS One, **3**, e3235.

Young, J. C., Barral, J. M. & Ulrich Hartl, F. (2003). More than folding: localized functions of cytosolic chaperones. Trends in Biochemical Sciences, **28**, 541-547.

Zhou, K. G., Chang, M. J., Wang, H. X., Xie, Y. L. & Zhang, H. L. (2012). Monitoring the layer-by-layer self-assembly of graphene and graphene oxide by spectroscopic ellipsometry. Journal of Nanoscience and Nanotechnology, **12**, 508-512.

Zhu, M., Li, J. & Fink, A. L. (2003). The association of alpha-synuclein with membranes affects bilayer structure, stability, and fibril formation. The Journal of Biological Chemistry, **278**, 40186-40197.

Zimmermann, R. (1998). The role of molecular chaperones in protein transport into the mammalian endoplasmic reticulum. Biological Chemistry, **379**, 275-282.